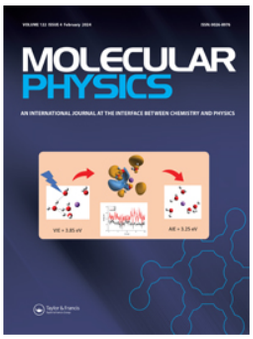

Taylor & Francis
Taylor & Francis Group

Molecular Physics

An International Journal at the Interface Between Chemistry and Physics

ISSN: (Print) (Online) Journal homepage: www.tandfonline.com/journals/tmph20

Theoretical investigation of electron interaction processes for furfural ($C_5H_4O_2$) and p-benzoquinone ($C_6H_4O_2$)

Dhaval Chauhan, Smruti Parikh, Nirav Thakkar & Chetan Limbachiya

To cite this article: Dhaval Chauhan, Smruti Parikh, Nirav Thakkar & Chetan Limbachiya (13 Feb 2024): Theoretical investigation of electron interaction processes for furfural ($C_5H_4O_2$) and p-benzoquinone ($C_6H_4O_2$), Molecular Physics, DOI: 10.1080/00268976.2024.2314706

To link to this article: https://doi.org/10.1080/00268976.2024.2314706

MOLECULAR PHYSICS e2314706
https://doi.org/10.1080/00268976.2024.2314706

Taylor & Francis
Taylor & Francis Group

RESEARCH ARTICLE

Theoretical investigation of electron interaction processes for furfural ($C_5H_4O_2$) and p-benzoquinone ($C_6H_4O_2$)

Dhaval Chauhan[a], Smruti Parikh[a], Nirav Thakkar[b] and Chetan Limbachiya[a]

[a]Department of Applied Physics, The M. S. University of Baroda, Vadodara, India; [b]Department of Physics, Sheth M. N. Science College, Patan, India

ABSTRACT

The present study aims to quantify the electron-induced inelastic and elastic processes for molecules of industrial relevance, furfural and p-benzoquinone. We have computed inelastic cross-sections (Q_{inel}), elastic cross-sections (Q_{el}) and total cross-sections (Q_T) through spherical complex optical potential (SCOP) formalism, from ionisation energy (IE) to 5000 eV. The continuum and discrete contributions of the Q_{inel} have been calculated in terms of ionisation (Q_{ion}) and excitation ($\sum Q_{exc}$) cross-sections, respectively, by employing the complex scattering potential-ionisation contribution (CSP-iC) method. A novel 2-parameter semi-empirical method (2p-SEM), a useful approach applicable for the large molecules $55 < Z < 95$ for calculating Q_T, has been proposed and validated. Computed results are compared with previous experimental and theoretical data. We have also estimated the dielectric constant (ε) using various methods and correlations with molecular ionisation for these applied molecules.

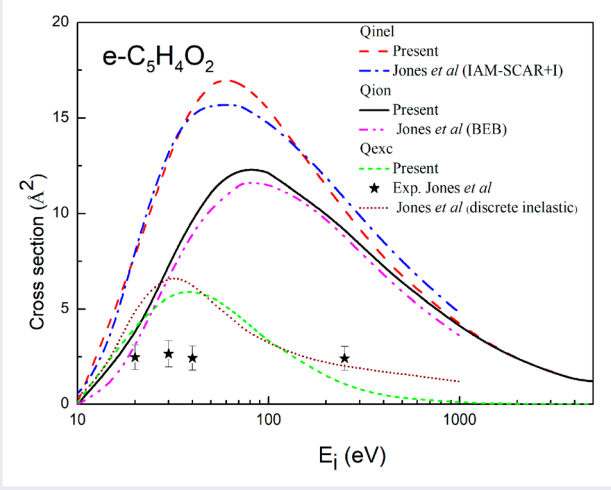

ARTICLE HISTORY
Received 18 May 2023
Accepted 31 January 2024

KEYWORDS
2-parameter semi-empirical method (2p-SEM); SCOP; CSP-ic; dielectric constant (ε); cross-sections

1. Introduction

A situation in which the rising global need for energy must be fulfilled while voicing concerns about climate change has ignited interest in devising new or improved (in terms of sustainability and low-cost) technologies over the last few decades, particularly for the conversion of lignocellulosic biomass into several biomaterials including biofuels [1–3]. Among all the issues to be surmounted, 'biomass recalcitrance' is the major contributor to the high price of converting lignocellulose into biomaterials with a high value. Theoretical and experimental studies conducted to deal with this issue found that radicals and free electrons produced within atmospheric pressure plasmas can aid in the breakdown of biomass through inducing dissociations, excitations and other fragmentation events [4,5]. In light of this, we have

CONTACT Chetan Limbachiya cglimbachiya-apphy@msubaroda.ac.in Department of Applied Physics, The M. S. University of Baroda, Vadodara 390001, India

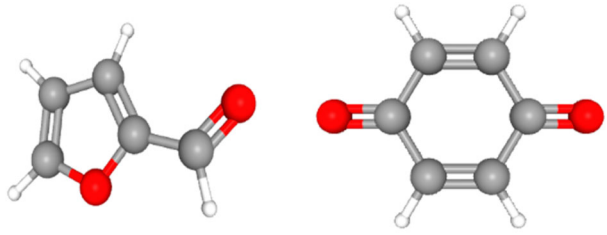

(A) Furfural ($C_5H_4O_2$) (B) p-benzoquinone ($C_6H_4O_2$)

Figure 1. Chemical structure of the molecules (https://pubchem.ncbi.nlm.nih.gov).

conducted the electron collision study with furfural, generated from the species of lignocellulose and a potential substitute for petrochemicals [6]. The chemical structure of the molecules is shown in Figure 1.

2-furaldehyde or furfural ($C_5H_4O_2$) is an essential component of green chemistry, as well as in petroleum, agrochemicals, pharmaceuticals and plastics [7]. Furthermore, it has been recognised as a crucial base chemical [6,8] for the commercialisation of bio-refineries. To provide a greater yield of biofuel conversion, biomass is first treated using electron beam irradiation techniques or atmospheric pressure plasma [3,4]. This and other modelling plasma applications [9] point to the requirement for precise and thorough electron scattering data for furfural [10].

Furthermore, with rising of the energy consumption, worldwide difficulties related to collecting and storing energy sustainably are becoming increasingly important. Knowing and imitating nature may allow developments that could assist in addressing these issues. The principal method for conversion of the energy on Earth is oxygenic photosynthesis, in which H_2O and CO_2 are transformed into O_2 and sugars [11]. Hence, improving our knowledge of these photosynthetic pathways may spur advancements in photocatalysis and photovoltaics [12] as well as the development of hybrid photo-bio electrochemical technologies [13]. Within the cellular respiration and electron transport sequence of photosynthesis, quinones [14] are crucial molecular components since they are capable of performing a reversible reduction process. As a result, they are proving to be a viable option as a long-term, cost-effective material in energy-storage and harvesting systems, such as artificial photosynthetic platforms, dye-sensitised solar cells, phototransistors, rechargeable batteries, plasmonic light harvesting and pseudo-capacitors [14]. The development of bio-inspired energy conversion and harvesting devices can be facilitated by an understanding of the special properties of quinone and its derivatives [14]. In this context, p-benzoquinone (pBQ), the simplest quinone, has served as a prototype structure in a variety of research seeking to understand the electrochemical and photo-induced behaviour of quinones in general [14].

A previous study on electron interactions with furfural and parabenzoquinone includes experimental studies of electron excitation [15] for 20-250 eV and total cross-sections measured using electron transmission technique [16] for 7-20 eV and Transmission-beam attenuation measurements [17] for 1-200 eV. Theoretical results are obtained by Binary-encounter-bethe (BEB) [10] methods, the Schwinger multichannel method with pseudopotentials (SMCPP) [17,18], Independent atomic model with Screening corrected additivity rule including interference (IAM-SCAR + I)[10]. A theoretical group [19] has used a well-established R-matrix method to study the elastic and inelastic collisions between electron and p-benzoquinone at low energy 0 eV to 8 eV.

For the present work, we have focused on these two molecules which have gained recent interest and studied their electron interaction processes for energies from molecular ionisation threshold to 5000 eV. We have quantified various electron-induced molecular processes for these compounds of great industrial applications. These processes are elastic and inelastic including excitations and ionisation.

2. Theoretical methodology

In this electron interaction study, we have computed various cross-sections using the established SCOP method and extracted ionisation cross-sections through the CSP-ic method. Furthermore, we have proposed a novel approach 2p-SEM, which is applicable for the larger and more complex molecules $55 < Z < 95$ for a wide energy range of 50 eV to 5000 eV.

2.1. Spherical complex optical potential formalism (SCOP)

To calculate Q_{inel} and Q_{el}, we have employed spherical complex optical potential formalism with group additivity rule [20,21] since present molecules have a larger physical size. This approach has been thoroughly discussed in our previous articles [21–23]. The complex potential is given as

$$V_{opt} = V_{real} + iV_{Ima} \tag{1}$$

The effects of static potential (V_s), exchange potential (V_{ex}) and polarisation potential (V_{pol}) are included through the real part of the complex potential (V_{real}) and inelastic effects are incorporated through the imaginary potential (V_{Ima}). To construct these potentials the primary input is the charge den$V_{opt} = V_{real} + iV_{Ima}$sity of

the target [24]. For exchange effects [25], the proposed model has been employed and for polarisation, Zhang *et al.* model potential is used.

$$V_{opt}(E_i, r) = V_{st}(r) + V_{ex}(E_i, r) + V_{pol}(E_i, r) + iV_{abs}(E_i, r) \quad (2)$$

To account inelastic effect, the quasi-free modified model potential [26] is used. The final V_{opt} is then fed into the Schroedinger equation, which is then solved numerically employing the partial wave approximation to compute the Q_{inel}, Q_{el} and finally Q_T. There are mainly two contributions that sum up to the Q_{inel}

$$Q_{inel}(E_i) = \sum Q_{exc}(E_i) + Q_{ion}(E_i) \quad (3)$$

where Q_{Ion} is the total ionisation cross-sections for all the permitted ionisation processes. $\sum Q_{exc}$ incorporates all the allowed electronic excitation processes.

2.2. Complex scattering potential-ionisation contribution (CSP-ic)

As the energy is increased above the ionisation energy, the $\sum Q_{exc}$ becomes less relevant than the Q_{ion}. Hence, we have

$$Q_{inel} \geq Q_{ion} \quad (4)$$

In the complex scattering potential-ionisation contribution (CSP-ic) formalism [27,28] we define a ratio$R(E_i) = Q_{ion}/Q_{inel}$. This ratio increases from zero at energy$E_i \leq IE$ (ionisation energy) and keeps growing as the incoming energy goes up, eventually approaching unity at very high energies. Thus, we may mathematically represent these criteria as

$$R(E_i) = \begin{cases} 0, \textit{ for } E_i \leq IE \\ R_P, \textit{ for } E_i = E_P \\ \sim 1, \textit{ for } E_i \gg E_P \end{cases} \quad (5)$$

The opening of the ionisation channel occurs at the molecule's ionisation energy (IE) as shown in the first condition of Equation (5). However, as needed by the third condition, ionisation predominates at very high energy and excitation cross-sections significantly decrease leading to $R(E_i) = R_P$. Q_{inel} attains maximum value, at this energy E_P, where E_P stands for incident energy at which $R(E_i) = 1$. According to theoretical predictions [20,29,30] and experimental findings for stable compounds [31], R_p is in the range of 0.7 and 0.8. Due to this characteristic, the theory is classified as semi-empirical and a range of 10-15% total uncertainty is introduced. Q_{ion} and Q_{exc} must be calculated with at least the accuracy demanded by users. Target properties are shown in Table 1.

Table 1. Target properties (http://www.chemspider.com).

Molecules	IE (eV)	Polarisability (α) (Å^3)	(a_0^3)
Furfural ($C_5H_4O_2$)	9.21	10.0	67.55
Parabenzoquinone ($C_6H_4O_2$)	10.01[32]	10.8	72.95

Table 2. Parameter for 50 eV–500 eV.

Targets	Adenine ($C_5H_5N_5$) (Z = 70)	Guanine ($C_5H_5N_5O$) (Z = 78)	Thymine ($C_5H_6N_2O_2$) (Z = 66)	Cytosine ($C_4H_5N_3O$) (Z = 58)	Uracil ($C_4H_4N_2O_2$) (Z = 58)
A	46.53	54.79	43.66	34.68	34.56
B	0.58	0.56	0.57	0.56	0.53

2.3. 2parameter-semi-empirical method formalism (2p-SEM)

The impact energy dependence of the Q_T for the intermediate energy[33,34] and high energy[35,36] have been previously studied and the proposed formula was as follows

$$Q_T = \frac{A}{E^B} \quad (6)$$

where parameter A is governed by molecular characteristics such as the size of the molecule and its polarisability. The value of B for the high energies, above 500 eV will be $\sim$0.7, which is proposed by Joshipura [35] and Garcia [36] for smaller molecules, i.e. for ten electrons (Z = 10) and up to Z = 22 electron systems, respectively. In the present work, this formula has been derived for large molecules with 55 < Z < 95. Also, the dependence of Q_T on E_i is different for diverse energy regimes. We have derived two different expressions for the intermediate (50 < E_i < 500 eV) and high energy regions (E_i > 500 eV) for the complex and larger molecular systems with 55 < Z < 95.

In Table 2, the parameters A and B have been tabulated for the DNA bases [37] and it is seen that the value of B is nearly the same for all the molecules and is $\sim$0.56. Our calculations reveal that the Q_T depends on energy and the dependence on incident energy is similar to that of Nishimura and Tawara [33] for 50-500 eV

$$Q_T = \frac{A}{\sqrt{E}} \quad (7)$$

However, the value of A is different for each molecule, suggesting its dependency on the number of target electrons (Z).

To observe this relation, we plotted the graph of A vs Z, as shown in Figures 2 and 3 for 50 < E_i < 500 eV and E_i > 500 eV, respectively. The linear relationship observed in Figure 2 is represented through the following

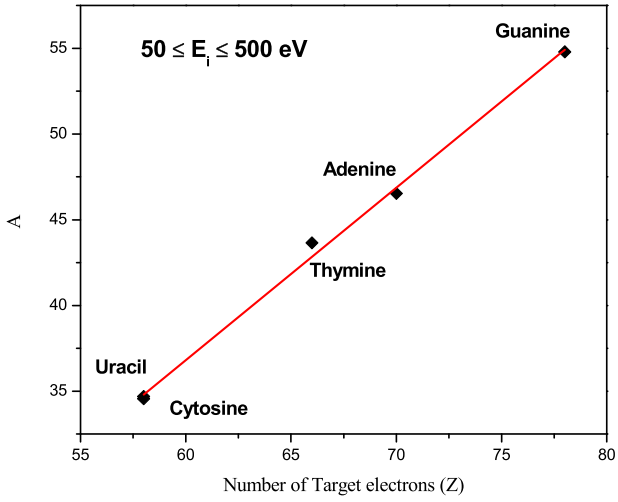

Figure 2. Parameter A vs. Z($50 \leq E_i \leq 500$ eV).

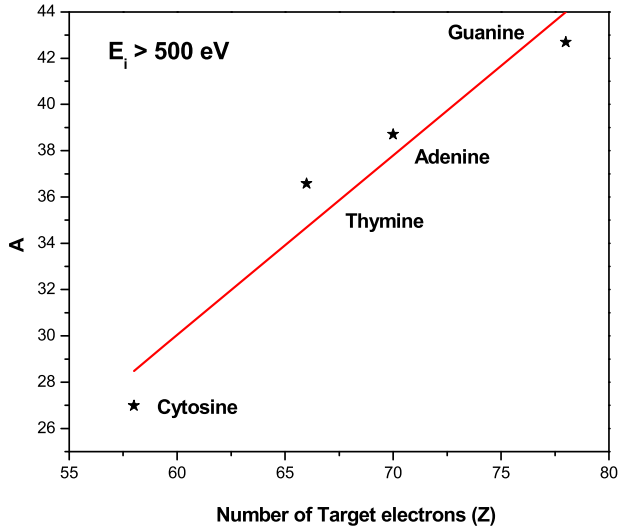

Figure 3. Parameter A vs. Z ($E_i > 500$ eV).

equation

$$A(Z) = Z - 23.54 \quad (\text{Correlation } r = 99\%) \qquad (8)$$

However, for a given Z, the precision of this approximation can be enhanced by considering the difference between the actual values of 'A' (from Table 2) and those derived from Equation (9) for each molecule. We have observed the dependency of this deviation (A – A(Z)) on the molecular size through the polarisability (α). The linear relationship between them is

$$A - A(Z) = -0.003\alpha + 0.63 \qquad (9)$$

Hence, from Equations (8) and (9), a two-parameter expression for Q_T can be formulated for the energy range from 50-500 eV

$$Q_T(E, Z, \alpha) = \frac{(Z) - 0.003(\alpha) - 22.91}{E^{0.56}} \qquad (10)$$

A similar method has been followed to derive the two-parameter expression of Q_T as a function of α and Z for the energies above 500 eV.

$$Q_T(E, Z, \alpha) = \frac{0.016(\alpha) + 0.776(Z) - 17.88}{E^{0.77}} \qquad (11)$$

We note the power of energy E is $E^{0.56}$ for lower side and $E^{0.77}$ for higher side of the incident energy.

Equations (10) and (11) provide the two-parameter expressions for Q_T for impact energy 50 eV $< E_i <$ 500 eV and $E_i >$ 500 eV, respectively allowing the estimation of Q_T for the entire energy range of the current study.

This method is employed to compute Q_{el} and Q_T for p-Benzoquinone (Z = 56) and extrapolated for Furfural (Z = 50).

3. Results and discussion

We calculated various cross-sections (Q_{inel}, Q_T, Q_{el}, Q_{ion}, and $\sum Q_{exc}$) for electron interactions with furfural ($C_5H_4O_2$) and p-benzoquinone ($C_6H_4O_2$) for the impact energy starting from IE to 5000 eV using SCOP, CSP-ic and recently developed 2p-SEM formalism. To facilitate our discussion, present results are shown in three sub-sections along with available comparisons. In sub-section 3.1, present total cross-sections are displayed in Figures 4–8. Sub-section 3.2 discusses validation of 2p-SEM and various correlations. Section 3.3 we presents the computation of the dielectric constant (ε).

3.1. Total cross-sections

Present inelastic, ionisation and excitation cross-sections for e-furfural are plotted in Figure 4.

The topmost curve shows Q_{inel}, which is compared with the only available data from Jones *et al.* [10]. They have used the Independent Atom Model with Screening Corrected Additivity Rule including the Interference (IAM-SCAR + I) method [10] for energies from 1 to 1000 eV. Throughout the energy range present Q_{inel} shows excellent accord with that of Jones *et al.* [10] except at the peak region, where present Q_{inel} slightly overestimates the IAM-SCAR + I result. Only Jones *et a. l*[10] have reported the Q_{ion} results using BEB theory and present data are seen to be in good accord with them within the mentioned 15% uncertainty of BEB[38]. The lowest curve represents the calculated $\sum Q_{exc}$. It is compared with both theoretical and experimental excitation cross-sections of Jones *et al.* [10]. Present $\sum Q_{exc}$ is close to theoretical results but overestimates of experimental

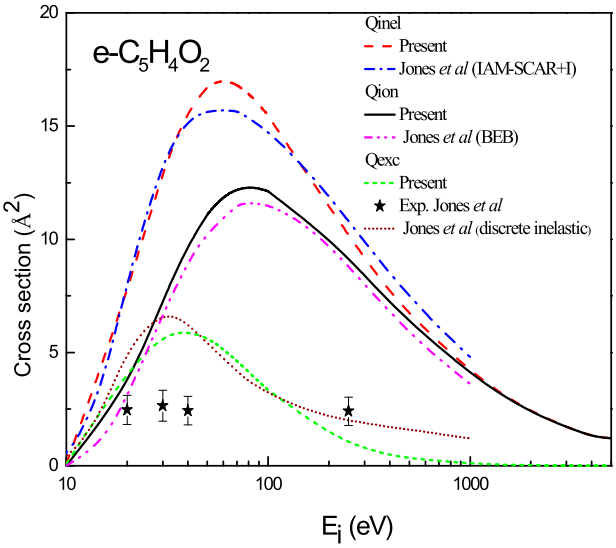

Figure 4. Q_{inel}, Q_{ion}, and $\sum Q_{exc}$ for e-$C_5H_4O_2$ Q_{inel}: Dash – Present, Dash dot – Jones *et al* [10] (IAM-SCAR + I), Q_{ion}: Solid – Present, Dash dot dot – Jones *et al.* [10], Q_{exc}: Short dash-Present, filled star – Jones *et al* [10] (exp.), Short dot- Jones *et al.* discrete inelastic.

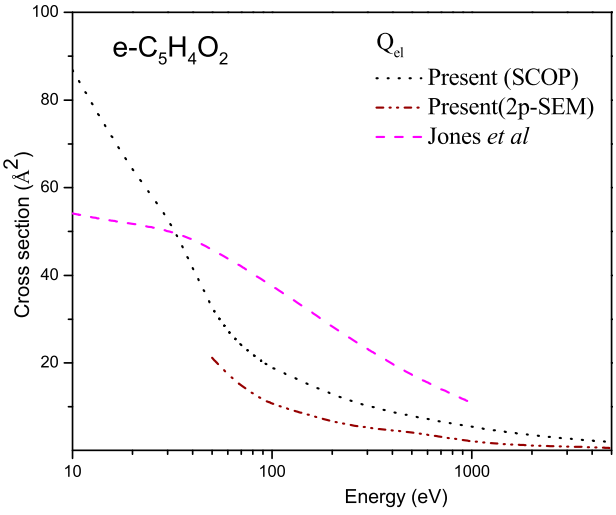

Figure 5. Q_{el} for e-$C_5H_4O_2$ Q_{el}: Dot -Present (SCOP), Dash dot dot -Present (2p-SEM), Dash - Jones *et al.* [10].

data of Jones *et al.* [10]. The experimental electronic excitation cross-sections for the bands I-VI separately and their $\sum Q_{exc}$ (band I + II + III + IV + V + VI), both are reported by Jones *et al.* [10] for the energy range 20-250 eV with the mentioned uncertainty 18% to 69%. This summed Q_{exc} is compared and seen to be of lower values as expected than present $\sum Q_{exc}$ which are calculated for all the allowed electronic excitations.

Figure 5 presents Q_{el} computed using SCOP and 2p-SEM is illustrated for the electron collision with furfural molecule. The only data of Jones *et al.* [10] for Q_{el} have been compared with the present one. At low energies, a

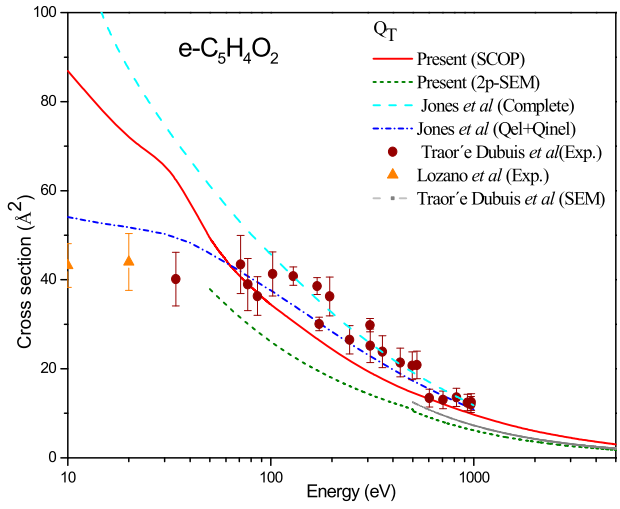

Figure 6. Q_T for e-$C_5H_4O_2$ Q_T: Solid - Present (SCOP), Short dash-Present (2p-SEM), Dash - Jones *et al.* [10] (complete), short dash dot- Jones *et al.* [10] ($Q_{el} + Q_{inel}$), solid circle- Traor´e Dubuis *et al.* [15], Solid triangle- Lozano *et al.* [16], Dash - Traor´e Dubuis *et al.* [15](SEM).

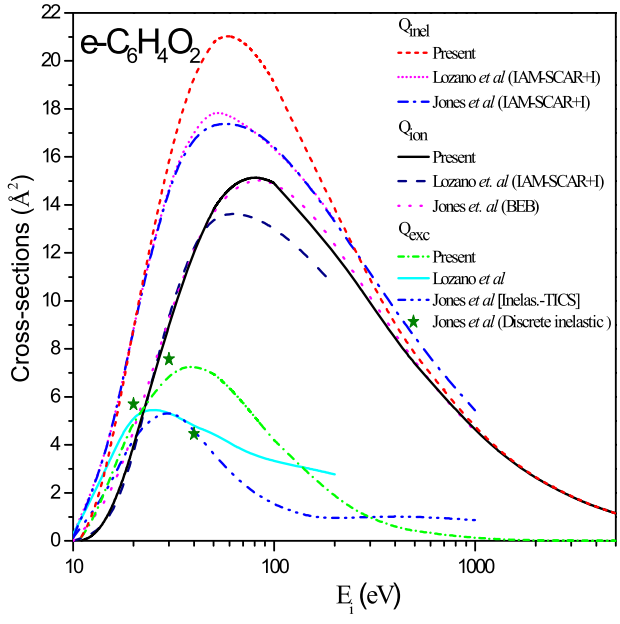

Figure 7. Q_{inel}, Q_{ion}, and $\sum Q_{exc}$ for e-$C_6H_4O_2$ [Q_{inel}: short dash -Present, short dot - Lozano *et al.* [17] (IAM-SCAR + I), dash dot - Jones *et al.* [18] (IAM-SCAR + I), Q_{ion}; solid -Present, dash -Lozano *et al.* [17] (IAM-SCAR + I), dot - Jones *et at* [18] (BEB), Q_{exc}; short dash dot -present, dash dot dot -Jones *et al.* [18] (Inelas.-TICS), solid star- Jones *et al.* [18] (Discrete inelastic)].

deviation between both of them can be observed, which is because the present Q_{el} has been calculated in the presence of inelastic channels while Jones *et al.* [10] have computed the pure Q_{el}. SCOP formalism allows for the flux competition between elastic and inelastic channels. We have computed elastic cross-sections by using the

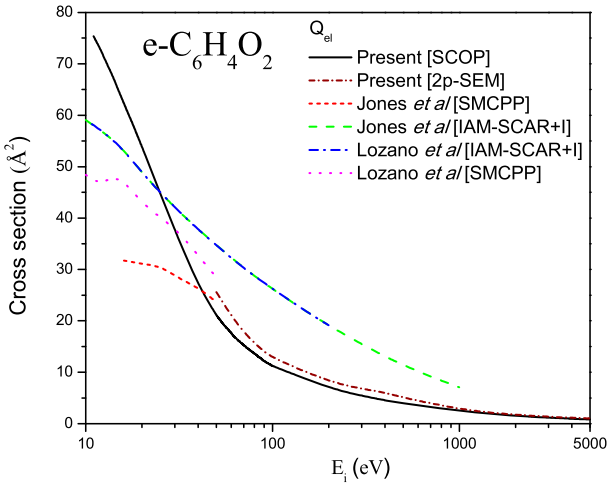

Figure 8. Q_{el} for e-$C_6H_4O_2$ Q_{el}: Solid - Present (SCOP), short dash- Present (2p-SEM), Dot- Lozano *et al.* [17] (SMCPP), dash dot - Lozano *et al.* [17] (IAM-SCAR + I), dash- Jones *et al.* [18] (IAM-SCAR + I), short dash- Jones *et at* [18] (SMCPP).

optical potential that includes an absorption potential. Hence, present elastic cross-sections are the results produced while considering the inelastic channels. Jones *et.al* [10] have reported the pure elastic cross-section data (i.e. no inelastic channels are considered in the computations). The authors reported uncertainty up to 43% at 1000 eV due to interference term added in the calculation of elastic cross-section.

The present Q_T calculated using the present SCOP method is plotted in Figure 6 with the existing data of Jones *et al.* [10], Lozano *et al.* [16] and Traoré Dubuis *et al.* [15]. The discrepancies between the present data and all the available data can be observed in Figure 6. However, the present results of Q_T show the same trend as that of Jones *et al.* [10]. While the present calculation does not involve the non-spherical effects, Jones *et al.* [10] have considered the involvement of rotational excitations in Q_T. This may be the reason for the discrepancy between the present data and the results of Jones *et al.* [10]. The experimental Q_T data of Traoré Dubuis *et al.* [15] are also seen in reasonable agreement with the present ones within the mentioned uncertainty of 4% – 22% above 50 eV[15]. Traoré Dubuis *et al.* [15] have also calculated the Q_T for energy above 500 eV, proposed by Garcia and Manero [39] for molecules having up to 22 electrons. These authors [15] claimed the SEM model has never been validated for ring molecular targets having higher atomic numbers. To estimate Q_{el} and Q_T we developed 2p-SEM and the results show a similar trend but underestimate at lower energies.

The topmost curve in Figure 7 displays the Q_{inel} for e^--$C_6H_4O_2$ collision with data from Lozano *et al.* [17] and Jones *et al.* [18]. Both authors[17,18] have employed the IAM-SCAR + I approach. Except for the peak region, present results show good agreement with the existing ones. Present ionisation cross-sections compared with available theoretical data obtained from IAM-SCAR + I [17] and BEB[18] approaches are shown in Figure 7. In Figure 7, it can be observed that the present Q_{ion} data matches excellently well with the result of Jones *et al.* [18]. However, the data of Lozano *et al.* [17] underestimate both, the present and Jones *et al.* [18] results. The data of Lozano et al. which are up to 200 eV underestimate both. Also in Figure 7, we represent $\sum Q_{exc}$ computed through the present methodology along with the available comparisons. The theoretical excitation cross-sections calculated using the IAM-SCAR + I method [17,18] are in good agreement with the present results below 25 eV, afterwards, they underestimate the present $\sum Q_{exc}$. Because Jones *et al.* [18] have also measured the electronic excitation cross-sections for each band 0-V from 20 to 40 eV energies. Their reported sum values have been compared here with the present $\sum Q_{exc}$ and good agreement can be observed for 20 and 30 eV.

Figure 8 presents Q_{el} for e-$C_6H_4O_2$ collision along with the available elastic results, computed using IAM-SCAR + I[17,18] and SMCPP [17,18] approach have been plotted. Up to 30 eV, present data overestimated with theoretical results. Beyond 30 eV present cross-sections show excellent matching with the data of Lozano *et al.* [17] and Jones *et al.* [18] obtained through SMCPP, while underestimating the results of IAM-SCAR + I [17]. The present 2p-SEM result shows excellent matching with the SCOP data. The total cross-sections along with available results are shown in Figure 9. Starting from the threshold to 30 eV our data underestimate theoretical results computed through [17] but show excellent matching with experimental [17] results within the uncertainty limit of ±5%. The present 2p-SEM result shows excellent matching with the current SCOP result. Present data include SCOP and 2p-SEM shows a similar trend with other available results.

3.2. Validation of 2p-SEM and various correlations

Several groups are involved in theoretical improvements to counter-balance the dearth of the experimental data, a situation that has improved but it is still challenging for many complex targets. Due to theoretical refinements, many models have been created, such as the Binary-encounter Bethe [38], the IAM-SCAR + I[40], the spherical complex optical potential [23,41] ab-initio R-matrix [42], complex Kohn and Schwinger multichannel methods [43,44] and so on. Above mentioned models are

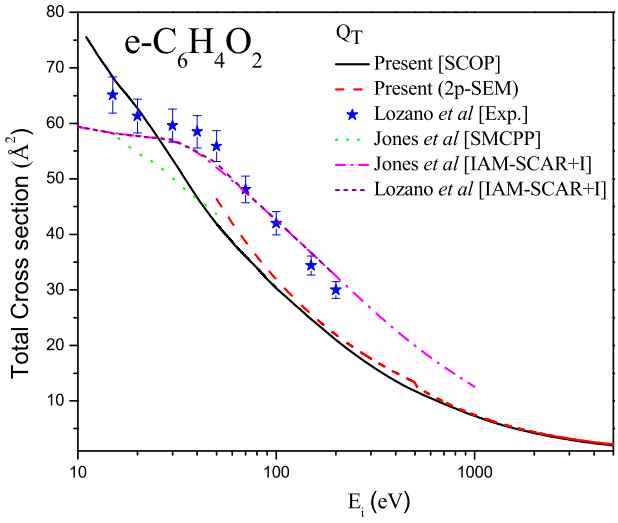

Figure 9. Q_T for e-$C_6H_4O_2$ Q_T: solid- Present, dash- Present (2p-SEM), solid star- Lozano *et al.* [17] (Exp.), dot - Jones *et al.* [18] (SMCPP), dash dot - Jones *et al.* [18] (IAM-SCAR + I), short dash - Lozano *et al.* [17] (IAM-SCAR + I).

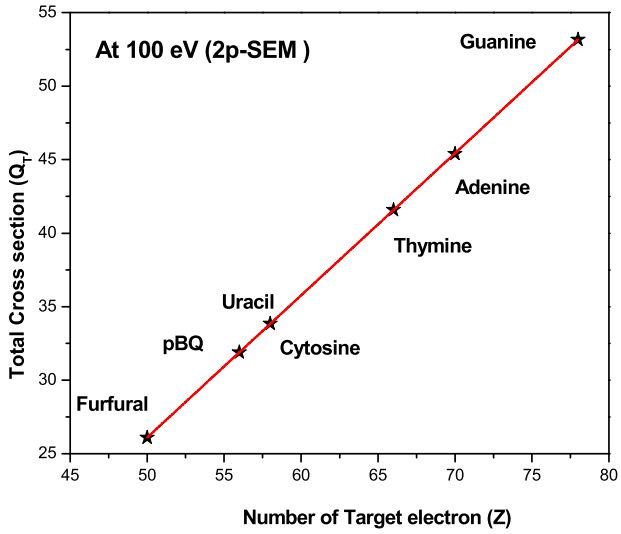

Figure 10. Correlation between Present Q_T (2p-SEM) and Z (Number of target electrons).

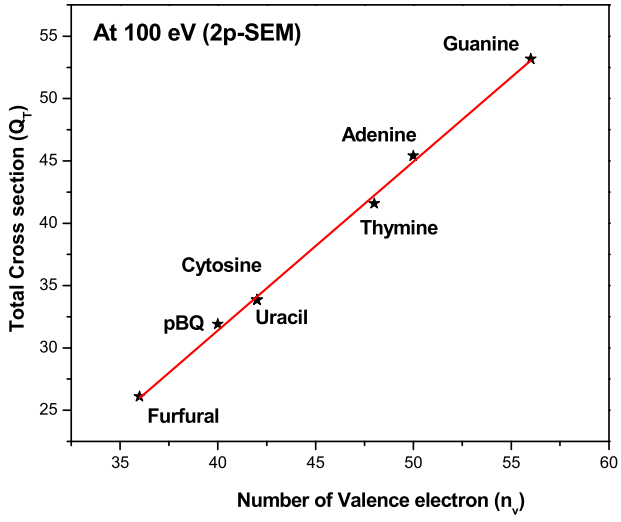

Figure 11. Correlation between Q_T (2p-SEM) and Number of valence electrons (n_v).

used to predict TCS upon electron impact within the computational complexity.

From the total electron scattering cross section data obtained through 2p-SEM, we have plotted various correlation graphs in Figures 10–15. For that we choose DNA/RNA bases [37] (Adenine, Guanine, Thymine, Cytosine), with $55 < Z < 95$. Total cross sections have been calculated analytically for the two different energy range 50 eV to 500 eV (Equation 10) and 500 eV to 5000 eV (Equation 11) as a function of the number of target electrons and the molecular polarisabilities. If there is no comparison provided by any group then the correlation is a very useful feature to evaluate the consistency and reliability of the cross sections data. The 2p-SEM method enables us to obtained reliable Q_T and Q_{el} for large and complex molecules $55 < Z < 95$ for a wide energy range 50–5000 eV.

To check the self-consistency of the present data we have plotted various graphs between Q_T(2p-SEM) vs Z (number of target electrons) and Q_T (2p-SEM) vs n_v (number of valence electrons) in Figures 10–11 at 100 eV respectively. We have shown exact correlation between them and it reflects the size dependency of target charge cloud. And also, we have plotted graph of Q_T vs polarisability (α) in Figures 12–13 at 100 eV & 1000 eV respectively. To include two ranges of energy as used in Equation 10,11. Further in Figure 14, we have shown linear correlation between Q_{ion}^{Max} and target polarisability.

3.3. Computation of dielectric constant, ε

The dielectric constant for p-benzoquinone and furfural molecules has potential applications for the study of electrical energy storage device, pseudo capacitor, photo transistor, dye-sensitised solar cells, artificial photosynthesis, rechargeable batteries, the evolution of new electronic devices and other electrical properties.

The Clausius-Mossotti equation [45] yields,

$$\frac{\varepsilon - 1}{\varepsilon + 2} = \frac{4\pi}{3} * N * \alpha \tag{13}$$

N is the number density of molecules in the material, and α is the molecular polarisability.

The number density can be calculated using the following equation [46],

$$N = \frac{N_A * \rho}{M} \tag{14}$$

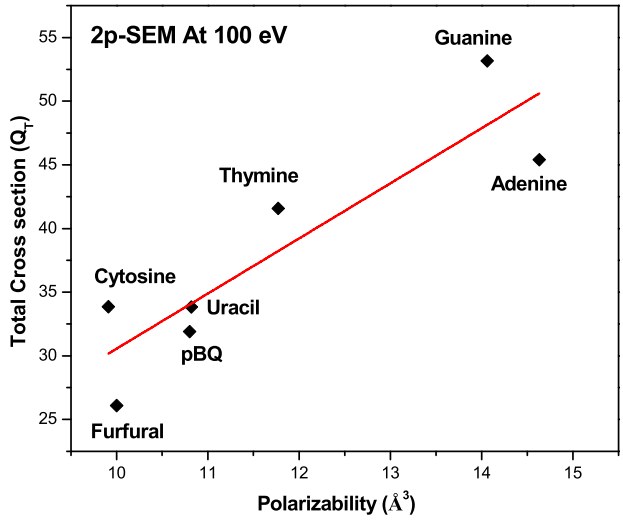

Figure 12. Correlation between Present Q_T (2p-SEM) along with the polarisability ($Å^3$).

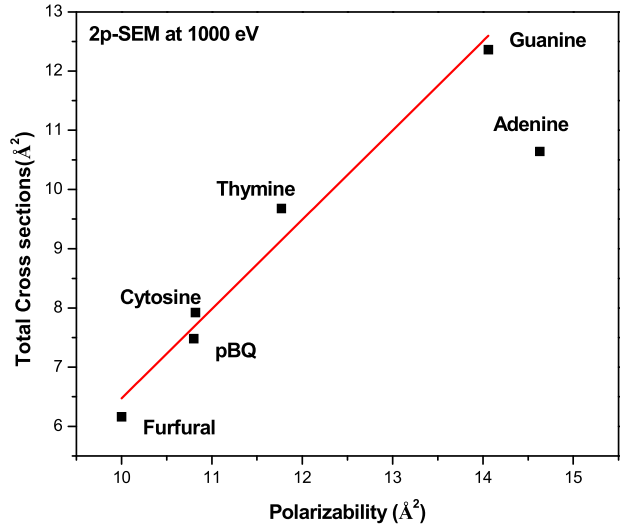

Figure 13. Correlation between Q_T and dipole polarisability (α).

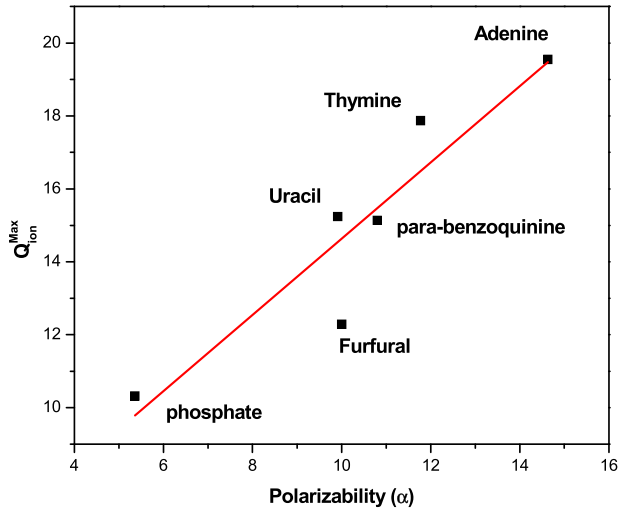

Figure 14. Correlation between $Q_{ion}{}^{Max}$ and dipole polarisability (α).

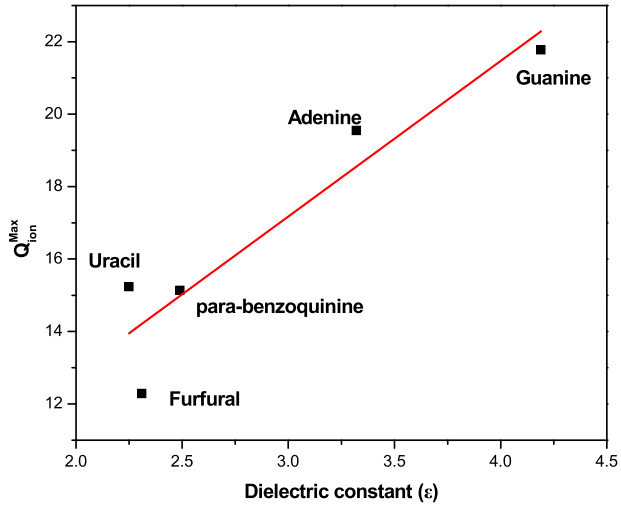

Figure 15. Correlation between $Q_{ion}{}^{Max}$ and dielectric constant (through Equation 13).

where, ρ is the density of the substance, N_A is Avogadro number (6.022×10^{23}), N is the number density of target and M is the molar mass of the molecule.

Secondly, the Onsager [47] equation yields,

$$\frac{\varepsilon - 1}{\varepsilon + 2} = \frac{4\pi}{3}\alpha N + \frac{(\varepsilon - \varepsilon_\infty)(2\varepsilon + \varepsilon_\infty)}{\varepsilon(\varepsilon_\infty + 2)^2} \tag{15}$$

where, ε_∞ is the high frequency dielectric constant.

Relation between $Q_{ion^{Max}}$ and dielectric constant (ε)

According to Harland's [48] proposed qualitative dependency nature of the $Q_{ion}{}^{Max}$ with its polarisability (α) using below Equation (16).

Then we correlate this equation with dielectric constant (using Equation 13),

$$Q_{ion^{Max}} = 11.92(\alpha) = 11.92\left(\frac{3 * (\varepsilon - 1/\varepsilon + 2)}{4\pi N * IE}\right)^{0.5} \tag{16}$$

Using above mentioned three methods, Clausius-Mossotti [45], Onsager [47] and by using the equation of Harland and vallance [48] (through Equations 13, 15,16 respectively), we have computed dielectric constant for present studied targets are shown in Table 3.

From Figure 15, we have observed linear relationship between maximum ionisation cross section and dielectric constant from Clausius- Mossootti Equation (13).

Table 3. Calculated Number density N and Dielectric constant (ε).

Mol.						Dielectric constant (ε)		
Mol.	Q_{ionMax} (Å^2)	α (10^{-24} cm^3)	ρ g/cm^3	M g/mol	N cm^{-3}	C.M. [45]	Onsager [47]	[48]
$C_5H_4O_2$	12.283	10	1.16	96.1	7.27×10^{21}	2.31	0.99	1
$C_6H_4O_2$	15.134	10.8	1.32	108.1	7.35×10^{21}	2.49	1	1

4. Conclusion

In this paper we have computed elastic, inelastic (including excitation and ionisation) and total cross sections for scattering of electrons by furfural and para-benzoquinone. The present cross sections were computed with the SCOP formalism and were compared with results available in the literature for energies above 10 eV. Furfural has many potential uses in bio-fuel, pharmaceutical, agrochemical industries, etc. whereas, p-benzoquinone is an important molecule in energy storage device, pseudo battery, artificial photosynthesis, rechargeable batteries, the evolution of new electronic devices etc. For these applied molecules, our cross-section data may be helpful in simulation. By using SCOP formalism, we quantified Q_T, Q_{el} and Q_{inel}, while Q_{ion} and $\sum Q_{exc}$ were computed through the CSP-ic method and compared with available results. A good agreement was noted between present total ionisation (Q_{ion}) through CSP-ic with BEB and IAM-SCAR + I. We have used a 2p-SEM for an energy range of 50–5 keV. This formalism may be useful for the estimation of Q_T, for those molecules/atoms whose experimental data are not available (especially due to experimental difficulties). In this paper, we have tested this method for larger and complex molecules with target electrons $55 < Z < 95$. By examining the available total electron scattering cross sections for several targets such as DNA constituents, we have observed that at intermediate to high energies the Q_T shows a significant correlation with ground state target dipole polarisability. We also computed dielectric constant ε using Clausius-Mossotti and Onsager and by making use of molecular ionisation cross sections. Furthermore, we have observed several correlations which may be helpful for the prediction of dipole polarisability and dielectric constant.

Disclosure statement

No potential conflict of interest was reported by the author(s).

References

[1] J.W. Tester, E.M. Drake, M.J. Driscoll, M.W. Golay and W.A. Peters, 2nd ed. (The MIT Press, Cambridge, 2012).

[2] J. Amorim, C. Oliveira, J.A. Souza-Correa and M.A. Ridenti, Plasma Processes Polym. **10**, 670 (2013). doi:10.1002/ppap.201200158

[3] N. Schultz-Jensen, F. Leipold, H. Bindslev and A. Thomsen, Appl. Biochem. Biotechnol. **163**, 558–572 (2011). doi:10.1007/s12010-010-9062-5

[4] J. Amorim, C. Oliveira, J.A. Souza-Corrêa and M.A. Ridenti, Plasma Process. Polym. **10**, 670 (2013).

[5] E.M. de Oliveira, R.F. da Costa, S.d. Sanchez, A.P.P. Natalense, M.H.F. Bettega, M.A.P. Lima and M.T.d.N. Varella, Phys. Chem. Chem. Phys. **15**, 1682–1689 (2013). doi:10.1039/C2CP43375C

[6] A.S. Mamman, J.-M. Lee, Y.-C. Kim, I.T. Hwang, N.-J. Park, Y.K. Hwang, J.-S. Chang and J.-S. Hwang, Biofuels, Bioprod. Biorefin. **2**, 438–454 (2008). doi:10.1002/bbb.95

[7] K. J. Zeitsch, *The Chemistry and Technology of Furfural and its Many By-Products*, 1st ed. Elsevier science (2000).

[8] H. Kobayashi and A. Fukuoka, Green Chem. **15**, 1740 (2013). doi:10.1039/c3gc00060e

[9] M.A. Ridenti, J.A. Filho, M.J. Brunger, R.F. da Costa, M.T.d.N. Varella, M.H.F. Bettega and M.A.P. Lima, Eur. Phys. J. D. **70**, 161 (2016). doi:10.1140/epjd/e2016-70272-8

[10] D.B. Jones, R.F. da Costa, M.T.d.N. Varella, M.H.F. Bettega, M.A.P. Lima, F. Blanco, G. Garcia and M.J. Brunger, J. Chem. Phys. **144**, 144303 (2016). doi:10.1063/1.4945562

[11] A. Zouni, H.-T. Witt, J. Kern, P. Fromme and N. Krauss, Nature. **409**, 739–743 (2001). doi:10.1038/35055589

[12] M. Hambourger, G.F. Moore, D.M. Kramer, D. Gust, A.L. Moore and T.A. Moore, Chem. Soc. Rev. **38**, 25–35 (2009). doi:10.1039/B800582F

[13] O. Yehezkeli, R. Tel-Vered, J. Wasserman, A. Trifonov, D. Michaeli, R. Nechushtai and I. Willner, Nature Comm. **3**, 742 (2012). doi:10.1038/ncomms1741

[14] D.B. Jones, F. Blanco, G. García, R.F. Da Costa, F. Kossoski, M.T.D.N. Varella, M.H.F. Bettega, M.A.P. Lima, R.D. White and M.J. Brunger, J. Chem. Phys. **147**, 244304 (2017). doi:10.1063/1.5010831

[15] A. Traoré Dubuis, A. Verkhovtsev, L. Ellis-Gibbings, K. Krupa, F. Blanco, D.B. Jones, M.J. Brunger and G. García, J. Chem. Phys. **147**, 054301 (2017). doi:10.1063/1.4996462

[16] A.I. Lozano, K. Krupa, F. Ferreira da Silva, P. Limão-Vieira, F. Blanco, A. Muñoz, D.B. Jones, M.J. Brunger and G. García, Eur. Phys. J. D. **71**, 226 (2017). doi:10.1140/epjd/e2017-80326-0.

[17] A.I. Lozano, J.C. Oller, D.B. Jones, R.F. Da Costa, M.T.D.N. Varella, M.H.F. Bettega, F. Ferreira Da Silva, P. Limão-Vieira, M.A.P. Lima, R.D. White, M.J. Brunger, F. Blanco, A. Muñoz and G. García, Phys. Chem. Chem. Phys. **20**, 22368–22378 (2018). doi:10.1039/C8CP03297A

[18] D.B. Jones, R.F. Da Costa, F. Kossoski, M.T.D.N. Varella, M.H.F. Bettega, G. García, F. Blanco, R.D. White, M.A.P. Lima and M.J. Brunger, J. Chem. Phys. **148**, 124312 (2018).

[19] A. Loupas and J.D. Gorfinkiel, Phys. Chem. Chem. Phys. **19**, 18252–18261 (2017). doi:10.1039/C7CP02916K

[20] M. Vinodkumar, H. Bhutadia, C. Limbachiya and K.N. Joshipura, Int. J. Mass Spectrom. **308**, 35–40 (2011). doi:10.1016/j.ijms.2011.07.017
[21] M. Vinodkumar, C. Limbachiya, A. Barot and N. Mason, Phys. Rev. A. **87**, 012702 (2013). doi:10.1103/PhysRevA.87.012702
[22] K.N. Joshipura, M. Vinodkumar, C.G. Limbachiya and B.K. Antony, Phys. Rev. A. **69**, 022705 (2004). doi:10.1103/PhysRevA.69.022705
[23] D. Chauhan and C. Limbachiya, Radiat. Phys. and Chem. **207**, 110802 (2023). doi:10.1016/j.radphyschem.2023.110802
[24] H.L. Cox and R.A. Bonham, J. Chem. Phys. **47**, 8 (1967).
[25] S. Hara, J. Phys. Soc. Jpn. **22**, 3 (1967). doi:10.1143/JPSJ.22.710
[26] G. Staszewska, D.W. Schwenke, D. Thirumalai and D.G. Truhlar, Phys. Rev. A. **28**, 2740–2751 (1983). doi:10.1103/PhysRevA.28.2740
[27] K.N. Joshipura, B.G. Vaishnav and C.G. Limbachiya, Pramana- J. Phys. **66**, 403–414 (2006). doi:10.1007/BF02704393
[28] C. Limbachiya, M. Vinodkumar, M. Swadia and A. Barot, Mol. Phys. **112**, 101–106 (2014). doi:10.1080/00268976.2013.802038
[29] H. Yadav, M. Vinodkumar, C. Limbachiya and P.C. Vinodkumar, Mol. Phys. **115**, 952–961 (2017). doi:10.1080/00268976.2017.1293306
[30] M. Vinodkumar, C. Limbachiya, H. Desai and P.C. Vinodkumar, Phys. Rev. A. **89**, 062715 (2014). doi:10.1103/PhysRevA.89.062715
[31] M.R. Chowdhury, D. Chauhan, C.G. Limbachiya, K. Tokési, C. Champion, P.F. Weck and L.C. Tribedi, J. Phys. B: At., Mol. Opt. Phys. **53**, 235201 (2020). doi:10.1088/1361-6455/abbe2b
[32] D.B. Jones, E. Ali, C.G. Ning, J. Colgan, O. Ing´olfsson, D.H. Madison and M.J. Brunger, J. Chem. Phys. **145**, 164306 (2016). doi:10.1063/1.4965919
[33] H. Nishimura and H. Tawara, J. Phys. B: At., Mol. Opt. Phys. **24**, L363–L366 (1991). doi:10.1088/0953-4075/24/15/002
[34] A. Zecca, G.P. Karwasz and R.S. Brusa, Phys. Rev. A. **45**, 2777 (1992). doi:10.1103/PhysRevA.45.2777.
[35] K.N. Joshipura and M. Vinodkumar, Pramana – J. Phys. **47**, 57 (1996). doi:10.1007/BF02847166
[36] G. García and F. Manero, Chem. Phys. Lett. **280**, 419–422 (1997). doi:10.1016/S0009-2614(97)01184-6
[37] M. Vinodkumar, C. Limbachiya, M. Barot, A. Barot and M. Swadia, Int. J. Mass Spectrom. **360**, 1–7 (2014). doi:10.1016/j.ijms.2013.12.027
[38] Y.K. Kim and M.E. Rudd, Phys. Rev. A. **50**, 3954–3967 (1994). doi:10.1103/PhysRevA.50.3954
[39] G. Garcıa and F. Maneró, Chem. Phys. Lett. **280**, 419–422 (1997). doi:10.1016/S0009-2614(97)01184-6
[40] F. Blanco, L. Ellis-Gibbings and G. García, Chem. Phys. Lett. **645**, 71–75 (2016). doi:10.1016/j.cplett.2015.11.056
[41] A. Jain, J. Chem. Phys. **86**, 1289–1300 (1987). doi:10.1063/1.452218
[42] L.A. Morgan, J. Tennyson and C.J. Gillan, Comput. Phys. Commun. **114**, 120–128 (1998). doi:10.1016/S0010-4655(98)00056-3
[43] K. Takatsuka and V. McKoy, Phys. Rev. A. **24**, 2473–2480 (1981). doi:10.1103/PhysRevA.24.2473
[44] C.W. McCurdy, T.N. Rescigno and B. Schneider, Phys. Rev. A. **36**, 2061–2066 (1987). doi:10.1103/PhysRevA.36.2061
[45] C. Kittel and D.F. Holcomb, *Introduction to Solid State Physics*, 8th ed (John Wiley and Sons Inc, 1967).
[46] P. Atkins and J. de Paula, *Atkins' Physical Chemistry* (Oxford university press (2014).
[47] L. Onsager, J. Am. Chem. Soc. **58**, 1486–1493 (1936). doi:10.1021/ja01299a050
[48] P.W. Harland and C. Vallance, Int. J. Mass Spectrom. Ion Process. **171**, 173–181 (1997). doi:10.1016/S0168-1176(97)00137-7

Radiation Physics and Chemistry 207 (2023) 110802

Contents lists available at ScienceDirect

Radiation Physics and Chemistry

journal homepage: www.elsevier.com/locate/radphyschem

Electron interactions with analogous of DNA/RNA nucleobases: 3-hydroxytetrahydroFuran and α-Tetrahydrofurfuryl alcohol

Dhaval Chauhan, Chetan Limbachiya *

Department of Applied Physics, The M.S. University of Baroda, Vadodara, 390001, India

ARTICLE INFO

Handling Editor: Dr. Chris Chantler

Keywords:
Electron scattering
Radiation-damage
Bio-molecules
Cross sections
Analogue of DNA/RNA nucleobases

ABSTRACT

We report quantitative results for electron induced molecular processes for DNA/RNA nucleobase analogous biomolecules, 3-hydroxytetrahydrofuran ($C_4H_8O_2$, 3hTHF) and α-tetrahydrofurfuryl alcohol ($C_5H_{10}O_2$, THFA), which are similar in structure and functional group to backbone of DNA and RNA. We have employed spherical complex optical potential (SCOP) formalism to compute total elastic (Q_{el}) and inelastic (Q_{inel}) cross sections and used Complex Scattering Potential-ionization contribution (CSP-ic) method to obtain total ionization (Q_{ion}) and summed total excitation ($\sum Q_{exc}$) cross sections. These results obtained for a wide energy range (10 eV - 5 keV) may serve as the input parameters in predicting damage in biomolecular systems induced by secondary electrons caused by primary ionization radiation. We have observed a correlation between maximum Q_{ion} and molecular polarizability volume (α), ionisation energy (IE) and number of valence electrons (N_v). This work includes an attempt to estimate $\sum Q_{exc}$ for these molecules in normal state.

1. Introduction

High-Resolution Electron Energy Loss Spectroscopy (HREELS) is a powerful technique (Bass and Sanche, 1998; Ibach and Mills, 1982) to measure and study absolute cross sections for Low Energy Electrons (LEEs) scattering from bio-molecules (Bouchiha et al., 2006; Boudaiffa et al., 2000). These cross sections are used for dose calculations in radiotherapy for cancer treatment. Radiotherapy is very effective and essential tool in cancer treatment (Kułakowski, 2011). These LEEs induced processes are relevant to many other fields involving high energy ionization radiation (HEIR) (Muñoz et al., 2008), and hence LEEs play an important role. These include Planetary Science (Lu and Sanche, 2001), astrochemistry (Kaiser, 2002), plasma science (Kong et al., 2009), extreme UV photon nanolithography, bio-medical imaging, and radioprotection (Eisenberg et al., 2011), dosimetry for irradiation in space (Sridharan et al., 2015). When HEIR (i.e. β-rays, ϒ-rays, X-rays and others) interact with bio molecules including DNA and its constituents and deposit their energy via biological medium several ions, radicals, secondary electrons (~10^4 electrons per MeV) are produced. By inelastic processes low energy secondary electrons interact with bio-molecules via biological medium. LEEs have the ability to cause cluster DNA/RNA damage through single-strand (SSBs) and double strand (DSBs) breaks, base dilation etc. To understand and predict these damages, Monte Carlo codes(Rogers, 2006) are used in nanoscopic scales which requires a vast number of variables relating to interaction probabilities including cross sections. Since LEEs are most abundant immediate species formed through irradiation it's necessary to comprehend and model their interactions within biological media.

It is challenging to comprehend electron interactions with DNA at low to intermediate energies because of a scarcity of the data and also its ultrafast reaction (10^{-18} to 10^{-15} sec). It is very useful to study the constituents of DNA and analogues of deoxyribose sugar molecules in the gas phase such as α-tetrahydrofurfuryl alcohol (THFA) and 3-hydroxytetrahydrofuran (3hTHF) molecules (Jin et al., 2018; Antic et al., 1999). The gas phase Deoxyribose is predominantly in the pyranose form of a six-membered ring and in order to study specifically the strength of the furanose ring under electron interactions, several analogues, α-tetrahydrofurfuryl alcohol (THFA), 3-hydroxytetrahydrofuran (3hTHF) and tetrahydrofuran (THF) (Limbachiya et al., 2015b) molecules, have been used as corresponding targets.

Our objective of the present study is to provide reliable probabilities for various molecular processes through estimation of inelastic, ionization, elastic, electronic excitation, and total cross sections for electron impact on the analogous molecule of sugar backbone of 2-deoxyribose such as THFA and 3hTHF. The schematic of these molecules are shown in Fig. 1. The literature survey on electron interaction processes

* Corresponding author
E-mail address: cglimbachiya-apphy@msubaroda.ac.in (C. Limbachiya).

https://doi.org/10.1016/j.radphyschem.2023.110802
Received 27 October 2022; Received in revised form 20 December 2022; Accepted 22 January 2023
Available online 1 February 2023

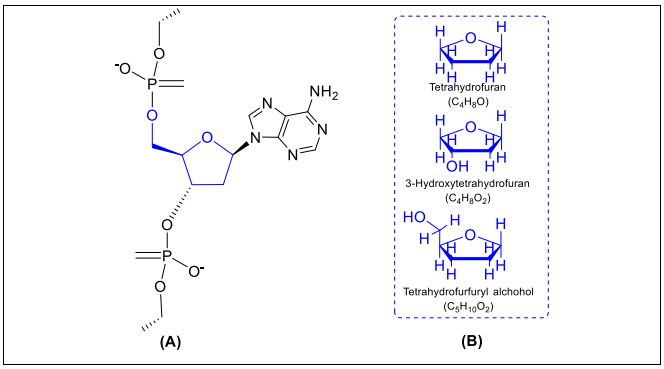

Fig. 1. Schematic diagram of (A) single-stranded deoxyribose backbone containing Sugar, base and phosphate group of DNA (B) deoxyribose analogue molecules.

Table 1
Literature survey

Mol.	Qty.	Methods	E_i (eV)	References
$C_4H_8O_2$	Q_{ion}	Binary-Encounter-Bethe (BEB) [Th.]	IE to 4000	Mozejko and Sanche (2005)
	Q_{inel}	IAM-SCAR [Th.]	5–10,000	Milosavljević et al. (2008)
	Q_{el}	Phase shift analysis approach [Ex; ±20%]	6,10,15,20	Vizcaino et al. (2008)
		IAM-SCAR [Th.]	5–10,000	Milosavljević et al. (2008)
	Q_T	IAM-SCAR [Th.]	5–10,000	Milosavljević et al. (2008)
$C_5H_{10}O_2$	Q_{ion}	Binary-Encounter-Bethe (BEB) [Th.]	IE to 4000	Mozejko and Sanche (2005)
		IAM-SCAR [Th.]	1–1000	Duque et al. (2014)
		Absolute Total Ionization cross section cell [Ex; ±4%]	10–285	Bull et al. (2014)
		Through swarm data [Th.]	10–1000	Stokes et al. (2021)
	Q_{inel}	IAM-SCAR [Th.]	5–5000	Milosavljević et al. (2006)
		IAM-SCAR [Th.]	1–1000	Duque et al. (2014)
	Q_{exc}	Electron monochromator [Ex.; ±30–45%]	20–50	Duque et al. (2014)
	Q_{el}	IAM [Th.]	50–2000	Mozejko and Sanche (2005)
		IAM-SCAR [Th.]	5–5000	Milosavljević et al. (2006)
		IAM-SCAR [Th.]	1–1000	Duque et al. (2014)
		Through swarm data [Th.]	10–1000	Stokes et al. (2021)
	Q_T	IAM and Binary-Encounter-Bethe (BEB) [Th.]	IE-4000	Mozejko and Sanche (2005)
		Linear transmission technique [Ex.]	1–370	Mozejko et al. (2006)
		IAM-SCAR [Th.]	5–5000	Milosavljević et al. (2006)
		IAM-SCAR [Th.]	1–10,000	Zecca et al. (2011)
		IAM-SCAR [Th.] and IAM-SCAR + R[Th.]	1–1000	Duque et al. (2014)
		Through swarm data [Th.]	10–1000	Stokes et al. (2021)

with present molecules is shown in Table 1.

2. Theoretical methodology

We investigate electron driven processes for 3hTHF and THFA, using two different theoretical approaches, SCOP (Jain, 1986; Jain and Baluja, 1992; Limbachiya et al., 2015a; Thakkar et al., 2021; Vinodkumar et al., 2013a, 2013b; Yadav et al., 2017) and CSP-ic (Vinodkumar et al., 2005, 2013b). We briefly present key points of these approaches.

2.1. Spherical complex optical potential formalism

To solve non-relativistic time independent Schrodinger Wave Equation for electrons interaction with the complex and heavier molecular target systems, we require an optical potential, to be written as

$$V_{opt}(E_i, r) = V_{st}(r) + V_{ex}(E_i, r) + V_{pol}(E_i, r) + iV_{abs}(E_i, r) \quad (1)$$

The electron cloud of the molecule defines the static potential (V_{st}) through its charge density $\rho(r)$. The identical incident and target electrons contribute to an exchange potential (V_{ex}). The static and an exchange potential dominate at short distances. For heavier molecules, it is very crucial to get an expression for $\rho(r)$. The static charge density and electrostatic potentials are obtained using improved version of RHF (Roothan-Hartree-Fock) wave functions (Cox and Bonham, 1967).

The strength of the exchange interaction depends on how long the impacting electron stays near the charge cloud. Hara (S. Hara, 1967), presented effective model potential called 'Free electron gas model' which is based on Fermi gas of non-interacting electrons when total wave function is anti-symmetrized in accordance with Pauli exclusion principle.

When dealing with elastic collision of electrons with target, the effect of the distortion on the target system is crucial. The temporary distortion of the target is induced by incident electrons. To model this, V_{pol} is added in an optical potential in equation (1).

In equation (1) the V_{abs}, the transfer of projectile flux into inelastic scattering channels that describe electronic excitation and ionization is represented by the imaginary term called absorption potential. The form of V_{abs} in a. u. is (Joshipura et al., 2004; Staszewska et al., 1983),

$$V_{abs} = -\frac{1}{2}\rho(r)v_{loc}\sigma_{ee} \quad (2)$$

Here, v_{loc} is the velocity of the incoming electrons and σ_{ee} is the mean total cross sections of the incident electron and target electron interaction.

Hence, we have used the dynamic, non-empirical, quasi-free, and Pauli-blocking model potential,

$$V_{abs}(r, E_i) = -\rho(r)\sqrt{\frac{T_{loc}}{2}} \times \left(\frac{8\pi}{10k_F^3 E_i}\right) \times\theta\left(p^2 - k_F^2 - 2\Delta\right)\cdot(A_1 + A_2 + A_3) \quad (3)$$

And the parameters A_1, A_2 and A_3 are defined as,

$$A_1 = 5\frac{k_f^3}{2\Delta};\quad A_2 = \frac{k_f^3\left(5p^2 - 3k_f^2\right)}{\left(p^2 - k_f^2\right)^2};$$
$$A_3 = \frac{2\theta\left(2k_f^2 + 2\Delta - p^2\right)\left(2k_f^2 + 2\Delta - p^2\right)^{5/2}}{\left(p^2 - k_f^2\right)^2}. \quad (4)$$

Where, $Tloc$ = local kinetic energy, $p^2 = 2E_i$ represents the kinetic energy of the incident electron in Hartree, and $k_F = [3\pi^2\,\rho(r)]^{1/3}$ is the Fermi wave vector. Also, $\theta(x)$ is the Heaviside unit step-function which depends on $\rho(r)$, Δ = cut off energy, such that $\theta(x) = 1$ for $x \geq 0$, and is zero otherwise.

Table 2
Target parameters

Target	C_1	C_2	a	R_p	E_P (eV)	Q_{ion}	Q_{inel}
$C_4H_8O_2$ (3-hTHF)	−0.865	−7.110	5.152	0.70	55	12.95	18.64
$C_5H_{10}O_2$ (THFA)	−0.836	−7.508	5.279	0.70	60	16.76	24.00

We have obtained $\rho(r)$ of constituent atoms through Hartree-Fock wave functions (Cox and Bonham, 1967) and have used the group additivity rule (GAR) (Vinodkumar et al., 2011, 2013a) to construct the total charge density which is fed to construct the optical potential. The electron molecular interaction for such a large target is more complicated as compared to electron-atom interaction. So, we have employed group additivity rule. The complexity is reduced by dividing the target into different groups. To get the total charge density of the target, we add the charge density of different groups.

For various angular moments, the SCOP approach works through the partial wave analysis and computations of complex phase-shifts $\delta_l(k)$, which give the detailed information about the electron-molecular interaction. Starting with the ionization threshold of the target only few (<10) phase shifts are significant, but when the energy increases more phase shifts are obtained for the convergence.

The scattering matrix is denoted as,

$$S_l(k) = exp[2i(Re\delta_l + iIm\delta_l)] \tag{5}$$

"Inelasticity" $\eta_l = \exp(-2\mathrm{Im}\delta_l)$ accounts for all possible inelastic effects within the spherical approximation that leads to inelastic cross-section, Q_{inel} (E_i).

2.2. Complex Scattering Potential-ionization contribution

Q_{inel} (E_i) is partitioned as follows,

$$Q_{inel}(E_i) = \sum Q_{exc}(E_i) + Q_{ion}(E_i) \tag{6}$$

First part of above equation (6) is excitation cross sections $\sum Q_{exc}$, which comes from discrete electronics dipole transition and second part consist of all allowed ionization processes.

The CSP-ic formalism is a semiempirical procedure developed by us to compute Q_{ion} from Q_{inel} through the dynamic ratio (Joshipura et al., 2006; Limbachiya et al., 2014).

We define a dynamic ratio,

$$R(E_i) = \frac{Q_{ion}(E_i)}{Q_{inel}(E_i)} \tag{7}$$

With $U = \frac{E_i}{I}$

$$R(E_i) = 1 - C_1\left(\frac{C_2}{U+a} + \frac{lnU}{U}\right) \tag{8}$$

Here, 'C_1', 'C_2' and 'a' are constants.

$$R(E_i) = \begin{cases} = 0 & for\ E_i \le I \\ = R_p & for\ E_i = E_p \\ \cong 1 & for\ E_i \gg E_p \end{cases} \tag{9}$$

Where E_P refers for the incident energy at which the computed Q_{inel} reaches maximum. R_P represents the value of ratio $R(E_i)$ at $E_i = E_P$. The value of R_P is close to 0.7–0.8 as we observed experimentally and theoretically for most stable molecules e.g. CH_4 (Joshipura et al., 2004), H_2O (Vinodkumar et al., 2003), N_2 (Chowdhury et al., 2020) etc. and for most complex targets such as bio-molecules (Vinodkumar et al., 2011) and perfluoroketones (Thakkar et al., 2021). For calculating the Q_{ion} from Q_{inel} we need R as a continuous function of energy E_i > IE. The values of target parameters 'C_1' 'C_2' and 'a' for the present molecules are shown in Table 2. The detailed procedure for obtaining the target parameters is given in previous paper (Joshipura et al., 2004).

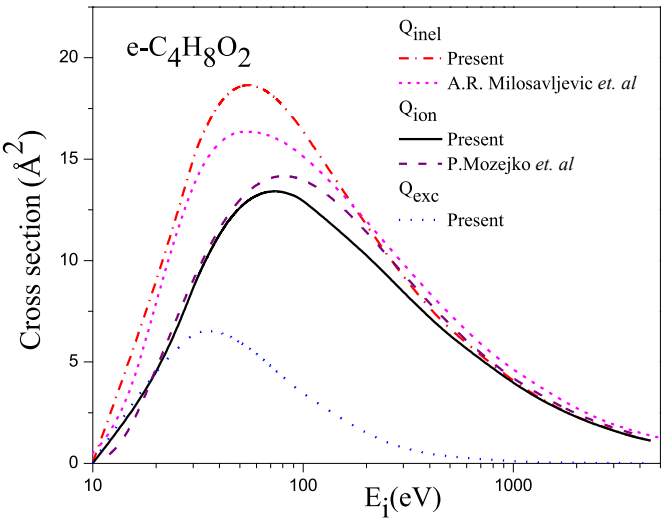

Fig. 2. Cross section for e−3hTHF collision
[Q_{inel}: dash dot line-Present, short dash line- (Milosavljević et al., 2008), Q_{ion}: solid line- Present, dash line- (Mozejko and Sanche, 2005), Q_{exc}: dot line- Present.].

Table 3
Cross sections data (Å^2)

Target	$C_4H_8O_2$			$C_5H_{10}O_2$		
E_i (eV)	Q_{ion}	Q_{el}	Q_T	Q_{ion}	Q_{el}	Q_T
10	0.00	69.50	69.54	0.00	92.61	92.66
20	4.03	46.15	54.62	4.67	62.11	72.56
30	8.64	33.31	48.33	10.36	44.89	63.36
40	11.26	26.22	44.31	13.85	35.08	57.30
50	12.59	21.75	41.04	15.81	28.94	52.62
60	13.19	18.82	38.39	16.84	24.93	48.94
70	13.40	16.57	35.94	17.29	21.83	45.56
80	13.37	14.93	33.88	17.39	19.71	42.86
90	13.22	13.50	31.92	17.30	17.88	40.31
100	12.99	12.50	30.30	17.05	16.64	38.29
200	10.32	7.46	20.29	13.65	10.10	25.60
300	8.44	5.41	15.50	11.17	7.28	19.44
400	7.18	4.29	12.65	9.46	5.78	15.84
500	6.26	3.53	10.71	8.22	4.77	13.40
1000	3.90	1.96	6.25	5.03	2.62	7.76
1500	2.86	1.37	4.47	3.65	1.84	5.54
2000	2.27	1.06	3.50	2.88	1.43	4.34
2500	1.88	0.88	2.90	2.38	1.18	3.58
3000	1.61	0.75	2.47	2.02	1.01	3.04
3500	1.39	0.67	2.16	1.77	0.89	2.66
4000	1.23	0.60	1.92	1.55	0.79	2.35
4500	1.11	0.55	1.74	1.40	0.73	2.13
5000	1.00	0.51	1.59	1.27	0.68	1.95

Considering the approximation involved in the theory it is difficult to estimate accuracy in a meaningful way. However, with nearly spherical targets such as CH_4, SiH_4 etc. our results usually fall within the experimentally quoted uncertainty (Limbachiya et al., 2015b; Vinodkumar et al., 2011; Joshipura et al., 2004). But for complex and big targets such as THFA and 3-hTHF the uncertainty is expected to be larger.

3. Results & discussion

In this section we describe the present results and compare them with available theoretical and experimental results.

In Fig. 2, we illustrate present Q_{inel}, Q_{ion}, and $\sum Q_{exc}$ for e-$C_4H_8O_2$ molecule. The cross-sections data are tabulated in Table 3. Here, we compare present Q_{inel} with available theoretical data (Milosavljević

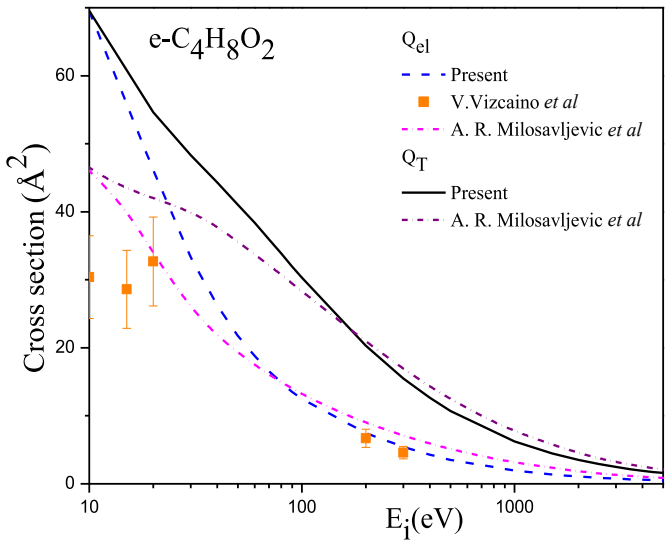

Fig. 3. Cross section for e−3hTHF collision.
[Q_{el}: Short dot dash - Present, short dot dash - (Milosavljević et al., 2008), Full Square- (Exp.) (Vizcaino et al., 2008), Q_T: solid line-Present, short dot dash-(Milosavljević et al., 2008)].

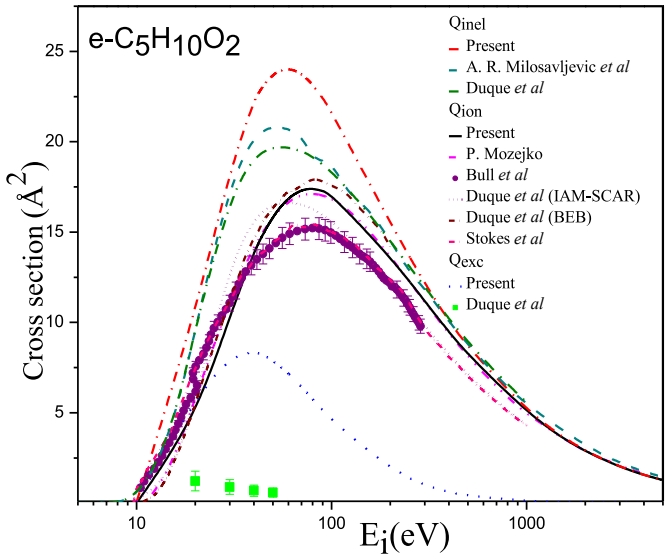

Fig. 4. Cross section for e-THFA collision.
[Q_{inel}: dash dot line-Present, dash line- (Milosavljević et al., 2006), dash dot line- (Duque et al., 2014)-Q_{ion}: Red Solid line- Present, dash dot dot line-(-Mozejko and Sanche, 2005), Dark pink solid line (Stokes et al., 2021), short dash dot (BEB) and short dot (IAM-SCAR) line- (Duque et al., 2014), Circle –(Bull et al., 2014), Q_{exc}: dot line- Present, square- (Duque et al., 2014).

et al., 2008). They have used IAM-SCAR method for 5 eV to 10 Kev. It's seen that present inelastic cross sections overestimate the IAM-SCAR result in the peak region. However, they (Milosavljević et al., 2008) show good accord at lower energies and beyond 200 eV. We show the Q_{ion} with the same energy range and compare with (Mozejko and Sanche, 2005). It gives good agreement with the BEB method proposed by (Mozejko and Sanche, 2005). To our knowledge, there is no direct experimental or theoretical data available to compare the present excitation cross sections ($\sum Q_{exc}$).

Our absolute elastic cross sections (Q_{el}) and total cross sections (Q_T) data for e-$C_4H_8O_2$ scattering are shown in Fig. 3. Present Q_{el} is compared with available experimental and theoretical data. Experimentally, an integral elastic cross sections has been measured by (Vizcaino et al.,

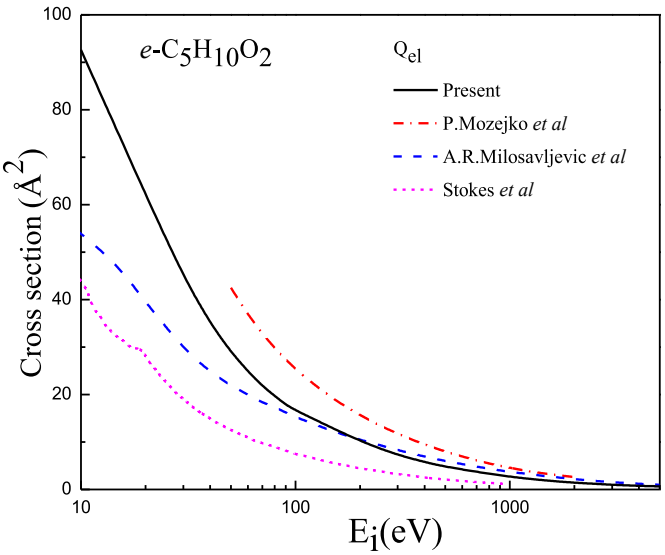

Fig. 5. Cross section for e-THFA collision.
[Q_T: solid Line-Present, dash dot line-(Mozejko and Sanche, 2005), dash line-(Milosavljević et al., 2008), short dash line- (Stokes et al., 2021).

2008) using a phase-shift analysis approach within certain energy 10,15, and 20 eV. For energy threshold to 100 eV, present Q_{el} is overestimated with available experimental data (Vizcaino et al., 2008) and for intermediate energy (200 eV & 300 eV), they show good agreement with the available experimental data.

Present Q_{el} and Q_T are matching well with theoretical data of (Milosavljević et al., 2008), they were obtained by the SCAR (Screen Corrected Additivity Rule) method and followed the same trend for intermediate energy to 5 keV.

In Fig. 4 we have presented Q_{inel}, Q_{ion}, and Q_{exc} for e-$C_5H_{10}O_2$ along with theoretical and experimental comparisons. The upper curve with a black solid line called Q_{inel}, which is shown in Fig. 4, contains all the present electronic excitation (Q_{exc}) and ionization (Q_{ion}) cross-sections. Present Q_{inel} data are compared with available theoretical data of (Duque et al., 2014) and (Milosavljević et al., 2006) [Excitation + Neutral dissociation + Ionization] and found good agreement with IAM-SCAR obtained by (Duque et al., 2014) and (Milosavljević et al., 2006) at an energy between 200 eV and -5 keV. Present Q_{ion} is in reasonably good accord with semi-classical (BEB) formalism by (Mozejko and Sanche, 2005). The ionization cross sections predicted by the IAM-SCAR model (Duque et al., 2014) is quite lower than present Q_{ion}. Experimentally, Q_{ion} data were measured using the absolute total ionization cross sections cell by (Bull et al., 2014) (under ±4% uncertainty). The data of (Bull et al., 2014) agrees quite well with the BEB results in terms of shape and position of the maximum cross sections, while being generally lower in magnitude compared to the theoretical results. Fig. 4 compares present electronic excitation cross sections data for e-THFA with experimental integral cross sections (ICS) data of (Duque et al., 2014). This author identified five Rydberg electronic-state bands reported Band 1 + 2, Band 3, and Band 4 + 5 with an energy range of 20, 30, 40, and 50 eV, which monotonically decreased with increased energy. Here, we compare present $\sum Q_{exc}$ with the sum of all Rydberg electronic-state with the stated uncertainty of 24%–34%. It underestimates with the present results.

Present total elastic cross sections (Q_{el}) values for e-THFA are reported in Table 3 and the graph is plotted in Fig. 5 with the available theoretical data of (Mozejko and Sanche, 2005), (Milosavljević et al., 2008) and (Stokes et al., 2021). At 10–90 eV, present data overestimates the data obtained through IAM-SCAR method (Milosavljević et al., 2008) and Neural network-based swarm data (Stokes et al., 2021). Present data gives good agreement with IAM-SCAR results

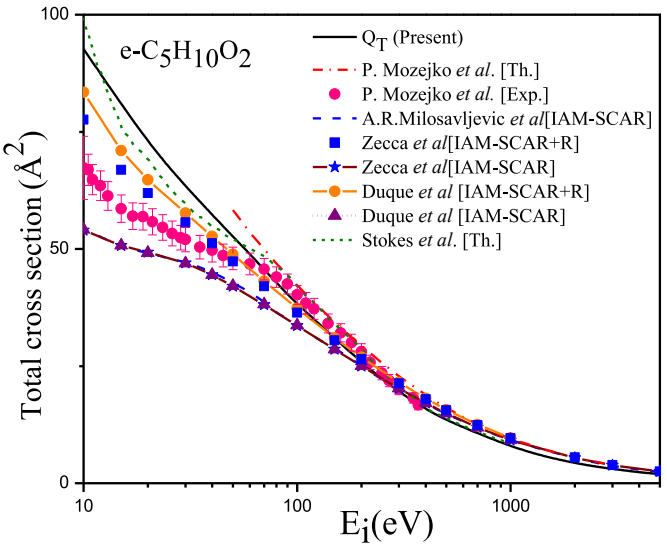

Fig. 6. Total cross section for e-$C_5H_{10}O_2$ collision.
[Q_T - solid line-Present, dash line- (Milosavljević et al., 2008), dash dot Line-(Mozejko and Sanche, 2005), circle- (Mozejko et al., 2006), Square-(Zecca et al., 2011), Short dash line - (Stokes et al., 2021), circle + line (IAM-SCAR + R) (Duque et al., 2014), short dash line + triangle -IAM-SCAR (Duque et al., 2014).

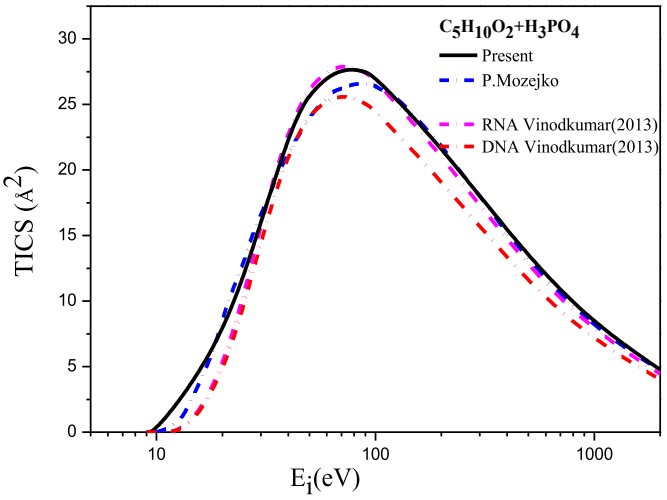

Fig. 7. Comparison of total ionization cross sections (TICS) of ($C_5H_{10}O_2$+H_3PO_4) and DNA, RNA backbone (Vinodkumar et al., 2013b).

(Milosavljević et al., 2008) beyond 100 eV and data of (Stokes et al., 2021) beyond 500 eV.

Present total cross sections, Q_T data for e-THFA are shown in Fig. 6. The experimental result of (Mozejko et al., 2006) and theoretical results of (Mozejko and Sanche, 2005), (Milosavljević et al., 2008), (Duque et al., 2014), (Stokes et al., 2021), (Zecca et al., 2011), are in excellent agreement with the present data beyond ~70–80 eV. Below ~70 eV the present data overestimates the experimental results of (Mozejko et al., 2006) within ~5–6% uncertainty. They also reproduced the TCS data by adding the elastic and ionization cross sections earlier calculated by (Mozejko and Sanche, 2005) using IAM and BEB methods respectively. It can be observed from the figure that the present results underestimate this reproduced data. This deviation is seen due to the fact that the theory which was used by them is not as reliable as to produce the data at lower energy (Mozejko and Sanche, 2005). Present Q_T, overestimates the available theoretical data obtain through IAM-SCAR method (Duque et al., 2014; Milosavljević et al., 2006), which includes all elastic and

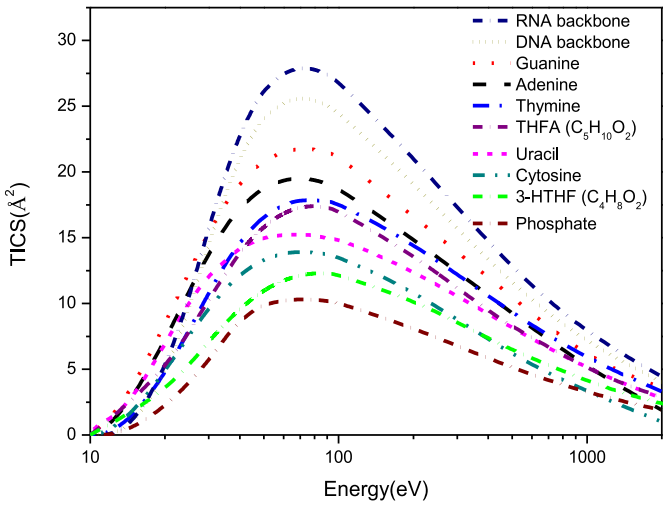

Fig. 8. Comparison of the e-TICS for RNA backbone (Vinodkumar et al., 2013b), DNA backbone (Vinodkumar et al., 2013b), guanine (Vinodkumar et al., 2013b), adenine (Vinodkumar et al., 2013b), thymine (Vinodkumar et al., 2013b), $C_5H_{10}O_2$ (THFA), uracil (Vinodkumar et al., 2013b), cytosine (Vinodkumar et al., 2013b), $C_4H_8O_2$ (3hTHF), and phosphoric acid molecules.

inelastic effect except DEA, rotational, vibrational excitation. The TCS computed by IAM-SCAR + R(Zecca et al., 2011). is in good accord, which includes rotational excitation but excludes DEA and vibrational excitations. The TCS data of (Duque et al., 2014) acquired by IAMSCAR + R method matches reasonably good with the present TCS data. It can be observed that the shape followed by their data is similar as that of the present results. The grand TCS data of (Stokes et al., 2021) is in good agreement with present result. To compute grand TCS (Stokes et al., 2021), first corrected the forward-scattering effect in experimental data of (Mozejko et al., 2006), by enlarging the cross sections magnitude at lower energies. At intermediate to high energy, they chose theoretical TCS data of (Duque et al., 2014) with their proposed DEA and vibrational excitation cross sections. Then, they scaled experimental data of (Mozejko et al., 2006) to best fit this approximation.

It has been shown that in some cases and within some approximations the electron-impact ionization cross sections for polyatomic molecules can be calculated by taking into account only basic atomic properties. From this assumption, we approximate ionization cross sections for the sugar-phosphate backbone of DNA/RNA by adding present results of ionization cross sections for $C_5H_{10}O_2$ and that of H_3PO_4, taken from (Vinodkumar et al., 2013b). In Fig. 7 the resulting values are compared with those of calculated by (Vinodkumar et al., 2013b) for the sugar-phosphate unit of DNA and RNA. Present $C_5H_{10}O_2$ + H_3PO_4 (Vinodkumar et al., 2013b) gives good accord with DNA and RNA backbone and (Mozejko and Sanche, 2005).

Fig. 8 compares total Q_{ion} data of DNA, RNA bases and phosphoric acid (Vinodkumar et al., 2013b) with the present studied molecular targets 3hTHF and THFA. In general, over the whole energy range examined (IE-2000 eV), the amplitude of the ionization cross sections follows the pattern, which is similar to (Mozejko and Sanche, 2005) and (Champion, 2013).

$$Q_{RNA} > Q_{DNA} > Q_{Guanine} > Q_{Adenine} > Q_{Thymine} > Q_{C5H10O2} > Q_{Uracil} > Q_{Cytosine} > Q_{C4H8O2} > Q_{Phosphoric\ acid}$$

The size of the molecular charge cloud is defined through the number of electrons of the molecule. When the number electrons of the molecule increases, the peak of the ionization cross sections increases, which is clearly reflected in Fig. 8.

Table 4
Proparties of target molecules and computed data

Target	IE (eV')	Polarizability (α)	Number of valance electrons (N_V)	Energy at peak of ionization (eV)	Peak Q_{ion} (Å^2)	Energy at peak of excitation (eV)	Peak $\sum Q_{exc}$ (Å^2)
C_4H_8O (Swadia et al., 2017)	9.38	8.00	30	76	12.50	–	–
$C_4H_8O_2$	9.51	8.60	36	74	13.41	35	6.518
$C_5H_{10}O_2$	9.47	10.40	42	80	17.394	40	8.362

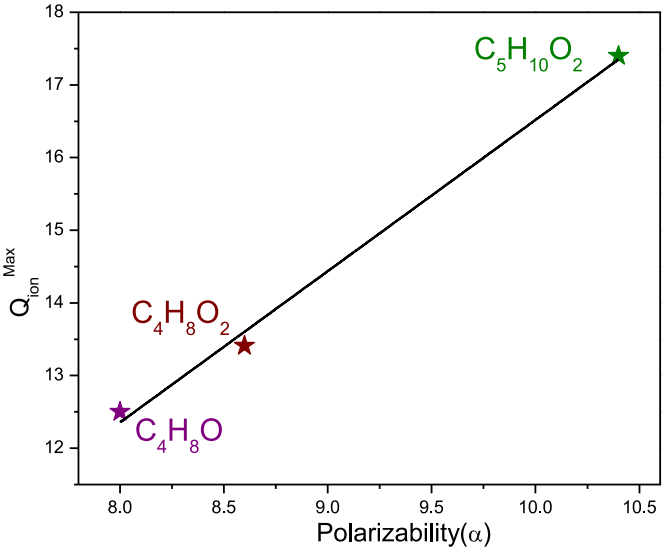

Fig. 9. correlation between Q_{ion}^{Max} and dipole polarizability (α).

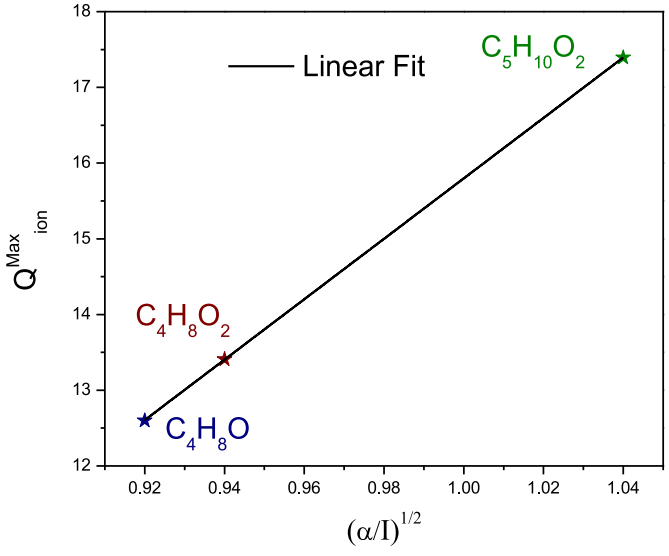

Fig. 10. correlation between Q_{ion}^{Max} and $\sqrt{\alpha/I}$

4. Correlation study and analysis of computed data

It is known that atomic and molecule characteristics like the ionization energy (IE), the intensity of the van der Waals contact, or the molecular volume are connected to the polarizability. The polarizability volume is proportional to the molecule's size as viewed by the incoming electron. Significant research of (Harland and Vallance, 1997) on such correlations has been conducted by atomic and molecular systems. When there is no comparison provided by any group then the correlation is a very useful feature to evaluate the consistency and reliability of the

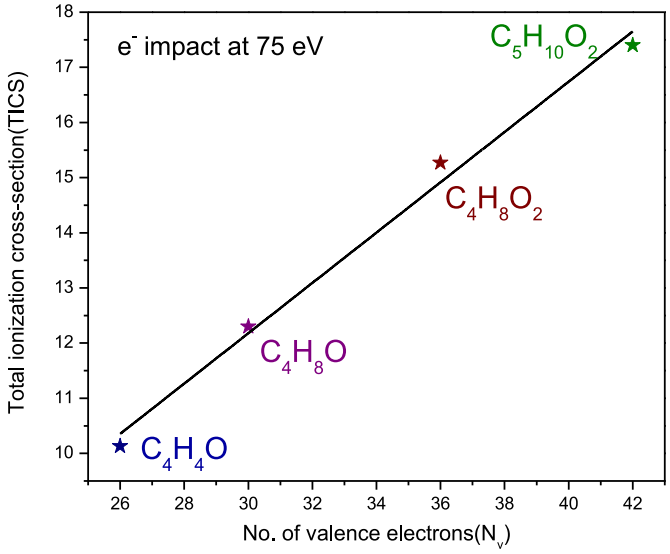

Fig. 11. TICS plotted vs No. of valence electron (N_V) for various Molecular target obtained at 75 eV for electron impact.

Table 5
Analytical relations for Q_{ion}^{Max}

	Linear fit	Linear fit passing through origin
Q_{ion}^{Max} as a function of α	Q = 2.09(α)-4.30	Q = 1.62(α)
Q_{ion}^{Max} as a function of $\sqrt{\alpha/I}$	Q = 39.91 ($\sqrt{\alpha/I}$)-24.11	Q = 14($\sqrt{\alpha/I}$)
Q_{ion}^{Max} as a function of N_V	Q = 0.45(N_V)-1.51	Q = 0.41(N_V)

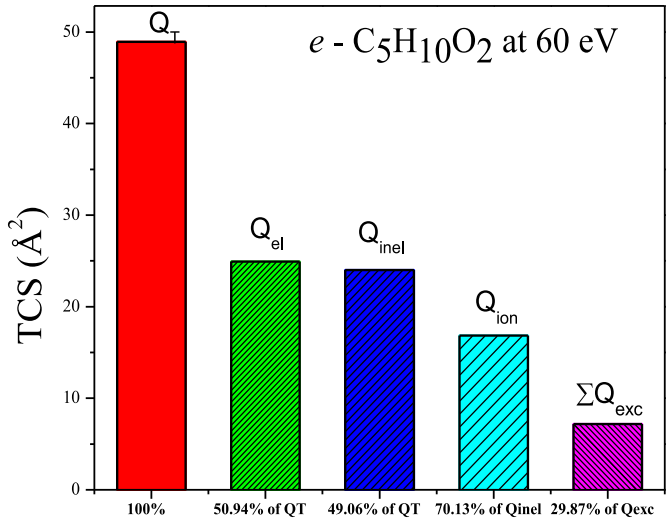

Fig. 12. Relative cross sections.

cross sections data. If we know either peak Q_{ion}^{Max} or dipole polarizability (α), this correlation is useful to estimate any of them roughly.

For the sake of consistency of current studied molecules and tetrahydrofuran (THF), we took Q_{ion}^{Max} data from (Swadia et al., 2017), presented in Table 4 to check linear correlation. In Fig. 9, we can see this correlation between maximum Q_{ion} and dipole polarizability(α). Slightly spread of the points has to be attributed to the uncertainty in the published polarizability and discrepancies in different group additivity rules used for calculating cross sections data of (Karwasz et al., 1999).

Further, we see the correlation between square root of the ratio of polarizability and ionization potential $\sqrt{\alpha/I}$ in Fig. 10. This feature allows to predict polarizability of a particular molecular target for which polarizability is not available in literature. Although accuracy of this procedure can be limited as it has been observed only for a very narrow range of values $\sqrt{\alpha/I}$.

Furthermore, we can see the scalability of total Q_{ion} is well proportional to number of valence electrons (N_V) of various target molecules at different electron impact energy range. In Fig. 11 we show Q_{ion} vs number of valence electrons (N_V) at 75 eV. In Table 5, we display the analytical equations for all these correlations for Q_{ion}^{Max} with α, IE and N_v obtained through linear fit. These equations readily predict the peak of Q_{ion} for targets of similar size and structures.

Fig. 12 exhibits a variety of total cross sections for e-THFA scattering at 60 eV peak of Q_{inel} computed using a single quantum mechanical theory. Since Total cross sections (Q_T) contain all scattering processes, they set the upper bound for all cross sections. The elastic cross sections (Q_{el}) is ~50.94% of Q_T and the inelastic cross sections (Q_{inel}) is ~49.06% of Q_T. The contribution from the Q_{inel} and Q_{el} cross-sections is nearly equal at the maxima of the inelastic cross sections (Charles, 1983). Due to the spherical approximation and GAR involved in present calculations the contribution of Q_{inel} to Q_T is not 50%. The contribution of the Q_{ion} is ~70.13% and Q_{exc} is ~29.87% of Q_{inel} is found as expected.

5. Conclusion

In this paper we carried out theoretical study of electron interaction (~10 eV - 5 keV) with biomolecular target: 3hTHF and THFA. For that we employed SCOP formalism along with CSP-iC formalism to compute Q_{el}, Q_T, Q_{inel}, $\sum Q_{exc}$, and Q_{ion} cross sections data shown in (Figs. 2–6). This is the first attempt to compute $\sum Q_{exc}$ for these molecules in normal state. In this study we have found the following empirical correlations: (1) The Q_{ion} (Figure: 8) rises as the geometric structure and the number of electrons (N) of molecules increase. (2) Peak of Q_{ion} is significantly influenced by the target's ionization threshold. (3) present study (figure: 9 & 10) has confirmed correlation between Q_{ion}^{Max} and dipole polarizability (α) of present molecules, also Q_{ion}^{Max} linearly dependent with $\sqrt{\alpha/I_p}$. (4) The results of this approach are in good accord with theoretical and experimental for the molecules discussed in this study. Present study enhances our confidence and also convinced for different methods that we have used to calculate cross sections for present complex biological molecules with adequate speed and accuracy.

Declaration of competing interest

The authors declare that they have no known competing financial interests or personal relationships that could have appeared to influence the work reported in this paper.

Data availability

Data will be made available on request.

References

Antic, D., Parenteau, L., Lepage, M., Sanche, L., 1999. Low-energy electron damage to condensed-phase deoxyribose analogues investigated by electron stimulated desorption of H- and electron energy Loss spectroscopy. J. Phys. Chem. B 103, 6611–6619. https://doi.org/10.1021/jp990686l.

Bass, A.D., Sanche, L., 1998. Absolute and effective cross-sections for low-energy electron-scattering processes within condensed matter. Radiat. Environ. Biophys. 37, 243–257. https://doi.org/10.1007/s004110050125.

Bouchiha, D., Gorfinkiel, J.D., Caron, L.G., Sanche, L., 2006. Low-energy electron collisions with tetrahydrofuran. J. Phys. B Atom. Mol. Opt. Phys. 39, 975. https://doi.org/10.1088/0953-4075/39/4/021.

Boudaiffa, B., Cloutier, P., Hunting, D., Huels, M.A., Sanche, L., 2000. Resonant Formation of DNA strand breaks by low-energy (3 to 20 eV) electrons. Science 287, 1658–1660.

Bull, J.N., Lee, J.W.L., Vallance, C., 2014. Absolute electron total ionization cross-sections: molecular analogues of DNA and RNA nucleobase and sugar constituents. Phys. Chem. Chem. Phys. 16, 10743–10752. https://doi.org/10.1039/c4cp00490f.

Champion, C., 2013. Quantum-mechanical predictions of electron-induced ionization cross sections of DNA components. J. Chem. Phys. 138, 184306 https://doi.org/10.1063/1.4802962.

Charles, Joachain, 1983. Quantum Collision Theory. North-Holland), Amsterdam.

Chowdhury, M.R., Chauhan, D., Limbachiya, C.G., Tokési, K., Champion, C., Weck, P.F., Tribedi, L.C., 2020. Double differential distributions of e-emission in ionization of N2by 3, 4 and 5 keV electron impact. J. Phys. B Atom. Mol. Opt. Phys. 53, 235201 https://doi.org/10.1088/1361-6455/abbe2b.

Cox, H.L., Bonham, R.A., 1967. J. Chem. Phys. 47, 8.

Duque, H.V., Chiari, L., Jones, D.B., Thorn, P.A., Pettifer, Z., da Silva, G.B., Limão-Vieira, P., Duflot, D., Hubin-Franskin, M.J., Delwiche, J., Blanco, F., García, G., Lopes, M.C.A., Ratnavelu, K., White, R.D., Brunger, M.J., 2014. Cross sections for electron scattering from α-tetrahydrofurfuryl alcohol. Chem. Phys. Lett. 608, 161–166. https://doi.org/10.1016/j.cplett.2014.05.087.

Eisenberg, M.J., Afilalo, J., Lawler, P.R., Abrahamowicz, M., Richard, H., Pilote, L., 2011. Cancer risk related to low-dose ionizing radiation from cardiac imaging in patients after acute myocardial infarction. CMAJ (Can. Med. Assoc. J.) 183, 430–436. https://doi.org/10.1503/cmaj.100463.

Hara, S., 1967. hara1967. J. Phys. Soc. Jpn. 22, 3.

Harland, P.W., Vallance, C., 1997. Ionization cross-sections and ionization efficiency curves from polarizability volumes and ionization potentials. Int. J. Mass Spectrom. Ion Process. 171, 173–181.

Ibach, H., Mills, D.L., 1982. Electron energy Loss spectroscopy and surface vibrations, electron energy Loss spectroscopy and surface vibrations. https://doi.org/10.1016/c2013-0-10894-x.

Jain, A., 1986. Total (elastic + absorption) cross sections fore- CH_4 collisions in a spherical model at 0.10–500 eV. Phys. Rev. A 34, 3707. https://doi.org/10.1103/PhysRevA.34.3707.

Jain, A., Baluja, K.L., 1992. A. Jain, K.L. Baluja, Total (elastic plus inelastic) cross sections for electron scattering from diatomic and polyatomic molecules at 10–5000 eV: H_2 , Li_2 , HF, CH_4 , N_2 , CO, C_2 H_2 , HCN, O_2 , HCl, H_2S, PH_3 , SiH_4 , and CO_2. Phys. Rev. A 45, 202. https://doi.org/10.1103/PhysRevA.45.202.

Jin, S., Hu, Y., Wang, P., Zhan, H., Lu, Q., Liu, F., Sheng, L., 2018. Hydrogen bonding and dominant conformations of hydrated sugar analogue complexes using tetrahydrofurfuryl alcohol as the model sugar molecule. Phys. Chem. Chem. Phys. 20, 7351–7360. https://doi.org/10.1039/c7cp07935d.

Joshipura, K.N., Vaishnav, B.G., Limbachiya, C.G., 2006. Ionization and excitation of some atomic targets and metal oxides by electron impact. Pramana- J. Phys. 66, 403–414.

Joshipura, K.N., Vinodkumar, M., Limbachiya, C.G., Antony, B.K., 2004. Calculated total cross sections of electron-impact ionization and excitations in tetrahedral (XY4) and SF6 molecules. Phys. Rev. 69, 022705 https://doi.org/10.1103/PhysRevA.69.022705.

Kaiser, R.I., 2002. Experimental investigation on the formation of carbon-bearing molecules in the interstellar medium via neutral-neutral reactions. Chem. Rev. 102, 1309–1358. https://doi.org/10.1021/cr970004v.

Karwasz, G.P., Brusa, R.S., Piazza, A., Zecca, A., 1999. Total cross sections for electron scattering on chloromethanes: formulation of the additivity rule. Phys. Rev. A 59, 1341–1347.

Kong, M.G., Kroesen, G., Morfill, G., Nosenko, T., Shimizu, T., van Dijk, J., Zimmermann, J.L., 2009. Plasma medicine: an introductory review. New J. Phys. 11 https://doi.org/10.1088/1367-2630/11/11/115012.

Kułakowski, A., 2011. The contribution of Marie Skłodowska-Curie to the development of modern oncology. Anal. Bioanal. Chem. 400, 1583–1586. https://doi.org/10.1007/S00216-011-4712-1/FIGURES/5.

Limbachiya, C., Chaudhari, A., Desai, H., Vinodkumar, M., 2015a. Electron Induced Chemistry of Thioformaldehyde, 5. The Royal Society of Chemistry Advances, pp. 103964–103976. https://doi.org/10.1039/c5ra19662k.

Limbachiya, C., Vinodkumar, M., Swadia, M., Barot, A., 2014. Electron impact total cross section calculations for CH3SH (methanethiol) from threshold to 5 keV. Mol Phys 112, 101–106. https://doi.org/10.1080/00268976.2013.802038.

Limbachiya, C., Vinodkumar, M., Swadia, M., Joshipura, K.N., Mason, N., 2015b. Electron-impact total cross sections for inelastic processes for furan, tetrahydrofuran and 2,5-dimethylfuran. Mol. Phys. 113, 55–62. https://doi.org/10.1080/00268976.2014.943314.

Lu, Q.B., Sanche, L., 2001. Effects of cosmic rays on atmospheric chlorofluorocarbon dissociation and ozone depletion. Phys. Rev. Lett. 87 https://doi.org/10.1103/PhysRevLett.87.078501, 78501-1-78501–4.

Milosavljević, A.R., Blanco, F., Šević, D., García, G., Marinković, B.P., 2006. Elastic scattering of electrons from tetrahydrofurfuryl alcohol. In: European Physical Journal D. Springer, New York, pp. 107–114. https://doi.org/10.1140/epjd/e2006-00138-7.

Milosavljević, A.R., Blanco, F., Maljković, J.B., Šević, D., García, G., Marinković, B.P., 2008. Absolute cross sections for elastic electron scattering from 3-hydroxytetrahydrofuran. New J. Phys. 10 https://doi.org/10.1088/1367-2630/10/10/103005.

Mozejko, P., Sanche, L., 2005. Cross sections for electron scattering from selected components of DNA and RNA. Radiat. Phys. Chem. 73, 77–84. https://doi.org/10.1016/j.radphyschem.2004.10.001.

Mozejko, P., Domaracka, A., Ptasińska-Denga, E., Szmytkowski, C., 2006. Total cross-section measurements for electron collisions with α-tetrahydrofurfuryl alcohol (C5H10O2). Chem. Phys. Lett. 429, 378–381. https://doi.org/10.1016/j.cplett.2006.08.077.

Muñoz, A., Blanco, F., Garcia, G., Thorn, P.A., Brunger, M.J., Sullivan, J.P., Buckman, S. J., 2008. Single electron tracks in water vapour for energies below 100 eV. Int. J. Mass Spectrom. 277, 175–179. https://doi.org/10.1016/j.ijms.2008.04.028.

Rogers, D.W.O., 2006. Fifty years of Monte Carlo simulations for medical physics. Phys. Med. Biol. https://doi.org/10.1088/0031-9155/51/13/R17.

Sridharan, D.M., Chappell, L.J., Whalen, M.K., Cucinotta, F.A., Pluth, J.M., 2015. Defining the biological effectiveness of components of high-LET track structure. Radiat. Res. 184, 105–119. https://doi.org/10.1667/RR13684.1.

Staszewska, G., Schwenke, D.W., Thirumalai, D., Truhlar, D.G., 1983. Quasifree-scattering model for the imaginary part of the optical potential for electron scattering. Phys. Rev. A 28, 2740. https://doi.org/10.1103/PhysRevA.28.2740.

Stokes, P.W., Foster, S.P., Casey, M.J.E., Cocks, D.G., González-Magaña, O., de Urquijo, J., García, G., Brunger, M.J., White, R.D., 2021. An improved set of electron-THFA cross sections refined through a neural network-based analysis of swarm data. https://doi.org/10.1063/5.0043759.

Swadia, M., Bhavsar, R., Thakar, Y., Vinodkumar, M., Limbachiya, C., 2017. Electron-driven processes for furan, tetrahydrofuran and 2, 5-dimethylfuran. Mol. Phys. 115, 2521–2527. https://doi.org/10.1080/00268976.2017.1333645.

Thakkar, N., Swadia, M., Vinodkumar, M., Mason, N., Limbachiya, C., 2021. Electron induced elastic and inelastic processes for perfluoroketone (PFK) molecules. Plasma Sources Sci. Technol. 30, 085008 https://doi.org/10.1088/1361-6595/AC17CA.

Vinodkumar, M., Joshipura, K.N., Limbachiya, C.G., Antony, B.K., 2003. Electron impact ionization of H2O molecule in crystalline ice. Nucl. Instrum. Methods Phys. Res. B 212, 63–66. https://doi.org/10.1016/S0168-583X(03)01480-0.

Vinodkumar, M., Joshipura, K.N., Limbachiya, C.G., Antony, B.K., 2005. Electron impact total and ionization cross-sections for some hydrocarbon molecules and radicals. The European Physical Journal D - Atomic, Molecular, Optical and Plasma Physics 37 (1 37), 67–74. https://doi.org/10.1140/EPJD/E2005-00257-7, 2005.

Vinodkumar, M., Bhutadia, H., Limbachiya, C., Joshipura, K.N., 2011. Electron impact total ionization cross sections for H_2S, PH_3, HCHO and HCOOH. Int. J. Mass Spectrom. 308, 35–40. https://doi.org/10.1016/j.ijms.2011.07.017.

Vinodkumar, M., Limbachiya, C., Barot, A., Mason, N., 2013a. Computation of electron-impact rotationally elastic total cross sections for methanol over an extensive range of impact energy (0.1 - 2000 eV). Phys. Rev. A 87, 012702. https://doi.org/10.1103/PhysRevA.87.012702.

Vinodkumar, M., Limbachiya, C., Barot, M., Swadia, M., Barot, A., 2013b. Electron impact total ionization cross sections for all the components of DNA and RNA molecule. Int. J. Mass Spectrom. 339–340. https://doi.org/10.1016/J.IJMS.2013.01.004, 16–23.

Vizcaino, V., Roberts, J., Sullivan, J.P., Brunger, M.J., Buckman, S.J., Winstead, C., McKoy, V., 2008. Elastic electron scattering from 3-hydroxytetrahydrofuran: experimental and theoretical studies. New J. Phys. 10 https://doi.org/10.1088/1367-2630/10/5/053002.

Yadav, H., Vinodkumar, M., Limbachiya, C., Vinodkumar, P.C., 2017. Scattering of electrons with formyl radical. Mol. Phys. 115, 952–961. https://doi.org/10.1080/00268976.2017.1293306.

Zecca, A., Chiari, L., García, G., Blanco, F., Trainotti, E., Brunger, M.J., 2011. Total cross-sections for positron and electron scattering from α-tetrahydrofurfuryl alcohol. New J. Phys. 13 https://doi.org/10.1088/1367-2630/13/6/063019.

Radiation Physics and Chemistry 214 (2024) 111248

Contents lists available at ScienceDirect

Radiation Physics and Chemistry

journal homepage: www.elsevier.com/locate/radphyschem

Scattering of electrons with aqueous biomaterials

Smruti Parikh [a], Dhaval Chauhan [a], Nirav Thakkar [b], Chetan Limbachiya [a,*]

[a] Department of Applied Physics, The Maharaja Sayajirao University of Baroda, Vadodara, 390001, India
[b] Sheth M. N. Science College, Patan, 384265, India

ARTICLE INFO

Handling Editor: Dr. Chris Chantler

Keywords:
Aqueous DNA compounds
Cross-sections
Dielectric constant
Polarisability

ABSTRACT

The aqueous phase of DNA, which is more realistic phase due to the presence of H-bonds is studied in this work for various molecular processes upon electron impact. We report computed probabilities of various interaction processes taking place during the collision of electrons with DNA molecules, viz., Adenine, Guanine, Cytosine, Thymine and Uracil in their aqueous phase. Modified spherical complex potential approach has been employed for the quantification of various (N+1) elastic and inelastic including ionisation interactions through the cross-sections. Since no study for electron scattering with aqueous DNA is available, we compared our results with condensed phase and also a new approach for estimating the elastic and total cross-sections has been proposed in the present work for larger and complex molecules ($55 < Z < 95$) like the DNA compounds and encouraging results are observed. Correlations of molecular ionisation with dielectric constant and polarisability of the compounds have also been investigated.

1. Introduction

The application of ionising radiation in the field of medicine is extremely common. It is frequently utilised in the medical field as a therapeutic agent and in the field of radio diagnostics as a probe. Ballistic impact was traditionally thought to be the mechanism that was responsible for the majority of the damage that high-energy incident radiation caused to living tissue. However, secondary species that result from primary ionisation are responsible for a significant radiation damage (Boudaïffa et al., 2002). The majority of the energy is deposited by the primary ionising particles once they enter the biological medium through several collision processes, including excitations and ionisations. Large amounts of secondary electrons are released as a result of this significant energy transfer, and these electrons can interact with a variety of biological substances causing the radiation damage. Among all the living tissues, DNA molecules are thought to be most sensitive to radiations. Exposure of DNA species to radiations result in multiple types of DNA damage (Nikjoo et al., 2016) through secondary species including electrons.

As primary as well as secondary species induces the radiation damage, it is essential to model their tracks through a biological medium. This makes it possible to anticipate and comprehend the type, location, and severity of cell damage. The route taken by the primary and secondary particles as they move through the medium is depicted by the charged-particle track structures (Goodhead, 1994). The entire range of interaction between the primary and secondary species at the level of each atom or molecule, is modelled in these aleatory (stochastic) simulations using the cross-section values. Hence, accurate cross-sections are crucial to the validity of these types of simulations.

Till now a lot of cross-sectional data has been reported for the DNA constituents upon electron impact in their gaseous phase (Mozejko and Sanche, 2005; Mokrani et al., 2020; Vinodkumar and Limbachiya, 2013; Rahman and Krishnakumar, 2016; Shafranyosh et al., 2015; Champion, 2013; Bull et al., 2014; Aouina and Chaoui, 2018; van der Burgt et al., 2014; Minaev et al., 2014; Zein et al., 2021). Such cross-sections (CSs) are also available for the condensed phase interaction processes but only for the low energy below 20 eV (Toburen, 1998; Bass and Sanche, 1998). But aqueous phase of the DNA rather than gaseous or condensed phase, presents more realistic picture, as they are always found covered with the water molecules through hydrogen bonding (Khesbak et al., 2011; Helmholtz Association of German Research Centres). This has motivated us to take up the work on electron interactions with aqueous DNA constituents. We have computed the ionisation CSs (Q_{ion}), inelastic CSs (Q_{inel}), elastic CSs (Q_{el}), and total CSs (Q_T) for all the five DNA constituents, viz. Adenine, Guanine, Thymine, Cytosine and Uracil upon electron collisions by considering their aqueous phase. This is the maiden attempt to investigate the electron induced processes for the aqueous DNA constituents for the energies from ionisation threshold of the

* Corresponding author.
E-mail address: cglimbachiya-apphy@msubaroda.ac.in (C. Limbachiya).

https://doi.org/10.1016/j.radphyschem.2023.111248
Received 3 May 2023; Received in revised form 22 August 2023; Accepted 27 August 2023
Available online 1 September 2023

molecules to 5000 eV.

Tan et al. (Tan et al., 2004) have reported the Q_{inel} data for the case of DNA in water using dielectric response theory and Penn's approximation for energy range from 20 to 10,000 eV. Recently, Vera et al. (De Vera et al., 2021) and Tan et al. (Tan et al., 2018) have reported the ionisation CSs data for DNA compounds by considering their condensed phase for impact energies from 1 to 10,000 eV and 10–500 eV, respectively. All of these groups (Tan et al., 2004, 2018; De Vera et al., 2021) have used a method that underlines the concept of dielectric response theory.

Since, to the best of our knowledge no work is available for the aqueous phase of DNA molecules; we have developed a new 2-parameter Semi-empirical method (2p-SEM) for computing the Q_T and Q_{el} for these applied biomaterials.

2. Theoretical methodology

The methodologies involved in the present study for the computations of inelastic and elastic interaction events as a result of electron interactions with the aqueous DNA constituents, have been described in this section.

2.1. Spherical complex optical potential approach (SCOP)

The energy-dependent modified complex potential is precisely treated in partial wave decomposition method (Vinodkumar et al., 2013a, 2013b, 2014a; Limbachiya et al., 2011, 2015) with respect to the DNA constituents in their aqueous phase in order to determine the CSs. In essence, a local version of the absorption potential (V_{ab}) (Staszewska et al., 1984) have been modified by keeping $\Delta = IE + E_{gap}$, due to the fact that when dealing with the aqueous or condensed phase, ionisation only occur when the projectile energy exceeds the ionisation energy, IE by an amount equal to the energy-band gap, E_{gap} (Pandya et al., 2012; Joshipura et al., 2007). Table 2 shows the target properties used for the present calculations.

This modified potential is given by,

$$V_{abs}(r, E_i) = -\rho(r)\sqrt{\frac{T_{loc}}{2}}\left(\frac{8\pi}{10{k_F}^3 E_i}\right)\Theta\left(p^2 - {k_F}^2 - 2\Delta\right) \times (A_1 + A_2 + A_3) \tag{1}$$

where, k_F is the appropriate fermi vector, and p is the incident momentum. The A_1, A_2 and A_3 are dynamic parameters, details of which already have been mentioned in our previous articles (Limbachiya et al., 2014, 2015; Vinodkumar et al., 2006, 2011; Joshipura et al., 2006). The local kinetic energy of the incident electron is, $T_{loc} = E_i - (V_s + V_e + V_p)$. Here, V_s is calculated using the Hartree-Fock wave functions (Cox and Bonham, 1967), is used to measure the undeformed molecule charge cloud. The exchange effect that took place between the target electrons and the incoming electrons, is taken into account through V_e (Hara, 1967). The charge cloud of the target system temporarily deforms in the response of the incoming electron. This polarisation effect has been considered through V_p (Zhang et al., 1992).

Since all of these potentials are constructed using the charge density of the molecule under study, it is crucial to represent it. The parameterized charge densities of constituent atomic systems to generate the total $\rho(r)$ of the target molecules have been introduced, which is input to the complex potential (Parikh et al., 2023; Parikh and Limbachiya, 2023).

The inelastic and elastic CSs, are computed by determining the scattering complex phase shifts (δ_l) (Parikh and Limbachiya, 2023). This Q_{inel} totals all the possible ionisations and electronic excitations:

$$Q_{inel} = Q_{ion} + \Sigma Q_{exc} \tag{2}$$

where, Q_{ion} stands for the total ionisation CSs for all permittable ionisations of the molecule and $\sum Q_{exc}$ represents all permitted electronic transitions that are influenced by low-lying states, which is less important than Q_{ion} for the incident energy higher than IE, hence,

$$Q_{inel} \geq Q_{ion} \tag{3}$$

2.2. Complex scattering potential-ionisation contribution (CSP-ic) method

Above inequality (equation (3)) is the cornerstone of this CSP-ic approach (Limbachiya et al., 2015; Vinodkumar et al., 2006; Thakkar et al., 2021) and implies to the ratio,

$$R(E_i) = \frac{Q_{ion}}{Q_{inel}} \tag{4}$$

The boundary conditions of which are as follows,

$$R(E_i) = \begin{cases} 0, for\ E_i \leq \Delta \\ R_P, for\ E_i = E_P \\ \sim 1, for\ E_i \gg \Delta \end{cases} \tag{5}$$

The ionisation events which are dominant part in the inelastic channel, begins to occur at the target's ionisation threshold, which is equal to Δ in this aqueous case. The inelastic CSs attains its peak at energy E_P. However, at high incident energy, ionisation dominates, and excitation CSs drastically drop, as seen by the final condition in equation (5). According to both experimental and theoretical results (Parikh et al., 2023; Swadia et al., 2017; Turner et al., 1982) of the stable targets, the value R_P will be within 0.7–0.8 when the impinging energy reaches E_P. This feature lends uncertainty of 10–15%.

2.3. 2-Parameter semi-empirical method (2p-SEM)

The impact energy dependence of the Q_T for the intermediate energy (Nishimura and Tawara, 1991a; Zecca et al., 1992) and high energy (Joshipura and Vinodkumar, 1996; García and Manero, 1997) have been previously studied and the proposed formula was as follows,

$$Q_T = \frac{A}{E^B} \tag{6}$$

where, parameter A is governed by the molecular characteristics such as molecular size and its polarisability. The value of B for the high energies, above 500 eV will be ~ 0.7, as proposed by Joshipura and Vinodkumar (1996) and García and Manero (1997) only for smaller molecules i.e., for ten electrons ($Z = 10$) and up to $Z = 22$ electrons systems respectively. However, Nishimura and Tawara (1991b) proposed the value of B ~ 0.5 for the intermediate energy range, 50–500 eV. In this work we have derived a single expression from our previous work (Vinodkumar et al., 2014b) and our current results for C_4F_7N, for the wide energy range, 50 $\leq E_i \leq$ 5000 eV and which is applicable for the complex and larger molecules with $55 < Z < 95$.

In Table 3, both the parameters A and B have been tabulated for the larger molecules whose Z ranges from 56 to 94, and it is seen that the

Table 2
Molecular characteristics.

DNA constituents	Aqueous phase IE (eV) (Crespo-Hernández et al., 2004; Fernando et al., 1998)	E_{gap} (eV)
Adenine	5.00	5.25 (Gop et al., 2019)
Cytosine	5.50	5.35 (Baei et al., 2014)
Guanine	4.80	4.80 (Di Felice et al., 2002)
Thymine	5.40	5.20 (MacNaughton et al., 2005)
Uracil	5.55	5.70 (Baei et al., 2014)

Table 3
Parameters vide equation (6).

Parameter	Adenine ($C_5H_5N_5$) (I)	Perfluoroisobutyronitrile (C_4F_7N) (II)	Thymine ($C_5H_6N_2O_2$) (III)	Cytosine ($C_4H_5N_3O$) (IV)	Uracil ($C_4H_4N_2O_2$) (V)
A	43.47	53.64	40.75	31.70	28.33
B	0.61	0.60	0.60	0.59	0.60

value of B (~0.6) is nearly same for all the molecules. However, the value of A is different for each molecule, suggesting its dependency on the number of target electrons (Z) and polarisability (α).

To observe this relation, we plotted the graph of A vs Z as shown in Fig. 1. The linear relationship observed in Fig. 1 is represented through the following equation,

$$A(Z) = 0.6413Z - 4.8016 \text{ (Correlation r = 95\%)} \quad (7)$$

However, for a given Z, the precision can be enhanced by inclusion of polarisability by considering the difference between the actual values of 'A' (from Table 3) and those derived from equation (7) for each molecule. We have observed the dependency of this deviation (A - $A(Z)$) on the molecular size through the polarisability (α). The linear relationship thus obtained from Fig. 2 is,

$$A - A(Z) = 0.1431\alpha - 10.5712 \text{ (Correlation r = 76\%)} \quad (8)$$

Hence, from the equations (6)–(8), a two-parameter expression for Q_T can be formulated for the wider energy range from 50 to 5000 eV for large molecules.

$$Q_T(E_i, Z, \alpha) = \frac{0.6413Z + 0.1431\alpha - 15.3728}{E_i^{0.60}} \quad (9)$$

We note the impact energy dependency as, $E_i^{0.60}$. Equation (9) provides the two-parameter expression for Q_T, which is applicable for the larger molecules with $55 < Z < 95$ and for the wider impact energy 50 eV $\leq E_i \leq$ 5000 eV. This 2p-SEM method provides total cross sections as well as total elastic cross sections for larger and complex molecules and could be very useful where experimental results are difficult to obtain as evident in the present case of aqueous DNA molecules.

3. Results and discussion

In this section, we present the results on Q_{inel}, Q_{ion}, Q_{el} and Q_T for the aqueous DNA compounds, by employing SCOP, CSP-ic and 2p-SEM. Numeric data for the CSs are provided in Appendix vide Tables 6–8 We also report various correlations (section 3.3) of peak ionisation leading to prediction of dipole polarisability (α) and dielectric constant

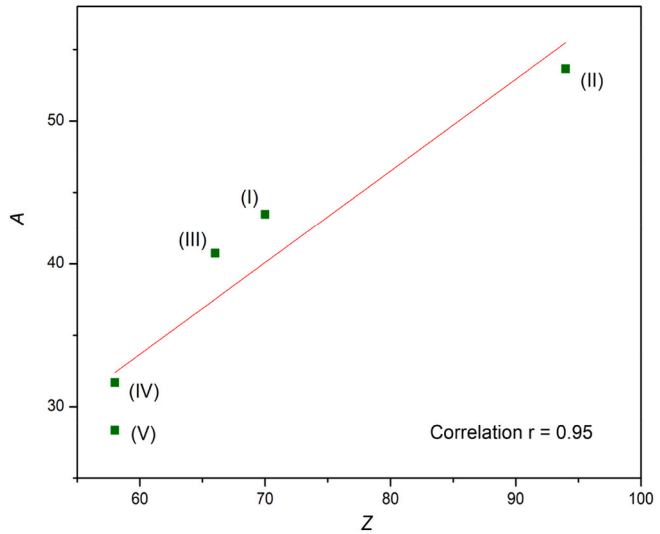

Fig. 1. Parameter A vs Z.

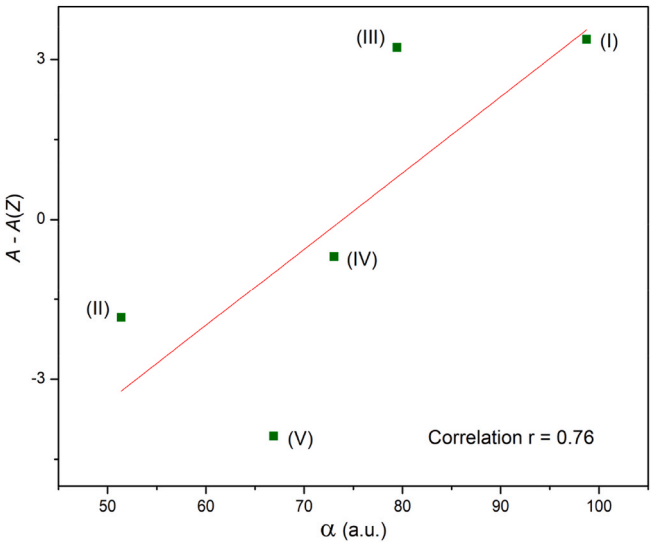

Fig. 2. A - $A(Z)$ vs α

(ε) for all the present aqueous molecules.

3.1. Inelastic contributions

Through Figs. 3–7, Q_{inel} and Q_{ion} are displayed for the investigated aqua-DNA constituents as a function of the electron energy along with the available results for condensed phase molecules (Tan et al., 2004, 2018; De Vera et al., 2021).

Top curves show total inelastic cross sections, Q_{inel}. Tan et al. (Tan et al., 2004) have reported the Q_{inel} data for the case of DNA in water using dielectric response theory and Penn's approximation. They took

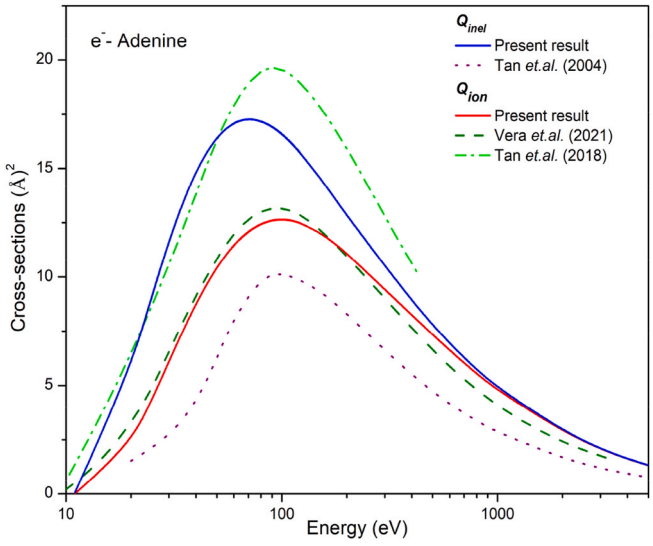

Fig. 3. Inelastic interaction CSs for Adenine
Blue solid: Present Q_{inel}; dot: Tan et al. Q_{inel} (Tan et al., 2004); red solid: Present Q_{ion}; olive green dash dot: Vera et al. Q_{ion} (De Vera et al., 2021); short dash: Tan et al. Q_{ion} (Tan et al., 2018).

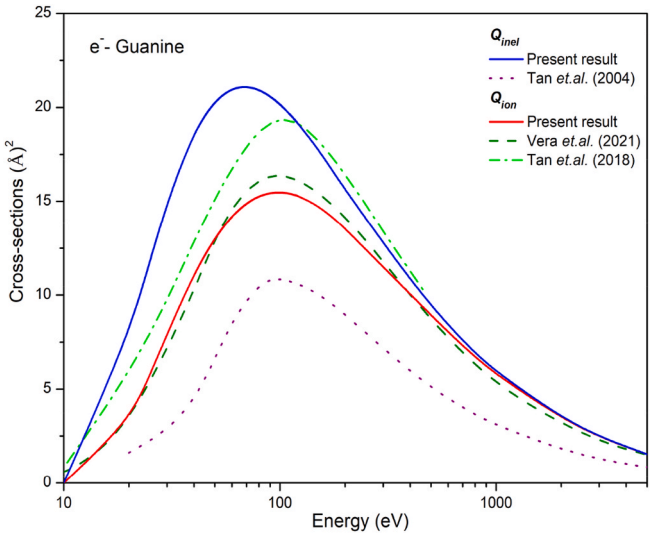

Fig. 4. Inelastic interaction CSs for Guanine
Blue solid: Present Q_{inel}; dot: Tan et al. Q_{inel} (Tan et al., 2004); red solid: Present Q_{ion}; olive green dash dot: Vera et al. Q_{ion} (De Vera et al., 2021); short dash: Tan et al. Q_{ion} (Tan et al., 2018).

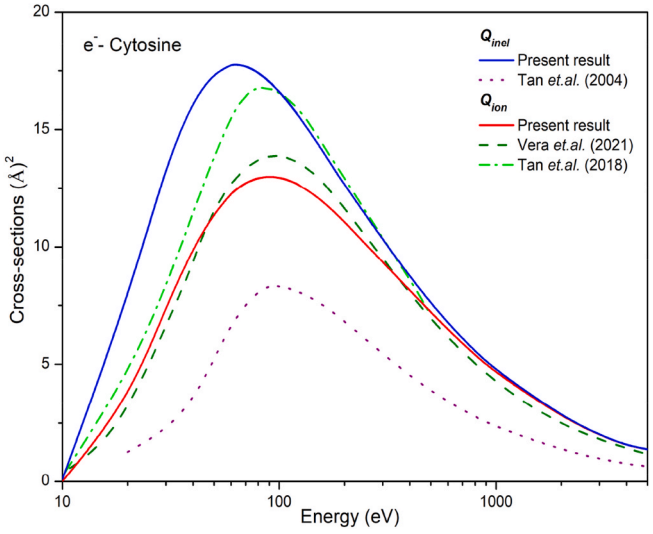

Fig. 5. Inelastic interaction CSs for Cytosine
Blue solid: Present Q_{inel}; dot: Tan et al. Q_{inel} (Tan et al., 2004); red solid: Present Q_{ion}; olive green dash dot: Vera et al. Q_{ion} (De Vera et al., 2021); short dash: Tan et al. Q_{ion} (Tan et al., 2018).

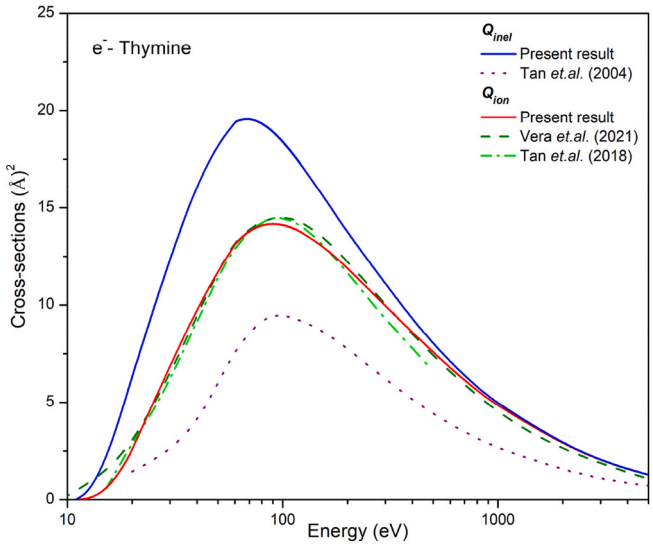

Fig. 6. Inelastic interaction CSs for Thymine
Blue solid: Present Q_{inel}; dot: Tan et al. Q_{inel} (Tan et al., 2004); red solid: Present Q_{ion}; olive green dash dot: Vera et al. Q_{ion} (De Vera et al., 2021); short dash: Tan et al. Q_{ion} (Tan et al., 2018).

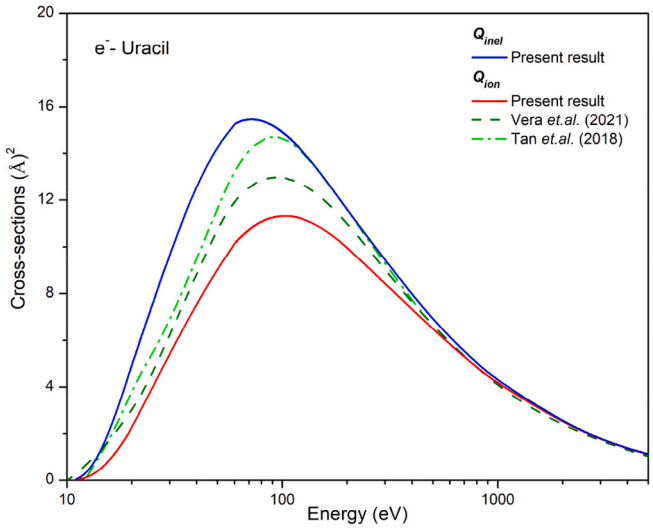

Fig. 7. Inelastic interaction CSs for Uracil Blue solid: Present Q_{inel}; dot: Tan et al. Q_{inel} (Tan et al., 2004); red solid: Present Q_{ion}; dash: Vera et al. Q_{ion} (De Vera et al., 2021); dash dot: Tan et al. Q_{ion} (Tan et al., 2018).

an equivalent unit of DNA molecule in water environment with 50% Guanine-Cytosine and 50% Adenine-Thymine and then separated into 5 constituents of DNA. However, their Q_{inel} underestimate present Q_{inel} and have lower values than even all the reported Q_{ion}.

Tan et al. (Tan et al., 2018) and Vera et al. (De Vera et al., 2021) have reported the Q_{ion} data for condensed DNA bases using the methodologies which underlines the dielectric response theory. The present results of Q_{ion} are observed to be in good accord with those of Vera et al. (De Vera et al., 2021) except in the case of Uracil. The minute deviation at the peak value of Q_{ion} may be because of the consideration of the different phases for the molecules.

As can be seen, the data of Tan et al. (Tan et al., 2018) overestimates both, present data and those of Vera et al. (De Vera et al., 2021) except for Thymine, in which case they show matching.

It is important to compare Q_{ion} for aqua and gas phase (Vinodkumar et al., 2003). Hence, apart from condensed phase results, the present aqueous phase Q_{ion} results are also compared with those of recent gas phase data (Rahman and Krishnakumar, 2015, 2016; Shafranyosh et al., 2015; Champion, 2013; Bull et al., 2014; van der Burgt et al., 2014; Minaev et al., 2014; van der Burgt, 2014, 2015) as shown in Figs. 8–12. As can be observed from the Figs. 8–12, gas phase results overestimate the present aqua phase data. This difference is because of the different threshold values for condensed and gas phase DNA compounds.

3.2. Elastic contributions

We have computed the elastic CSs (Q_{el}) and the total CSs (Q_T) for the electron energies from molecular IE to 5000 eV using the SCOP and 2p-SEM approach.

Figs. 13–17 show the Q_{el} and Q_T plots against the incident electron energies for aqueous Adenine, Cytosine, Guanine, Thymine and Uracil, respectively. We also show recent data of Q_{el} and Q_T in the gas phase.

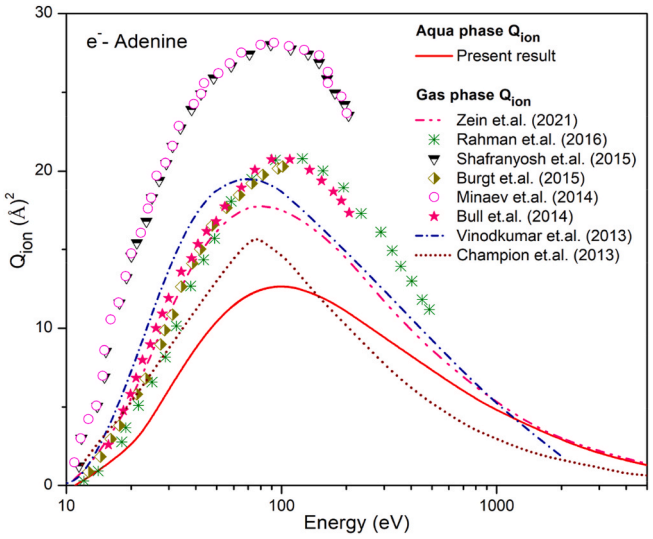

Fig. 8. Q_{ion} for Adenine in aqua and gas phase
Solid: Present Q_{ion} (aqua phase); pink dash dot: Zein et al. (Zein et al., 2021); asterisk: Rahman et al. (Rahman and Krishnakumar, 2016); inverted half-filled triangles: Shafranyosh et al. (Shafranyosh et al., 2015); half-filled diamonds: Burgt et al. (van der Burgt, 2015); open circles: Minaev et al. (Minaev et al., 2014); filled stars: Bull et al. (Bull et al., 2014); short dash dot: Vinodkumar et al. (Vinodkumar and Limbachiya, 2013); short dot: Champion (Champion, 2013).

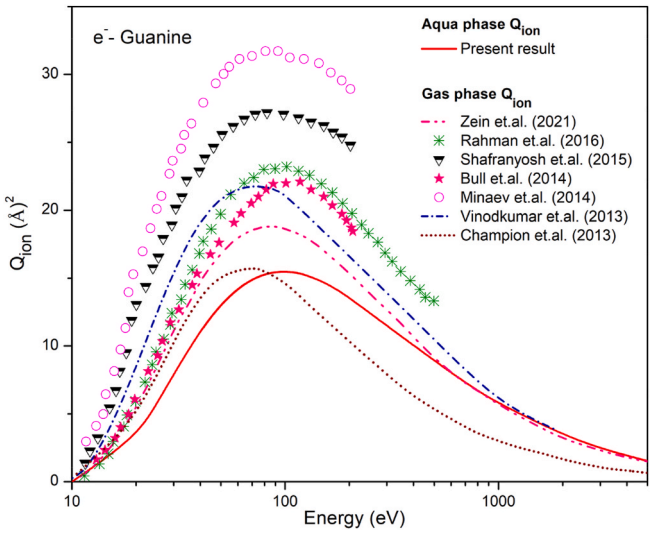

Fig. 9. Q_{ion} for Guanine in aqua and gas phase
Solid: Present aqua phase result; pink dash dot: Zein et al. (Zein et al., 2021); asterisk: Rahman et al. (Rahman and Krishnakumar, 2016); inverted half-filled triangles: Shafranyosh et al. (Shafranyosh et al., 2015); open circles: Minaev et al. (Minaev et al., 2014); filled stars: Bull et al. (Bull et al., 2014); short dash dot: Vinodkumar et al. (Vinodkumar and Limbachiya, 2013); short dot: Champion (Champion, 2013).

The results obtained from 2p-SEM and those from SCOP formalism are seen in good agreement with each other confirming the recently developed 2p-SEM method for larger and complex molecules.

The Q_{el} results from both the methodologies (2p-SEM and SCOP) are observed to be in excellent accord with each other for all the present studied molecules, which validate the newly proposed 2p-SEM formalism even for the aqueous phase molecules.

The gas phase results of Aouina (Aouina and Chaoui, 2018), Vinodkumar et al. (Vinodkumar et al., 2014b), Mokrani et al. (Mokrani et al., 2020) and Gurung (Devi Gurung and Ariyasinghe, 2017) are seen to be deviated at low energy side, which is due to the fact that at lower energies these Q_{el} and Q_T are highly sensitive to threshold values as well as polarisabilities. We observe that Q_{el} data of Zein et al. (Zein et al., 2021) shows significant deviation from the other existing Q_{el} data, mainly at the lower to intermediate energies. This deviation then reduces as we move towards high energy regime.

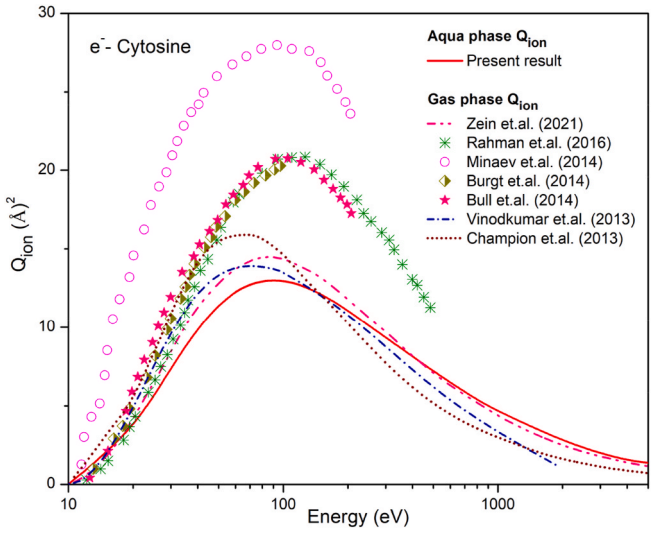

Fig. 10. Q_{ion} for Cytosine in aqua and gas phase
Solid: Present aqua phase result; Solid: Present aqua phase result; pink dash dot: Zein et al. (Zein et al., 2021); asterisk: Rahman et al. (Rahman and Krishnakumar, 2016); open circles: Minaev et al. (Minaev et al., 2014); half-filled diamonds: Burgt (van der Burgt, 2014); filled stars: Bull et al. (Bull et al., 2014); short dash dot: Vinodkumar et al. (Vinodkumar and Limbachiya, 2013); short dot: Champion (Champion, 2013).

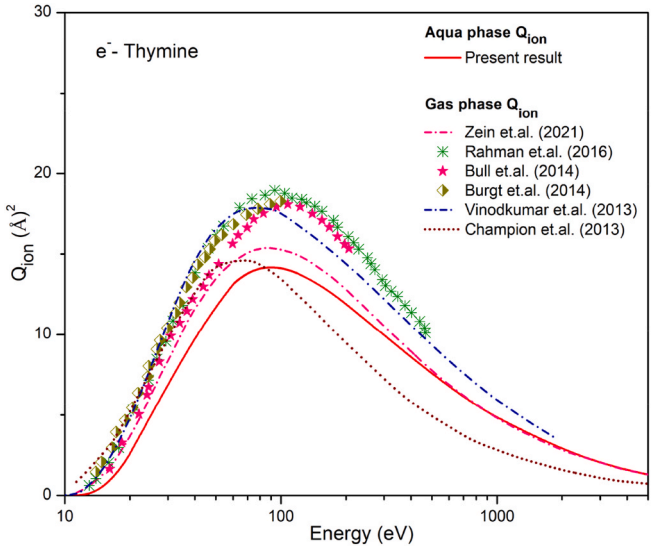

Fig. 11. Q_{ion} for Thymine in aqua and gas phase
Solid: Present aqua phase result; Solid: Present aqua phase result; pink dash dot: Zein et al. (Zein et al., 2021); asterisk: Rahman et al. (Rahman and Krishnakumar, 2016); half-filled diamonds: Burgt et al. (van der Burgt et al., 2014); filled stars: Bull et al. (Bull et al., 2014); short dash dot: Vinodkumar et al. (Vinodkumar and Limbachiya, 2013); short dot: Champion (Champion, 2013).

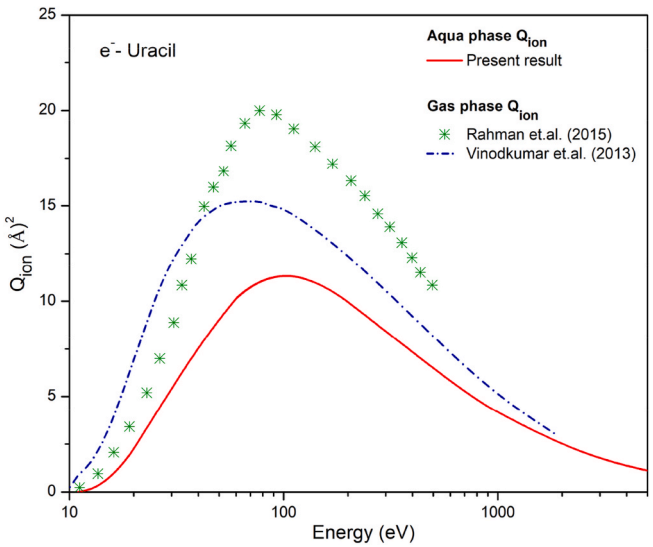

Fig. 12. Q_{ion} for Uracil in aqua and gas phase
Solid: Present aqua phase result; asterisks: Rahman (Rahman and Krishnakumar, 2015); short dash dot: Vinodkumar et al. (Vinodkumar and Limbachiya, 2013).

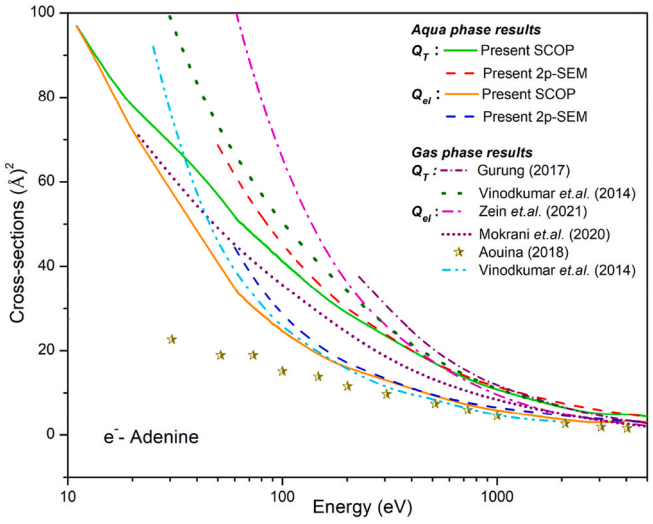

Fig. 13. Elastic and total interaction CSs for Adenine
Aqua phase results
Green solid: Present SCOP Q_T; red dash: Present 2p-SEM Q_T; Present SCOP Q_{el}; blue dash: Present 2p-SEM Q_{el}
Gas phase results
Short dash dot: Gurung Q_T (Devi Gurung and Ariyasinghe, 2017); olive green dot: Vinodkumar et al. Q_T (Vinodkumar et al., 2014b); pink dash dot: Zein et al. Q_{el} (Zein et al., 2021); short dot: Mokrani et al. Q_{el} (Mokrani et al., 2020); half-filled stars: Aouina Q_{el} (Aouina and Chaoui, 2018); dash dot: Vinodkumar et al. (Vinodkumar et al., 2014b).

3.3. Various correlations: prediction of polarisability (α) and dielectric constant (ε)

We have used the calculated total ionisation cross sections to compute useful parameters, polarisability (α) and dielectric constant (ε) for aqua-DNA molecules which are not found in literature.

3.3.1. Polarisability (α)

According to Harland's proposed qualitative dependency nature of the maximum ionisation CSs, ($Q_{ion(m)}$) with its polarisability (α)

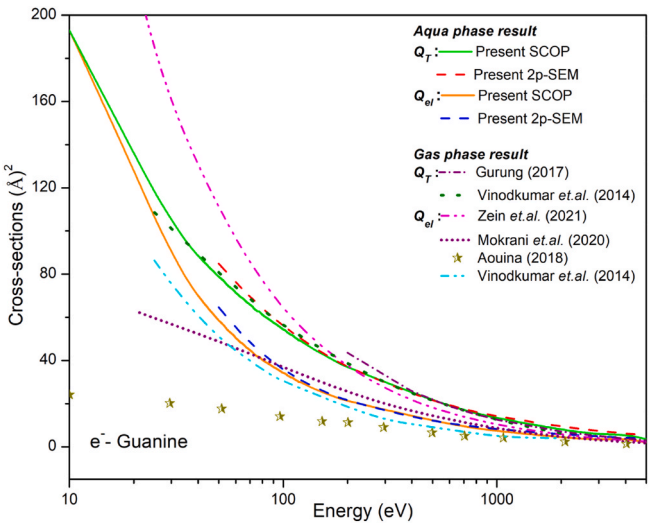

Fig. 14. Elastic and total interaction CSs for Guanine
Aqua phase results
Green solid: Present SCOP Q_T; red dash: Present 2p-SEM Q_T; Present SCOP Q_{el}; blue dash: Present 2p-SEM Q_{el}
Gas phase results
Short dash dot: Gurung Q_T (Devi Gurung and Ariyasinghe, 2017); olive green dot: Vinodkumar et al. Q_T (Vinodkumar et al., 2014b); Pink dash dot: Zein et al. Q_{el} (Zein et al., 2021); short dot: Mokrani et al. Q_{el} (Mokrani et al., 2020); half-filled stars: Aouina Q_{el} (Aouina and Chaoui, 2018); dash dot: Vinodkumar et al. (Vinodkumar et al., 2014b).

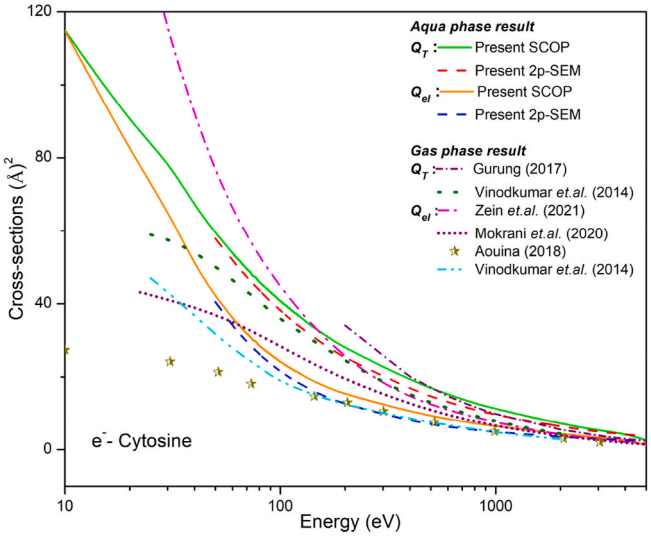

Fig. 15. Elastic and total interaction CSs for Cytosine
Aqua phase results
Green solid: Present SCOP Q_T; red dash: Present 2p-SEM Q_T; orange solid: Present SCOP Q_{el}; blue dash: Present 2p-SEM Q_{el}
Gas phase results
Short dash dot: Gurung Q_T (Devi Gurung and Ariyasinghe, 2017); olive green dot: Vinodkumar et al. Q_T [53]; pink dash dot: Zein et al. Q_{el} (Zein et al., 2021); short dot: Mokrani et al. Q_{el} (Mokrani et al., 2020); half-filled stars: Aouina Q_{el} (Aouina and Chaoui, 2018); dash dot: Vinodkumar et al. (Vinodkumar et al., 2014b).

(Harland and Vallance, 1997),

$$Q_{ion(\mathrm{m})} = \frac{e}{4\varepsilon_o}\sqrt{\frac{\alpha}{\Delta}} \tag{10}$$

Harland proposed the Δ will be equal to *IE* in case of gas phase of the

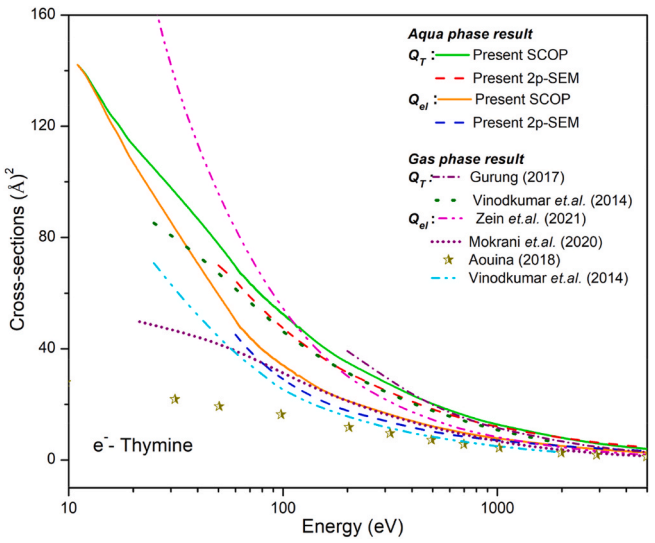

Fig. 16. Elastic and total interaction CSs for Thymine
Aqua phase results
Green solid: Present SCOP Q_T; red dash: Present 2p-SEM Q_T; orange solid: Present SCOP Q_{el}; blue dash: Present 2p-SEM Q_{el}
Gas phase results
Short dash dot: Gurung Q_T (Devi Gurung and Ariyasinghe, 2017); olive green dot: Vinodkumar et al. Q_T (Vinodkumar et al., 2014b); pink dash dot: Zein et al. Q_{el} (Zein et al., 2021); short dot: Mokrani et al. Q_{el} (Mokrani et al., 2020); half-filled stars: Aouina Q_{el} (Aouina and Chaoui, 2018); dash dot: Vinodkumar et al. (Vinodkumar et al., 2014b).

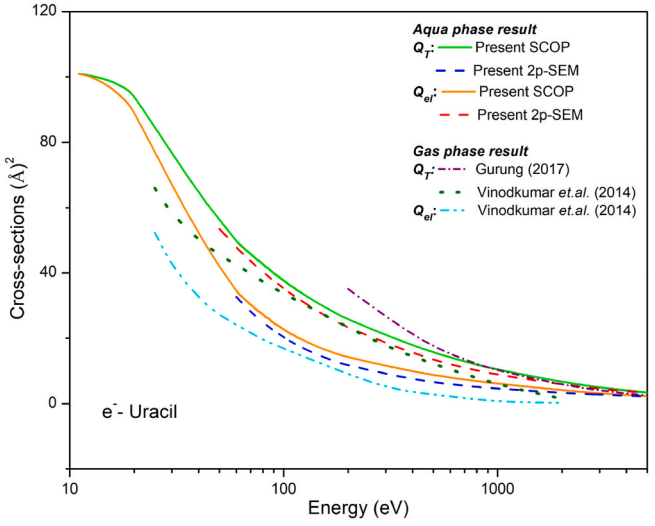

Fig. 17. Elastic and total interaction CSs for Uracil
Aqua phase results
Green solid: Present SCOP Q_T; red dash: Present 2p-SEM Q_T; orange solid: Present SCOP Q_{el}; blue dash: Present 2p-SEM Q_{el}
Gas phase results
Short dash dot: Gurung Q_T (Devi Gurung and Ariyasinghe, 2017); olive green dot: Vinodkumar et al. Q_T (Vinodkumar et al., 2014b); dash dot: Vinodkumar et al. (Vinodkumar et al., 2014b).

target system. While, in the present case of aqueous phase species, the $\Delta = IE + E_{gap}$, and the ionisation of the system actually occurs when the incoming energy is greater than the threshold value, $\Delta = IE + E_{gap}$.

Using this equation (10), we have predicted the α values for the present studied targets as given in the Table 4.

From the table it can be observed that the present predicted α for the aqueous molecules find good agreement with those of Nakagawa (2007), who calculated the α for condensed molecules.

Table 4
Predicted polarisability α (Å^3).

Target	Δ (eV)	$Q_{ion(m)}$ (Å^2)	Predicted α (Å^3)	Reference value of α for condensed phase (Å^3) (Nakagawa, 2007)
Adenine	10.25	12.65	11.54	14.33
Guanine	9.60	15.47	16.17	15.26
Thymine	10.60	14.17	14.99	13.35
Cytosine	10.85	12.99	12.88	11.47
Uracil	11.25	11.32	10.15	10.41

3.3.2. Dielectric constant (ε)

The two expressions for dielectric constant (ε) have been derived in the present work using the dependency of the $Q_{ion(m)}$ on α and ε. The first proposed expression of dielectric constant as a function of $Q_{ion(m)}$, derived using the dependency of $Q_{ion(m)}$ with α (equation (10)) and the Clausius-Mosotti (CM) equation,

$$\frac{\varepsilon-1}{\varepsilon+2} = C\cdot\left(Q_{ion(m)}\right)^2 N\Delta \tag{11}$$

where, C is the constant $= \frac{64\pi}{3}\left(\frac{\varepsilon_0}{e}\right)^2$ and N is the number density of the molecule.

Secondly, the Onsager dielectric equation (Onsager, 1936; Valiskó and Boda, 2005), which works well for the case of liquids is given by,

$$\frac{\varepsilon-1}{\varepsilon+2} = \frac{4\pi}{3}\alpha N + \frac{(\varepsilon-\varepsilon_\infty)(2\varepsilon+\varepsilon_\infty)}{\varepsilon(\varepsilon_\infty+2)^2} \tag{12}$$

This equation is thought to be more applicable in the present aqueous phase study, and again the equation of dielectric constant as a function of $Q_{ion(m)}$ is proposed as,

$$\frac{\varepsilon-1}{\varepsilon+2} = C\cdot\left(Q_{ion(m)}\right)^2 N\Delta + \frac{(\varepsilon-\varepsilon_\infty)(2\varepsilon+\varepsilon_\infty)}{\varepsilon(\varepsilon_\infty+2)^2} \tag{13}$$

where, ε_∞ is the high frequency dielectric constant, which can be obtained from the CM equation. The computed ε values are listed in Table 5.

Form the Table 5 and it can be observed as expected that the ε values computed through equation (13), are in good agreement with those of Szarek (2017).

Conclusion

The aqueous phase of DNA is explored here for several molecular processes upon electron impact, as it is a more realistic phase of DNA due to the presence of H-bonds. Radiation induced damage assessment of DNA due to the single and double strand breaks requires electron interacting with aqueous DNA inelastically. Present study quantifies various interaction processes in response to the impact of electrons on aqueous DNA constituents, viz., Adenine, Guanine, Thymine, Cytosine and Uracil through cross-sections. In order to provide Q_{el} and Q_T results for these biomaterials we have proposed a method 2p-SEM and

Table 5
Computed dielectric constants (ε).

Target	$Q_{ion(m)}$ (Å^2)	Dielectric constant (ε) (vide equation (11))	Dielectric constant (ε) (vide equation (13))	Reference value of ε for condensed phase (Szarek, 2017)
Adenine	12.65	2.22	1.00	1.59
Guanine	15.47	3.23	0.85	1.77
Thymine	14.17	3.39	0.99	1.59
Cytosine	12.99	2.84	1.03	1.71
Uracil	11.32	2.29	0.98	–

encouraging results are observed (Figs. 13–17). The proposed expression for Q_T (equation (9)) is applicable for the larger molecular systems ($55 < Z < 95$) and wider energy range. Numeric data for the CSs are provided in Appendix vide Tables 6–8 Further, from the correlation study of molecular ionisation, we have computed molecular polarisability and dielectric constant. The dielectric constant is obtained from the Q_{ion} using the Clausius-Mosotti (CM) and Onsager approaches (vide equations (11) and (13) respectively). The computed results are compared with previous data. In absence of previous study involving aqueous DNA constituents, this estimation of various cross-sections, computation of polarisability and dielectric constant may prove to be very useful.

CRediT author statement

Smruti Parikh: Data curation, Writing- Original draft preparation, Formal analysis, Conceptualization, Methodology, software. **Dhaval Chauhan:** Data curation, Methodology. **Nirav Thakkar:** Formal analysis. **Chetan Limbachiya:** Reviewing and Editing, Validation, Visualization, Investigation, Supervision.

Declaration of competing interest

The authors declare that they have no known competing financial interests or personal relationships that could have appeared to influence the work reported in this paper.

Data availability

Data will be made available on request.

APPENDIX

Table 6
Numeric data for cross-sections of Aqueous Adenine and Guanine (in Å^2)

E_i (eV)	Adenine					Guanine				
	Q_{ion}	Modified SCOP		2p-SEM		Q_{ion}	Modified SCOP		2p-SEM	
		Q_{el}	Q_T	Q_{el}	Q_T		Q_{el}	Q_T	Q_{el}	Q_T
10	–	–	–	–	–	0.00	192.94	192.95	–	–
11	0.004	96.82	96.88	–	–	0.021	188.95	189.16	–	–
20	2.35	72.02	77.85	–	–	3.27	128.23	136.08	–	–
40	8.76	48.42	63.27	–	–	11.04	70.00	88.51	–	–
60	11.46	34.79	51.86	44.49	61.56	14.17	50.40	71.35	55.34	76.29
70	12.08	31.17	48.43	38.87	56.13	14.87	44.76	65.84	48.47	69.55
80	12.43	28.59	45.76	34.64	51.80	15.25	40.28	61.20	43.28	64.20
100	12.65	24.60	41.18	28.73	45.31	15.47	34.26	54.41	36.00	56.15
400	8.25	11.04	19.91	10.86	19.72	10.04	14.30	25.07	13.67	24.44
800	5.54	6.74	12.47	7.29	13.01	6.71	8.56	15.48	9.20	16.13
1000	4.79	5.81	10.72	6.47	11.38	5.78	7.34	13.27	8.18	14.10
3000	2.07	2.69	4.78	3.80	5.89	2.48	3.17	5.66	4.80	7.30
5000	1.33	3.07	4.40	3.00	4.33	1.53	2.00	3.54	3.84	5.37

Table 7
Numeric data for cross-sections of Aqueous Cytosine and Thymine (in Å^2)

E_i (eV)	Cytosine					Thymine				
	Q_{ion}	Modified SCOP		2p-SEM		Q_{ion}	Modified SCOP		2p-SEM	
		Q_{el}	Q_T	Q_{el}	Q_T		Q_{el}	Q_T	Q_{el}	Q_T
10	0.01	114.81	114.92	–	–	–	–	–	–	–
11	0.08	109.80	110.29	–	–	0.001	142.10	142.12	–	–
20	3.42	82.11	89.88	–	–	2.55	106.87	113.23	–	–
40	9.94	50.70	66.94	–	–	10.01	70.34	87.17	–	–
60	12.26	36.26	54.00	34.14	51.88	13.13	50.41	69.81	45.06	64.46
70	12.71	31.81	49.49	29.62	47.29	13.79	43.97	63.52	39.21	58.76
80	12.93	28.52	45.93	26.25	43.65	14.09	39.72	59.05	34.91	54.24
100	12.95	24.15	40.75	21.58	38.18	14.12	34.05	52.44	29.05	47.44
400	8.13	10.45	19.12	7.95	16.62	8.58	13.73	22.93	11.45	20.65
800	5.40	7.23	12.78	5.41	10.97	5.60	8.88	14.67	7.84	13.62
1000	4.64	6.46	11.21	4.84	9.59	4.81	7.74	12.66	6.99	11.92
3000	1.98	3.35	5.34	2.97	4.96	2.03	3.78	5.82	4.12	6.16
5000	1.37	1.23	2.60	2.27	3.65	1.29	2.69	3.98	3.24	4.54

Table 8
Numeric data for cross-sections of Aqueous Uracil (in Å^2)

E_i (eV)	Uracil				
	Q_{ion}	Modified SCOP		2p-SEM	
		Q_{el}	Q_T	Q_{el}	Q_T
11	0.007	100.96	100.99	–	–
20	2.24	89.44	94.39	–	–
40	7.69	50.97	64.10	–	–
60	10.14	34.53	49.79	32.63	47.88
70	10.73	30.30	45.75	28.20	43.65
80	11.08	27.23	42.62	24.90	40.29
100	11.32	22.71	37.62	20.34	35.24
400	7.33	9.78	17.69	7.43	15.34
800	4.83	6.90	11.91	5.11	10.12
1000	4.15	6.14	10.42	4.58	8.85
3000	1.76	3.20	4.98	2.80	4.58
5000	1.12	2.31	3.43	2.25	3.37

References

Aouina, N.Y., Chaoui, Z.-E.-A., 2018. Simulation *of Positron and electron elastic mean free Path and diffusion Angle on DNA Nucleobases from 10 eV to 100 KeV*. Surf. Interface Anal. 50, 939.

Baei, M.T., Taghartapeh, M.R., Lemeski, E.T., Soltani, A., 2014. A computational study of adenine, Uracil, and cytosine adsorption upon AlN and BN nano-cages. Phys. B Condens. Matter 444, 6.

Bass, A., Sanche, L., 1998. Absolute and effective cross-sections for low-energy electron-scattering processes within condensed matter. Radiat. Environ. Biophys. 37, 243.

Boudaïffa, B., Cloutier, P., Hunting, D., Huels, M.A., Sanche, L., 2002. Cross sections for low-energy (10-50 EV) electron damage to DNA. Radiat. Res. 157, 227.

Bull, J.N., Lee, J.W.L., Vallance, C., 2014. Absolute *electron total ionization cross-sections: molecular Analogues of DNA and RNA Nucleobase and sugar constituents*. Phys. Chem. Chem. Phys. 16, 10743.

Champion, C., 2013. Quantum-mechanical predictions of electron-induced ionization cross sections of DNA components. J. Chem. Phys. 138, 184306.

Cox, H.L., Bonham, R.A., 1967. Elastic electron scattering amplitudes for neutral atoms calculated using the partial wave method at 10, 40, 70, and 100 KV for Z = 1 to Z = 54. J. Chem. Phys. 47, 2599.

Crespo-Hernández, C.E., Arce, R., Ishikawa, Y., Gorb, L., Leszczynski, J., Close, D.M., 2004. Ab initio ionization energy thresholds of DNA and RNA bases in gas phase and in aqueous solution. J. Phys. Chem. A 108, 6373.

De Vera, P., Abril, I., Garcia-Molina, R., 2021. Excitation and ionisation cross-sections in condensed-phase biomaterials by electrons down to very low energy: application to liquid water and genetic building blocks. Phys. Chem. Chem. Phys. 23, 5079.

Devi Gurung, Meera, Ariyasinghe, W.M., 2017. Total electron scattering cross sections of some important biomolecules at 0.2 – 6.0keV energies. Radiat. Phys. Chem. 141, 1.

Di Felice, R., Calzolari, A., Molinari, E., Garbesi, A., 2002. Ab initio study of model guanine assemblies: the role of (formula presented) coupling and band transport. Phys. Rev. B Condens. Matter 65, 1.

Fernando, H., Papadantonakis, G.A., Kim, N.S., Lebreton, P.R., 1998. Conduction-band-edge ionization thresholds of DNA components in aqueous solution. Proc. Natl. Acad. Sci. U. S. A. 95, 5550.

García, G., Manero, F., 1997. Correlation of the total cross section for electron scattering by molecules with 10-22 electrons, and some molecular parameters at intermediate energies. Chem. Phys. Lett. 280, 419.

Goodhead, D.T., 1994. Initial events in the cellular effects of ionizing radiations: clustered damage in DNA. Int. J. Radiat. Biol. 65, 7.

Gop, S., Sutradhar, R., Chakraborty, S., Sinha, T.P., 2019. The study of energetic and electronic properties of metal-adenine complex in solvent phase: a density functional theory approach. In: AIP Conference Proceedings, vol. 2162. American Institute of Physics Inc.

Hara, S., 1967. The scattering of slow electrons by hydrogen molecules. J. Phys. Soc. Jpn. 22, 710.

Harland, P.W., Vallance, C., 1997. Ionization cross-sections and ionization efficiency curves from polarizability volumes and ionization potentials. Int. J. Mass Spectrom. Ion Process. 171, 173.

Helmholtz Association of German Research Centres. Water molecules characterize the structure of DNA genetic material. https://www.sciencedaily.com/releases/2011/04/110426091122.htm#citation_apa.

Joshipura, K.N., Vinodkumar, M., 1996. *Cross Sections and other Parameters of e^- - H_2O scattering (Ei≥50eV)*. Pramana - J. Phys. 47, 57.

Joshipura, K.N., Vaishnav, B.G., Limbachiya, C.G., 2006. Ionization and excitation of some atomic targets and metal oxides by electron impact. Pramana - J. Phys. 66, 403.

Joshipura, K.N., Gangopadhyay, S., Limbachiya, C.G., Vinodkumar, M., 2007. Electron impact ionization of water molecules in ice and liquid phases. J. Phys. Conf. Ser. 80, 012008.

Khesbak, H., Savchuk, O., Tsushima, S., Fahmy, K., 2011. The role of water H-bond imbalances in B-DNA substate transitions and peptide recognition revealed by time-resolved FTIR spectroscopy. J. Am. Chem. Soc. 133, 5834.

Limbachiya, C., Vinodkumar, M., Mason, N., 2011. *Calculation of electron-impact rotationally elastic total cross Sections for NH_3, H_2S, and PH_3 over the energy Range from 0.01 eV to 2 KeV*. Phys. Rev. 83, 042708.

Limbachiya, C., Vinodkumar, M., Swadia, M., Barot, A., 2014. *Electron impact total cross section Calculations for CH_3SH (methanethiol) from Threshold to 5 KeV*. Mol. Phys. 112, 101.

Limbachiya, C., Vinodkumar, M., Swadia, M., Joshipura, K.N., Mason, N., 2015. Electron-impact total cross sections for inelastic processes for furan, tetrahydrofuran and 2,5-dimethylfuran. Mol. Phys. 113, 55.

MacNaughton, J., Moewes, A., Kurmaev, E.Z., 2005. Electronic structure of the nucleobases. J. Phys. Chem. B 109, 7749.

Minaev, B.F., Shafranyosh, M.I., Yu Svida, Yu., Sukhoviya, M.I., Shafranyosh, I.I., Baryshnikov, G.V., Minaev, V.A., 2014. Fragmentation of the adenine and guanine molecules induced by electron collisions. J. Chem. Phys. 140, 175101.

Mokrani, S., Aouchiche, H., Champion, C., 2020. Elastic scattering of electrons by DNA bases. Radiat. Phys. Chem. 172, 108735.

Mozejko, P., Sanche, L., 2005. Cross sections for electron scattering from selected components of DNA and RNA. Radiat. Phys. Chem. 73, 77.

Nakagawa, S., 2007. Polarizable model potential function for nucleic acid bases. J. Comput. Chem. 28, 1538.

Nikjoo, H., Taleei, R., Liamsuwan, T., Liljequist, D., Emfietzoglou, D., 2016. Perspectives in radiation biophysics: from radiation track structure simulation to mechanistic models of DNA damage and repair. Radiat. Phys. Chem. 128, 3.

Nishimura, H., Tawara, H., 1991a. Some aspects of total scattering cross sections of electrons for simple hydrocarbon molecules. J. Physiol. Biochem.: At Mol. Opt. Phys. 24, L363.

Nishimura, H., Tawara, H., 1991b. Some aspects of total scattering cross sections of electrons for simple hydrocarbon molecules. J. Physiol. Biochem.: At Mol. Opt. Phys. 24, L363.

Onsager, L., 1936. Electric moments of molecules in liquids. J. Am. Chem. Soc. 58, 1486.

Pandya, S.H., Vaishnav, B.G., Joshipura, K.N., 2012. Electron inelastic mean free paths in solids: a theoretical approach. Chin. Phys. B 21.

Parikh, S., Limbachiya, C., 2023. Electron driven molecular processes for nucleosides. Radiat. Phys. Chem. 208, 110940.

Parikh, S., Vinodkumar, M., Limbachiya, C., 2023. Electron impact inelastic molecular processes for deuterated compounds. Chem. Phys. 565, 111766.

Rahman, M.A., Krishnakumar, E., 2015. Absolute partial and total electron ionization cross sections of Uracil. Int. J. Mass Spectrom. 392, 145.

Rahman, M.A., Krishnakumar, E., 2016. Communication: electron ionization of DNA bases. J. Chem. Phys. 144, 161102.

Shafranyosh, I.I., Svida, Yu. Yu., Sukhoviya, M.I., Shafranyosh, M.I., Minaev, B.F., Baryshnikov, G.V., Minaev, V.A., 2015. Absolute effective cross sections of ionization of adenine and guanine molecules by electron impact. Tech. Phys. 60, 1430.

Staszewska, G., Schwenke, D.W., Truhlar, D.G., 1984. Investigation of the shape of the imaginary part of the optical-model potential for electron scattering by rare gases. Phys. Rev. 29, 3078.

Swadia, M., Thakar, Y., Vinodkumar, M., Limbachiya, C., 2017. *Theoretical electron impact total cross Sections for tetrahydrofuran (C_4H_8O)*. Eur. Phys. J. D 71, 85.

Szarek, P., 2017. Electric permittivity in individual atomic and molecular systems through direct associations with electric dipole polarizability and chemical hardness. J. Phys. Chem. C 121, 12593.

Tan, Z., Xia, Y., Liu, X., Zhao, M., Ji, Y., Li, F., Huang, B., 2004. Cross sections of electron inelastic interactions in DNA. Radiat. Environ. Biophys. 43, 173.

Tan, H.Q., Mi, Z., Bettiol, A.A., 2018. Simple and universal model for electron-impact ionization of complex biomolecules. Phys. Rev. E 97, 1.

Thakkar, N., Swadia, M., Vinodkumar, M., Mason, N., Limbachiya, C., 2021. Electron induced elastic and inelastic processes for perfluoroketone (PFK) molecules. Plasma Sources Sci. Technol. 30, 085008.
Toburen, L., 1998. Ionization and charge-transfer: basic data for track structure calculations. Radiat. Environ. Biophys. 37, 221.
Turner, J.E., Paretzke, H.G., Hamm, R.N., Wright, H.A., Ritchie, R.H., 1982. Comparative study of electron energy deposition and yields in water in the liquid and vapor phases. Radiat. Res. 92, 47.
Valiskó, M., Boda, D., 2005. Dielectric constant of the polarizable dipolar hard sphere fluid studied by Monte Carlo simulation and theories. Condens. Matter Phys. 8, 357.
van der Burgt, P.J.M., 2014. Electron impact fragmentation of cytosine: partial ionization cross sections for positive fragments. Eur. Phys. J. D 68, 135.
van der Burgt, P.J.M., 2015. Electron impact fragmentation of adenine: partial ionization cross sections for positive fragments. Eur. Phys. J. D 69, 173.
van der Burgt, P.J.M., Mahon, F., Barrett, G., Gradziel, M.L., 2014. Electron impact fragmentation of thymine: partial ionization cross sections for positive fragments. Eur. Phys. J. D 68, 151.
Vinodkumar, M., Limbachiya, C., 2013. Electron impact total and ionization cross-sections for DNA based compounds. Mol. Phys. 111, 215.
Vinodkumar, M., Joshipura, K.N., Limbachiya, C.G., Antony, B.K., 2003. *Electron impact Ionization of H_2O Molecule in crystalline ice*. Nucl. Instrum. Methods Phys. Res. B 212, 63.
Vinodkumar, M., Joshipura, K.N., Limbachiya, C., Mason, N., 2006. Theoretical calculations of the total and ionization cross sections for electron impact on some simple biomolecules. Phys. Rev. 74, 022721.
Vinodkumar, M., Bhutadia, H., Limbachiya, C., Joshipura, K.N., 2011. *Electron impact total ionization cross Sections for H_2S, PH_3, HCHO and HCOOH*. Int. J. Mass Spectrom. 308, 35.
Vinodkumar, M., Limbachiya, C., Barot, M., Swadia, M., Barot, A., 2013a. Electron impact total ionization cross sections for all the components of DNA and RNA molecule. Int. J. Mass Spectrom. 339–340, 16.
Vinodkumar, M., Limbachiya, C., Barot, A., Mason, N., 2013b. Computation of electron-impact rotationally elastic total cross sections for methanol over an extensive range of impact energy (0.1 – 2000 eV). Phys. Rev. 87, 012702.
Vinodkumar, M., Limbachiya, C., Desai, H., Vinodkumar, P.C., 2014a. Electron-impact total cross sections for phosphorous triflouride. Phys. Rev. 89, 062715.
Vinodkumar, M., Limbachiya, C., Barot, M., Barot, A., Swadia, M., 2014b. Electron impact total cross sections for components of DNA and RNA molecules. Int. J. Mass Spectrom. 360, 1.
Antonio Zecca, Grzegorz P. Karwasz, and R. S. Brusa, *Total-Cross-Section Measurements For Electron Scattering by NH_3, SiH_4, and H_2S in the Intermediate-Energy Range*, vol. 45, (1992)..
Zein, S.A., Bordage, M.C., Francis, Z., Macetti, G., Genoni, A., Dal Cappello, C., Shin, W. G., Incerti, S., 2021. Electron transport in DNA bases: an extension of the geant4-DNA Monte Carlo toolkit. Nucl. Instrum. Methods Phys. Res. B 488, 70.
Zhang, X., Sun, J., Liu, Y., 1992. A new approach to the correlation polarization potential-low-energy electron elastic scattering by He atoms. J. Physiol. Biochem.: At Mol. Opt. Phys. 25, 1893.

Eur. Phys. J. D (2024)78:62
https://doi.org/10.1140/epjd/s10053-024-00858-y

THE EUROPEAN PHYSICAL JOURNAL D

Regular Article - Molecular Physics and Chemical Physics

Electron-driven processes for perfluoronitriles

Nirav Thakkar[1], Dhaval Chauhan[2,3], Smruti Parikh[2], and Chetan Limbachiya[2,a]

[1] Sheth M. N. Science College, Patan 384 265, India
[2] Department of Applied Physics, The M S University of Baroda, Vadodara 390001, India
[3] Faculty of Science, Sigma University, Vadodara 390019, India

Received 29 January 2024 / Accepted 3 May 2024

Abstract. We report the results of the study on electron-driven molecular processes for the perfluoronitriles, C_3F_5N and C_4F_7N for a wide energy range, from the ionisation potential to 5000 eV. These compounds have been shown to have extremely low global warming potential, suggesting they could be useful in gas discharges and plasma reactors. Calculations of ionisation cross sections (Q_{ion}) are made using the complex scattering potential-ionisation contribution (CSP-ic) method and are shown to be in good agreement with the available data. Elastic (Q_{el}), inelastic (Q_{inel}) and total (Q_T) cross sections are computed through spherical complex optical potential formalism. We have recently developed two-parameter semi-empirical method (2p-SEM) for large molecules with $55 < Z < 95$ to report Q_{el} and Q_T. This work is a maiden report of Q_{el} and Q_T for C_3F_5N and C_4F_7N. We present various correlation studies between the cross sections and target parameters, leading to a prediction of polarizability. We have derived dielectric constant using number density and molar mass and have correlated Q_{ion} (max) with dielectric constant.

1 Introduction and literature survey

As an insulating gas, sulphur hexafluoride (SF_6) is commonly used in high-voltage devices [1]. Non-toxicity, a low boiling point, and excellent insulating performance are just a few of the many physicochemical features of SF_6 that lead in this direction. However, SF_6 does not decompose very quickly in the atmosphere and has a GWP that is 22,800 times higher than that of carbon dioxide. SF_6 insulated equipment is extensively used in high-voltage, extra-high-voltage, and ultra-high-voltage power systems because of its excellent dependability, low electromagnetic radiation, and little land demand. Nonetheless, the failure of equipment insulation would result in enormous economic loss. Thus, finding a suitable alternative to SF_6 has become one of the most critical issues in high-voltage mechatronics. The fluoronitrile (C_3F_5N and C_4F_7N) gases have been studied intensively [2–4] in recent years as a potential alternative to SF_6. The dielectric strength $\boldsymbol{\varepsilon_r}$ is 2.00 [5] and 2.74 [6] related to SF_6. The other parameter, i.e. GWP of C_4F_7N is 2100 [6], and for SF6, it is 23,900 [7].

Thus, fluoronitriles have low GWP and high dielectric strength compared to SF_6, which makes them most suitable alternative to SF_6 in various applications.

However, there has been comparatively less research into microscopic parameters such as the ionisation cross sections (Q_{ion}) upon electron impact. This Q_{ion} is a key variable in the study of electron avalanche and gas breakdown mechanisms [8, 9].

Figure 1 displays graphical representations of fluoronitriles studied here.

Gas electron transport coefficients and discharge reaction rates can be calculated using either Boltzmann's computations or Monte Carlo calculations [8, 9], with Q_{ion} serving as an input. Q_{ion} can be measured experimentally. Theoretical methods become potent tools for obtaining Q_{ion}, which might be used as a reference in the investigation of the insulating properties of gases. CSP-ic technique [10], Binary-Encounter Bethe (BEB) method [11], and Deutsche-Mark (DM) method [6] are the most well-known theoretical approaches.

Our group has developed a CSP-ic technique [12], which is used in the present work to calculate the Q_{ion} for the molecules of interest in the present work.

Constructing a complete set of electron scattering cross sections is essential for predicting the performance of fluoronitriles in plasma reactors, industrial gas discharges, gas insulated transmission line (GIL), and gas insulated switchgear (GIS). Only a handful of electron interaction investigations have been conducted with fluoronitriles, and a literature survey reveals that there are no results for Q_{el}, elastic cross sections, or, Q_T total cross sections (Table 1).

This work examines the fluoronitrile molecules in depth, from IP (ionisation potential) to 5 keV, reporting probabilities of occurrence of numerous molecular reactions upon electron impact due to their significance to the environment and relevance to plasma physics.

[a] e-mail: cglimbachiya-apphy@msubaroda.ac.in (corresponding author)

Published online: 21 May 2024

Table 1 Prior investigations of e-fluoronitriles scattering

Molecule	Reported quantity	Impact energy (E_i)	References
C_3F_5N	Q_{ion}	IP-1000 eV	Wang et al. [5]
C_4F_7N	Q_{ion}	IP-1000 eV	Wang et al. [5]
	Q_{ion}	IP-2000 eV	Xiong et al. [6]
	Q_{ion}	IP-100 eV	Rankovic et al. [13]
	Q_{inel}, Q_{ion}, ΣQ_{exc}	IP-5000 eV	Sinha et al. [14]

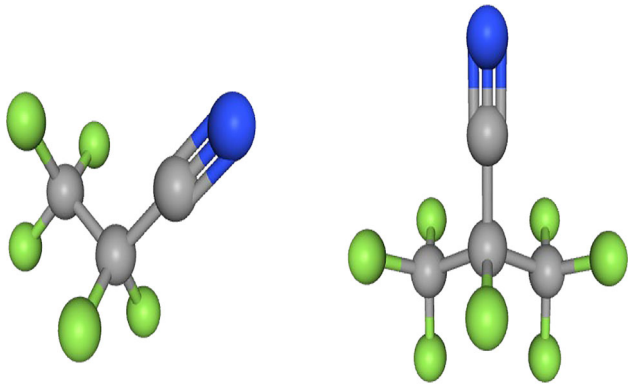

C_3F_5N **C_4F_7N**

Fig. 1 Diagrammatic representations. (https://pubchem.ncbi.nlm.nih.gov)

2 Computational methods

In this investigation, three distinct methodologies are used to investigate electron-driven molecular processes, viz. the spherical complex optical potential (SCOP) [15–18], the complex scattering potential- ionisation contribution (CSP-ic) [19–22], and recently developed two-parameter semi-empirical method (2p-SEM) [23]

2.1 SCOP formalism: calculation of Q_{el}, Q_{inel} and Q_T

Under the fixed nuclei approach of the SCOP formalism, these interaction processes are characterised by an optical potential,

$$V_{opt}(E_i, r) = V_{st}(r) + V_{ex}(E_i, r) + V_{pol}(E_i, r) + iV_{abs}(E_i, r) \quad (1)$$

The short-ranged static potential (V_{st}) quantifies the cloud of charges in the molecular system and is constructed by employing the Hartree–Fock wave functions [24]. Exchange potential (V_{ex}) [25] governs the exchange of the incident electrons with the target electrons. Due to the induced multipole moments, the approaching electron temporarily distorts the target, which is an attractive phenomenon. The asymptotic polarisation potential is given by an adiabatic equation [25–27],

$$V_{pol} = -\frac{\alpha_d}{2r^4} - \frac{\alpha_q}{2r^6} \quad (2)$$

Here, we have disregarded the multipolar terms of higher order. The static dipole and quadrupole polarizabilities are denoted by α_d and α_q, respectively.

Within the absorption potential (V_{abs}), electronic excitation and ionisation are described by transfer of projectile flux into inelastic scattering channels. We used the following form of V_{abs} [28, 29] provided in a.u.

This absorption potential V_{abs} is given as,

$$V_{abs}(r, Ei) = -\rho(r)\left(\frac{T_{loc}}{2}\right)^{\frac{1}{2}}\left(\frac{8\pi}{10k_F^3 Ei}\right)\theta(p^2 - k_F^2 - 2\Delta)(A_1 + A_2 + A_3) \quad (3)$$

The local kinetic energy of the incident electron is obtained from

$$T_{loc} = E_i - V_R = E_i - (V_{st} + V_{ex} + V_p)$$

Here, $p^2 = 2\,E_i$, k_F is the Fermi wave vector and Δ is an energy parameter, $\theta(x)$ is the Heaviside step function, such that $\theta(x) = 1$ for $x > 0$, and is zero otherwise. The dynamic functions A_1, A_2 and A_3 depend differently on $\rho(r)$, I, Δ and E_i. The parameter Δ assumed to be fixed in the original model determines a threshold below which $V_{abs} = 0$, and the ionisation or excitation is prevented energetically [29].

We have improved this potential to allow the inelastic processes even below the ionisation potential of the target. Partial wave approach yields the dynamic phase shifts that bear the signature of the molecular process which is finally utilised in quantification of elastic (Q_{el}) and inelastic cross sections (Q_{inel}) as described in our earlier papers [20, 30].

2.2 CSP-ic formalism: calculation of Q_{ion} and ΣQ_{exc}

The total ionisation cross section is a quantity of substantial practical relevance. The current work to find all these cross sections is undertaken from IP of the molecule to 5000 eV. The cross section of interest in many applications is Q_{ion}, which is contained in Q_{inel}. There is no rigorous way to project out the former from the latter. The present method the CSP-ic approach

defines a ratio $R(E_i)$ such that [19, 20].

$$R(E_i) = \frac{Q_{\text{ion}}(E_i)}{Q_{\text{inel}}(E_i)};\ E_i \text{ is the incident energy.} \quad (4)$$

The ratio $R(E_i)$ takes the following form due to the Bethe form at high energies and the nature of Q_{inel} at the peak region.

$$R(E_i) = 1 - C_1\left(\frac{C_2}{U+a} + \frac{lnU}{U}\right) \quad (5)$$

where U = $\frac{E_i}{I}$. To calculate the three constants C_1, C_2, and a, we need to meet the following three requirements:

$$R(E_i) = \begin{cases} 0, \text{ for } E_i \le I \\ R_P, \text{ for } E_i = E_P \\ \sim 1, \text{ for } E_i \gg E_P \end{cases} \quad (6)$$

The opening of the ionisation channel occurs at the molecule's ionisation threshold (I), which is justified through the first condition (Eq. 6). However, as needed by the third condition, ionisation predominates at very high energy and excitation cross sections significantly decrease. The value of the ratio $R(E_i)$ at impact energy E_{p} (incident energy where Q_{inel} is maximum) is denoted by R_{p}. According to theoretical predictions [31, 32] and experimental findings for stable compounds like the ones reported in [33–35], contribution of Q_{ion} is about 70–80% of Q_{inel}, which leads to the value of R_p in the range of 0.7 to 0.8. While the SCOP method is a quantum mechanical theory, it involves the model potentials to account for different electron–molecule interactions. The used model potentials have some approximations incorporated for the development of the potential. Further, owing to partial wave approach, the spherical approximation is considered under SCOP formalism. For the estimations of Q_{ion}, the semi-empirical CSP-ic method is used. These are major sources of uncertainties in the present theory. Due to these factors, an overall uncertainty of about 10–15% [36].

2.3 2p-SEM formalism: calculation of Q_{el} and Q_T

The impact energy dependence of the Q_{T} for the intermediate energy [37, 38] and high energy [39, 40] has been previously studied, and the proposed formula is as follows:

$$Q_T = \frac{A}{E^B} \quad (7)$$

where parameter A is governed by the molecular characteristics such as size of the molecule and its polarizability. The value of B for the high energies above 500 eV will be ∼ 0.7, which is proposed by Joshipura [39] and Garcia [40] for smaller molecules, i.e. for (Z = 10) and up to (Z = 22) electrons systems, respectively.

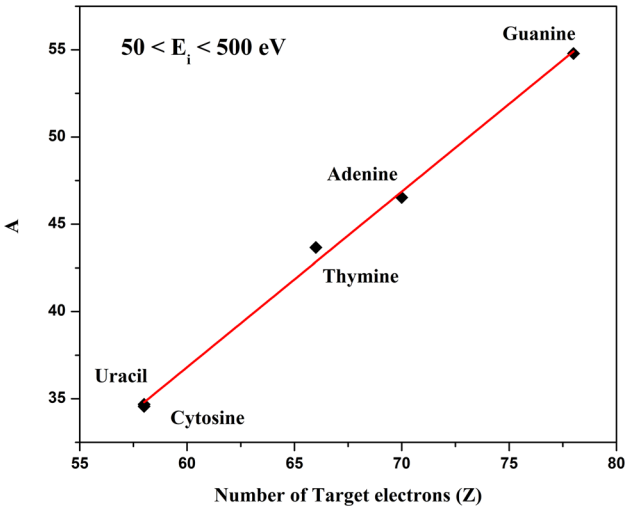

Fig. 2 Parameter A vs. Z ($50 < E_i < 500$ eV)

In the current work, this formula is obtained for larger molecules with 55 < Z < 95 for two distinct energy range ($50 < E_i < 500$ eV) and high energy regions ($E_i > 500$ eV) [23].

Table 2 displays the parameters A and B for the DNA bases in the intermediate energy range (50–500 eV). It is evident that the value of B, which is around 0.5, is consistent for every molecule. According to our estimates, the Q_{T} is energy-dependent [41], and for 50–500 eV, its dependency on incoming energy is comparable to that of Nishimura and Tawara [37] as,

$$Q_T = \frac{A}{\sqrt{E}} \quad (8)$$

However, the value of A is different for each molecule, suggesting its dependency on the number of target electrons (Z).

In order to observe this relationship, we plotted the A vs. Z graph for $50 < E_i < 500$ eV and $E_i > 500$ eV, respectively, as shown in Figs. 2 and 3. The linear relationship depicted in Fig. 2 is represented by the equation,

$$A(Z) = Z - 23.54 \qquad (\text{Correlation r} = 99\%) \quad (9)$$

Through the polarizability (α), we discovered that this deviation (A–A(Z)) is dependent on molecular size. Their linear relationship is as follows:

$$A - A(Z) = -0.003\alpha + 0.63 \quad (10)$$

Thus, for the energy range of 50–500 eV, two-parameter expression for Q_T can be derived from Eqs. (8), (9) and (10).

$$Q_T(Z, \alpha) = \frac{Z - 0.003\alpha - 22.91}{E^{0.56}} \qquad (50 < E_i < 500 \text{ eV}) \quad (11)$$

Table 2 A and B parameters for the DNA basis

Targets	Adenine	Guanine	Thymine	Cytosine	Uracil
A	46.53	54.79	43.66	34.68	34.56
B	0.58	0.56	0.57	0.56	0.53

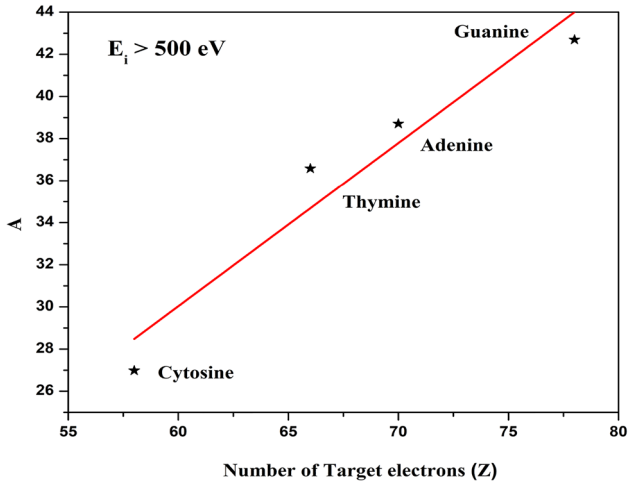

Fig. 3 Parameter A vs. Z ($E_i > 500$ eV)

Similarly for above 500 eV,

$$Q_T(Z, \alpha) = \frac{0.016\alpha + 0.776Z - 17.88}{E^{0.77}} \qquad (E_i > 500 \text{ eV}) \tag{12}$$

We observe the power of energy E is $E^{0.56}$ for lower side and $E^{0.77}$ for higher side of the incident energy.

These equations are also used to estimate Q_{el} for the studied molecules.

3 Results and discussion

In this study, we provide a complete analysis of the electron interaction with two ecologically and plasma-relevant fluoronitrile compounds, including graphs of the total cross sections for various interaction processes. This section is divided into four subsections: (1) Inelastic processes (2) Elastic processes and (3) Study of various correlations (4) Computation of dielectric constant ε.

3.1 Inelastic processes

In Figs. 4 and 5, we have provided Q_{ion}, for C_3F_5N and C_4F_7N, respectively.

Figure 4 displays results of e- C_3F_5N. The current Q_{ion} for C_3F_5N matches reasonably well with the BEB estimation of Wang et al. [5] across the whole energy range. Our Q_{ion} values increase more slowly than the BEB data that reported uncertainty of 10% [19, 32, 42].

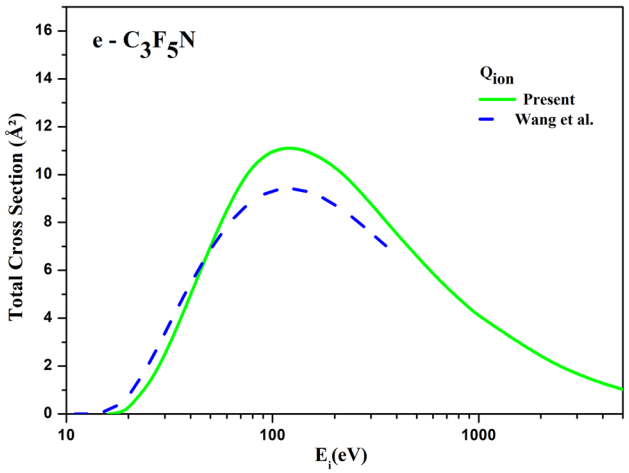

Fig. 4 Ionisation processes for C_3F_5N. line: Present Q_{ion}; Dashed: Wang et al. [5] Q_{ion} (BEB)

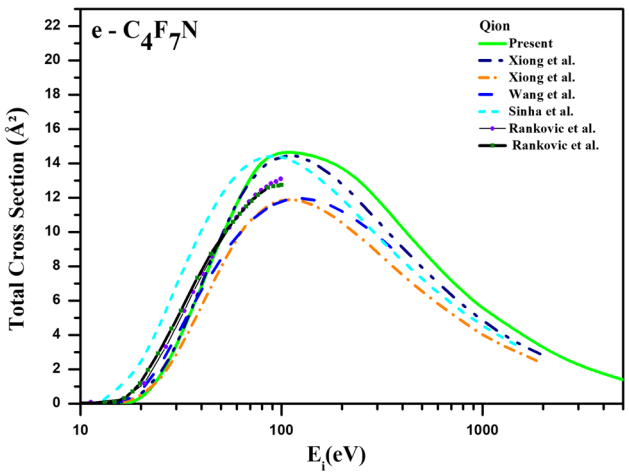

Fig. 5 Ionisation processes for C_4F_7N. line: Present Q_{ion}; Dashed: Wang et al. [5] Q_{ion} (BEB); Dash Dot Dotted: Xiong et al. [6] Q_{ion} (Modified DM); Short Dashed Dot: Xiong et al. [6] Q_{ion} (DM); Short Dashed: Sinha et al. [14] Q_{ion}; -●- Rankovic et al. [13] (BEB) Q_{ion}; -■- Rankovic et al. [13] (Experiment) Q_{ion};

Figure 5 depicts the electron scattering cross sections for C_4F_7N. In Fig. 5, Sinha et al.'s [14] Q_{ion} result is slightly left shifted. This difference may be due to the incorporation of nuclear charge into the calculation, which affects both the position and peak value, as Sinha et al. [14] have mentioned. The modified DM results provided by Xiong et al. [6] are consistent with the present Q_{ion} data. While showing reasonable agreement up to Q_{ion}'s peak, the BEB and DM results are

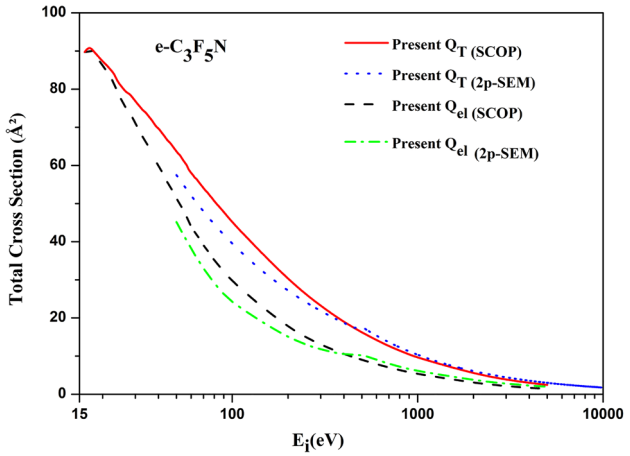

Fig. 6 Elastic processes for C_3F_5N. Line: Present Q_T (SCOP); Dotted: Present Q_T (2p-SEM); Dashed: Present $Q_{\rm el}$ (SCOP); Dash Dotted: Present $Q_{\rm el}$ (2p-SEM)

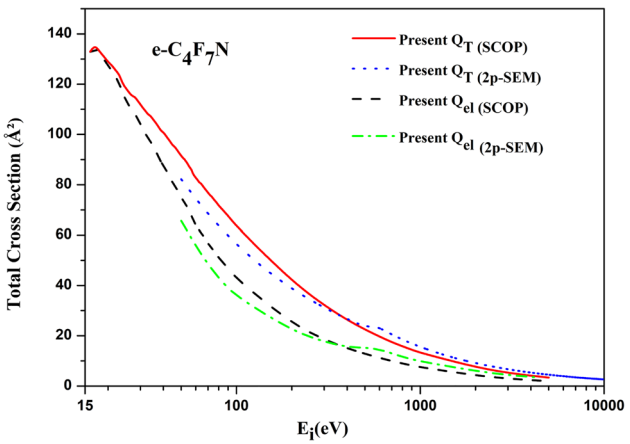

Fig. 7 Elastic processes for C_4F_7N. Line: Present Q_T (SCOP); Dotted: Present Q_T (2p-SEM); Dashed: Present $Q_{\rm el}$ (SCOP); Dash Dotted: Present $Q_{\rm el}$ (2p-SEM)

lower for the higher energy levels. In addition to these findings, the present CSP-ic result is in rather good agreement with the experimental data of the ionisation cross section by Rankovic et al. [13] at lower energies.

3.2 Elastic processes

In this subsection, we display the current $Q_{\rm el}$ and Q_T for fluoronitrile molecules through Figs. 6 and 7.

Using the SCOP approach, we are able to compute $Q_{\rm el}$ in addition to $Q_{\rm inel}$ such that,

$$Q_T(E_i) = Q_{\rm el}(E_i) + Q_{\rm inel}(E_i)$$

We show SCOP and 2p-SEM results for $Q_{\rm T}$ in Figs. 6 and 7 through the top curves for C_3F_5N and C_4F_7N, respectively. $Q_{\rm T}$ expresses the probability of all electron-induced molecular processes, and it finds use in a variety of modelling methodologies [33, 43].

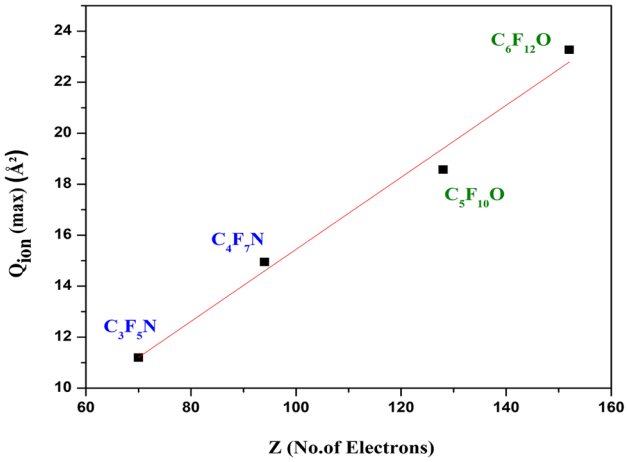

Fig. 8 Variation of $Q_{\rm ion}$(max) with Z

At higher energies, as expected, $Q_{\rm T}$ decreases as a function of $\frac{1}{E_i}$ in accordance with the Born-Bethe trend. The reported $Q_{\rm T}$ and $Q_{\rm el}$ using recently developed 2p-SEM method gives excellent agreement. This is the first effort to describe the $Q_{\rm el}$ and $Q_{\rm T}$ by two various methods upon electron impact for these key compounds that are crucial to environmental and plasma studies.

3.3 Various correlations: prediction of polarizability and dielectric constant

The SCOP technique discusses how the interactions between electrons and charged cloud of the molecule takes place and allows for an estimation of the possibility of various electron-assisted chemical processes. The molecular cloud size determined by the number of electrons (Z) plays an important role for the peak of $Q_{\rm ion}$ of each molecule. The size of the cloud through the number of electrons of the target molecule has a great influence on the peak of $Q_{\rm ion}$.

In addition to the target cloud size, $Q_{\rm ion}$ are reliant on the ionisation potential that does not vary significantly for very large molecules (Table 3). Hence, a linear relationship is seen for $Q_{\rm ion}$ (max) and number of electrons (Z) for fluoroketones [18] and fluoronitriles (Fig. 8).

We observe similar trend for fluoroketones [18] and fluoronitriles in Fig. 9 for $Q_{\rm ion}$ (max) with the number of carbon atoms (n_c) that are present in the target. These correlations can be utilised with some basic extrapolation to get an estimate for the $Q_{\rm ion}$ (max) of such massive compounds.

Our findings confirm the linear relationship between $Q_{\rm ion}$ (max) and polarizability as reported by Bart et al. [44] (Fig. 10) with $R^2 = 0.942$ and $\chi 2 = 0.2327$, The deviation is due to the spherical approximations involved in constructing charge density and potentials as well as due to the semi-empirical nature of CSP-ic formalism. Our findings confirm the linear relationship between $Q_{\rm ion}$ (max) and polarizability, as reported by

Table 3 Molecular properties and predicted α

Target	Z	Ionisation Potential (eV)	Polarizability (10^{-24}cm^{-3})		
			Reported	Estimated	Found at www.chemspider.com
C_3F_5N	70	15.20 [5]	5.72 [45]	5.34	6.60 (deviation 19%)
C_4F_7N	94	15.10 [5]	6.82 [45]	7.65	8.50 (deviation 10%)
$C_5F_{10}O$	128	12.02 [46]	8.83 [47]	9.84	10.60 (deviation 7.1%)
$C_6F_{12}O$	152	11.41 [48]	11.44 [49]	12.54	12.60 (deviation 0.4%)

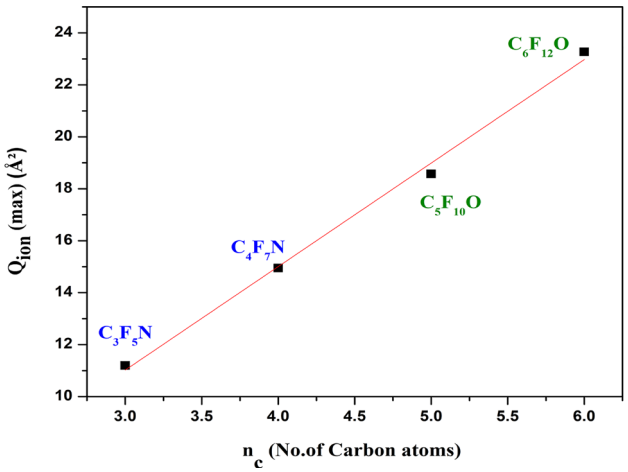

Fig. 9 Variation of Q_{ion}(max) with n_c

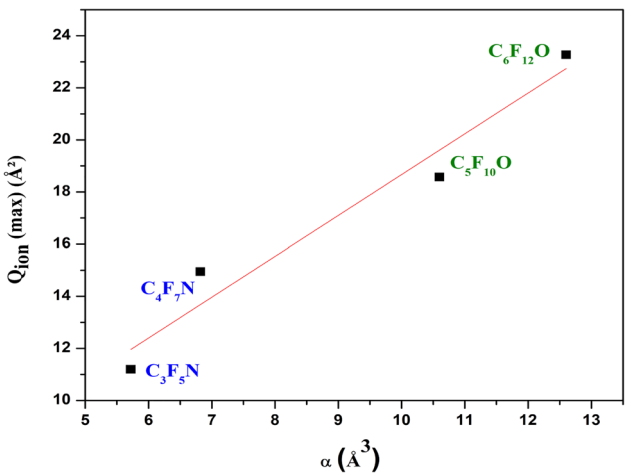

Fig. 10 Variation of Q_{ion}(max) with α

Bart et al. [44] (Fig. 10), through which we can predict polarizability for similar compounds. Table 3 shows various properties including polarizability of C_3F_5N, C_4F_7N, and perfluoroketone (PFK) (C_X $F_{2X}O$, x = 5–6) [18] molecules. The total number of electrons (Z) decides the dimension of the molecular charge density cloud.

3.4 Computation of dielectric constant, ε

As demonstrated by J. C. Devins's experiments, fluoronitrile organic gases like C_3F_5N and C_4F_7N can have double electric strengths than that of SF_6 [50]. The electrical properties of a composite material made of C_3F_5N and epoxy resin showed improved dielectric strength and thermal stability compared to pure epoxy resin. The dielectric constant of the material made of C_3F_5N was used as a key parameter in the design and optimisation of such composite material [51].

The dielectric properties of C_4F_7N lead to its potential use as a high-performance insulating gas in power equipment. The dielectric constant of C_4F_7N was found to be significantly greater to that of the SF_6, a widely employed insulating gas, which suggests that C_4F_7N could be a promising alternative for use in power equipment [52, 53].

The Clausius–Mossotti equation [54] yields,

$$\frac{\varepsilon - 1}{\varepsilon + 2} = \frac{4\pi}{3} * N * \alpha \tag{13}$$

N is the number density of molecules in the material, and α is the molecular polarizability.

The number density can be calculated using the following equation [55]:

$$N = \frac{N_A * \rho}{M} \tag{14}$$

where ρ is the density of the substance, N_A is Avogadro number (6.022×10^{23}), and M is the molar mass of the molecule. Thus, we compute the dielectric constant, ε, using Eq. (13). Required material properties are shown in Table 4.

4 Conclusion

We report quantified probabilities of various electron-assisted molecular processes for fluoronitriles C_3F_5N and C_4F_7N for wide impact energies (IP to 5 keV). We performed calculations for Q_{el}, Q_{inel}, and Q_{T} using the SCOP formalism, obtained Q_{ion} and ΣQ_{exc} through CSP-ic method, and displayed results graphically in Figs. 4, 5, 6 and 7 along with available comparison. The present Q_{ion} agrees reasonably well with adjusted DM

Table 4 Calculated dielectric constant ε

Target	Density, ρ (g cm^{-3}) (Gas phase)	Molar mass, M (g mol^{-1})	Number density, N (10^{21} cm^{-3})	Dielectric constant (ε)
C_3F_5N	1.50 [56]	145.03 [56]	6.23	1.52
C_4F_7N	1.50 ± 0.1 [56]	195.03 [56]	4.65	1.46
$C_5F_{10}O$	1.53 [56]	266.04 [56]	3.46	1.54
$C_6F_{12}O$	1.61 [56]	316.04 [56]	3.06	1.58

data [6] and BEB [5] for present compounds (Figs. 4 and 5). Since there is no previous data on Q_{el} and Q_T, we have compared present Q_{el} and Q_T computed through SCOP with results of newly developed two-parameter semi-empirical method (2p-SEM) in Figs. 6 and 7. This new method is applicable for large molecules ($55 < Z < 95$) and over a wide energy range 50 eV $< E_i <$ 5000 eV. We observed excellent agreement.

We also verified the sensitivity of Q_{ion} to size of the molecule (Z) as well as total number of carbon atoms (n_c) and observed a linear relationship Q_{ion}(max) with them (Figs. 8 and 9). We found a linear correlation between Q_{ion}(max) and polarizability shown in Fig. 10 as expected [44, 57] using which we can predict polarizability for similar compounds.

These two significant environmental and plasma-relevant compounds, C_3F_5N and C_4F_7N, have an exceptionally greater dielectric strength and lower GWP, making them appealing for commercial prospects and effective alternative for SF_6. For these applied molecules, we also computed dielectric constant ε.

While this work is the maiden report of ΣQ_{exc} and Q_{inel} for C_3F_5N, it is the first study of Q_{el} and Q_T for both these fluoronitriles. Reported theoretical results in this work may encourage experimentalists to embark on similar projects.

Author's contribution

All authors contributed equally to this submitted manuscript.

Data Availability Statement This manuscript has no associated data, or the data will not be deposited. [Authors' comment: The datasets generated during and/or analyzed during the current study are available from the corresponding author on reasonable request.]

References

1. B. Zhang, M. Hao, Y. Yao, J. Xiong, X. Li, A.B. Murphy, N. Sinha, B. Antony, H.B. Ambalampitiya, Determination and assessment of a complete and self-consistent electron-neutral collision cross-section set for the C4F7N molecule. J. Phys. D Appl. Phys. **56**, 134001 (2023). https://doi.org/10.1088/1361-6463/ACBD5D
2. J. Zhang, N. Sinha, M. Jiang, H. Wang, Y. Li, B. Antony, C. Liu, DC Breakdown characteristics of CFN/CO mixtures with particle-in-cell simulation. IEEE Trans. Dielectr. Electr. Insul. **29**, 1005–1010 (2022). https://doi.org/10.1109/TDEI.2022.3173505
3. M. Flynn, J. Agan, A. Neuber, J. Stephens, Generation and optimization of cross-sections for electron-C4F7N collisions. J. Phys. D Appl. Phys. **56**, 485207 (2023). https://doi.org/10.1088/1361-6463/ACF3DB
4. X. Zhang, Y. Li, S. Xiao, J. Tang, S. Tian, Z. Deng, Decomposition mechanism of C5F10O: an environmentally friendly insulation medium. Environ. Sci. Technol. **51**, 10127–10136 (2017). https://doi.org/10.1021/acs.est.7b02419
5. F. Wang, Q. Dun, S. Chen, L. Zhong, X. Fan, L.L. Li, Calculations of total electron impact ionization cross sections for fluoroketone and fluoronitrile. IEEE Trans. Dielectr. Electr. Insul. **26**, 1693–1700 (2019). https://doi.org/10.1109/TDEI.2019.008255
6. J. Xiong, X. Li, J. Wu, X. Guo, H. Zhao, Calculations of total electron-impact ionization cross sections for Fluoroketone C5F10O and Fluoronitrile C4F7N using modified Deutsch-Märk formula. J. Phys. D Appl. Phys. **50**, 2–9 (2017). https://doi.org/10.1088/1361-6463/aa881d
7. S. Tian, X. Zhang, S. Xiao, J. Zhang, Q. Chen, Y. Li, Application of $C_6F_{12}O/CO_2$ mixture in 10 kV medium-voltage switchgear. IET Sci. Meas. Technol. **13**, 1225–1230 (2019). https://doi.org/10.1049/iet-smt.2018.5482
8. M. Vinodkumar, H. Bhutadia, C. Limbachiya, K.N. Joshipura, Electron impact total ionization cross sections for H_2S, PH_3, HCHO and HCOOH. Int. J. Mass Spectrom. **308**, 35–40 (2011). https://doi.org/10.1016/J.IJMS.2011.07.017
9. K.N. Joshipura, B.G. Vaishnav, C.G. Limbachiya, Ionization and excitation of some atomic targets and metal oxides by electron impact. Pramana - J. Phys. **66**, 403–414 (2006). https://doi.org/10.1007/BF02704393/METRICS
10. C. Limbachiya, M. Vinodkumar, M. Swadia, K.N. Joshipura, N. Mason, Electron-impact total cross sections for inelastic processes for furan, tetrahydrofuran and 2,5-dimethylfuran. Mol. Phys. **113**, 55–62 (2015). https://doi.org/10.1080/00268976.2014.943314
11. Y.K. Kim, W. Hwang, N.M. Weinberger, M.A. Ali, M.E. Rudd, Electron-impact ionization cross sections of atmospheric molecules. J. Chem. Phys. **106**, 1026–1033 (1997). https://doi.org/10.1063/1.473186
12. D. Prajapati, H. Yadav, P.C. Vinodkumar, C. Limbachiya, A. Dora, M. Vinodkumar, Computation of electron impact scattering studies on benzene. Eur. Phys.

J. **72**(12), 72 (2018). https://doi.org/10.1140/EPJD/E2018-90078-X
13. M. Ranković, J. Chalabala, M. Zawadzki, J. Kočišek, P. Slavíček, J. Fedor, Dissociative ionization dynamics of dielectric gas C_3F_7CN. Phys. Chem. Chem. Phys. **21**, 16451–16458 (2019). https://doi.org/10.1039/c9cp02188d
14. N. Sinha, V.M. Patel, B. Antony, Ionization cross sections for plasma relevant molecules. J. Phys. B: Atomic, Molec. Opt. Phys. **53**, 145101 (2020). https://doi.org/10.1088/1361-6455/ab8e26
15. A. Jain, Total (elastic+ absorption) cross sections for eletron—CH_4 collisions in a spherical model 0.10–500 eV. Phys. Rev. A **34**, 3707–3722 (1986)
16. A. Jain, K.L. Baluja, Total (elastic plus inelastic) cross sections for electron scattering from diatomic and polyatomic molecules at 10–5000 eV. Phys. Rev. A **45**, 202 (1992). https://doi.org/10.1103/PhysRevA.45.202
17. M. Vinodkumar, C. Limbachiya, H. Desai, P.C. Vinodkumar, Electron-impact total cross sections for phosphorous triflouride. Phys. Rev. A **89**, 062715 (2014). https://doi.org/10.1103/PHYSREVA.89.062715/FIGURES/7/MEDIUM
18. N. Thakkar, M. Swadia, M. Vinodkumar, N. Mason, C. Limbachiya, Electron induced elastic and inelastic processes for perfluoroketone (PFK) molecules. Plasma Sources Sci. Technol. **30**, 085008 (2021). https://doi.org/10.1088/1361-6595/ac17ca
19. C. Limbachiya, M. Vinodkumar, M. Swadia, A. Barot, Electron impact total cross section calculations for CH_3SH (methanethiol) from threshold to 5 keV. Mol. Phys. **112**, 101–106 (2014). https://doi.org/10.1080/00268976.2013.802038
20. K.N. Joshipura, M. Vinodkumar, C.G. Limbachiya, B.K. Antony, Calculated total cross sections of electron-impact ionization and excitations in tetrahedral [Formula Presented] and [Formula Presented] molecules. Phys. Rev. A **69**, 6 (2004). https://doi.org/10.1103/PhysRevA.69.022705
21. D. Chauhan, C. Limbachiya, Electron interactions with analogous of DNA/RNA nucleobases: 3-hydroxytetrahydroFuran and α-Tetrahydrofurfuryl alcohol. Rad. Phys. Chem. **207**, 110802 (2023). https://doi.org/10.1016/j.radphyschem.2023.110802
22. N. Barad, C. Limbachiya, Electron- and positron-driven molecular processes for H_2O, CO_2, and NH_3 in their gas and ice phases. Phys. Chem. Chem. Phys. (2024). https://doi.org/10.1039/D3CP04675C
23. S. Parikh, D. Chauhan, N. Thakkar, C. Limbachiya, Scattering of electrons with aqueous biomaterials. Radiat. Phys. Chem. **214**, 111248 (2024). https://doi.org/10.1016/J.RADPHYSCHEM.2023.111248
24. R.A. Bonham, J.L. Peacher, H.L. Cox, On the calculation of multicenter two-electron repulsion integrals involving slater functions. J. Chem. Phys. **40**, 3083–3086 (1964). https://doi.org/10.1063/1.1724953
25. H. Yadav, M. Vinodkumar, C. Limbachiya, P.C. Vinodkumar, Scattering of electrons with formyl radical. Mol. Phys. **115**, 952–961 (2017). https://doi.org/10.1080/00268976.2017.1293306
26. M.A. Krestyanikova, V.I. Shematovich, Stochastic models of hot planetary and satellite coronas: a hot oxygen corona of Mars. Sol. Syst. Res. **40**, 384–392 (2006). https://doi.org/10.1134/S0038094606050030
27. G. Staszewska, D.W. Schwenke, D.G. Truhlar, Investigation of the shape of the imaginary part of the optical-model potential for electron scattering by rare gases. Phys. Rev. A **29**, 3078–3091 (1984). https://doi.org/10.1103/PhysRevA.29.3078
28. C. Limbachiya, A. Chaudhari, H. Desai, M. Vinodkumar, Electron induced chemistry of thioformaldehyde. RSC Adv. **5**, 103964–103976 (2015). https://doi.org/10.1039/c5ra19662k
29. G. Staszewska, D.W. Schwenke, D. Thirumalai, D.G. Truhlar, Quasifree-scattering model for the imaginary part of the optical potential for electron scattering. Phys. Rev. A **28**, 2740–2751 (1983). https://doi.org/10.1103/PHYSREVA.28.2740
30. C. Limbachiya, M. Vinodkumar, N. Mason, Calculation of electron-impact rotationally elastic total cross sections for NH_3, H_2S, and PH_3 over the energy range from 0.01 to 2 keV. Phys. Rev. A **83**, 1–9 (2011). https://doi.org/10.1103/PhysRevA.83.042708
31. M. Vinodkumar, C. Limbachiya, A. Barot, N. Mason, Theoretical total cross sections for e-SO_2 scattering over a wide energy range (01–2000 eV) revealing a 3.4-eV shape resonance. Phys. Rev. A (2012). https://doi.org/10.1103/PhysRevA.86.012706
32. Y.K. Kim, P.M. Stone, Ionization of boron, aluminum, gallium, and indium by electron impact. Phys. Rev. A **64**, 11 (2001). https://doi.org/10.1103/PhysRevA.64.052707
33. M. Vinodkumar, C. Limbachiya, A. Barot, N. Mason, Computation of electron-impact rotationally elastic total cross sections for methanol over an extensive range of impact energy (01–2000 eV). Phys. Rev. A **87**, 1–10 (2013). https://doi.org/10.1103/PhysRevA.87.012702
34. M. Vinodkumar, K.N. Joshipura, C.G. Limbachiya, B.K. Antony, Electron impact ionization of H_2O molecule in crystalline ice. Nucl. Instrum. Methods Phys. Res. B **212**, 63–66 (2003). https://doi.org/10.1016/S0168-583X(03)01480-0
35. K.N. Joshipura, S. Gangopadhyay, C.G. Limbachiya, M. Vinodkumar, Electron impact ionization of water molecules in ice and liquid phases. J. Phys. Conf. Ser. **80**, 012008 (2007). https://doi.org/10.1088/1742-6596/80/1/012008
36. M.A. Rahman, S. Gangopadhyay, C. Limbachiya, K.N. Joshipura, E. Krishnakumar, Electron ionization of NF_3. Int. J. Mass Spectrom. **319–320**, 48–54 (2012). https://doi.org/10.1016/j.ijms.2012.05.005
37. H. Nishimura, H. Tawara, Some aspects of total scattering cross sections of electrons for simple hydrocarbon molecules. J. Phys. B At. Mol. Opt. Phys. **24**, L363–L366 (1991). https://doi.org/10.1088/0953-4075/24/15/002
38. A. Zecca, G.P. Karwasz, R.S. Brusa, Total-cross-section measurements for electron scattering by NH_3, SiH_4, and H_2S in the intermediate-energy range. Phys. Rev. A **45**, 2777–2783 (1992). https://doi.org/10.1103/PHYSREVA.45.2777

39. K.N. Joshipura, M. Vinodkumar, Cross sections and other parameters of e^-–H_2O scattering (Ei≥50eV). Pramana J. Phys. **47**, 57–63 (1996). https://doi.org/10.1007/BF02847166
40. G. García, F. Manero, Correlation of the total cross section for electron scattering by molecules with 10–22 electrons, and some molecular parameters at intermediate energies. Chem. Phys. Lett. **280**, 419–422 (1997). https://doi.org/10.1016/S0009-2614(97)01184-6
41. M. Vinodkumar, C. Limbachiya, M. Barot, A. Barot, M. Swadia, Electron impact total cross sections for components of DNA and RNA molecules. Int. J. Mass Spectrom. **360**, 1–7 (2014). https://doi.org/10.1016/j.ijms.2013.12.027
42. Y.K. Kim, J.P. Desclaux, Ionization of carbon, nitrogen, and oxygen by electron impact. Phys. Rev. A **66**, 127081–1270812 (2002). https://doi.org/10.1103/PhysRevA.66.012708
43. M. Swadia, R. Bhavsar, Y. Thakar, M. Vinodkumar, C. Limbachiy, Electron-driven processes for furan, tetrahydrofuran and 2, 5-dimethylfuran. Mol. Phys. **115**, 2521–2527 (2017). https://doi.org/10.1080/00268976.2017.1333645
44. M. Bart, P.W. Harland, J.E. Hudson, C. Vallance, Absolute total electron impact ionization cross-sections for perfluorinated hydrocarbons and small halocarbons. Phys. Chem. Chem. Phys. **3**, 800–806 (2001). https://doi.org/10.1039/B009243F
45. Y. Wu, C. Wang, H. Sun, A.B. Murphy, M. Rong, F. Yang, Z. Chen, C. Niu, X. Wang, Properties of C_4F_7N-CO_2 thermal plasmas: thermodynamic properties, transport coefficients and emission coefficients. J. Phys. D Appl. Phys. **51**, 155206 (2018). https://doi.org/10.1088/1361-6463/aab421
46. L. Zhong, J. Wang, X. Wang, M. Rong, Calculation of electron-impact ionization cross sections of perfluoroketone (PFK) molecules C_xF2_xO (x = 1–5) based on binary-encounter-bethe (BEB) and Deutsch–Märk (DM) methods. Plasma Sources Sci. Technol. **27**, 095005 (2018). https://doi.org/10.1088/1361-6595/aad4d2
47. Y. Wu, C. Wang, H. Sun, M. Rong, A.B. Murphy, T. Li, J. Zhong, Z. Chen, F. Yang, C. Niu, Evaluation of SF6-alternative gas C5-PFK based on arc extinguishing performance and electric strength. J. Phys. D Appl. Phys. **50**, 385202 (2017). https://doi.org/10.1088/1361-6463/aa800b
48. X. Zhang, S. Tian, S. Xiao, Z. Deng, Y. Li, J. Tang, Insulation strength and decomposition characteristics of a $C_6F_{12}O$ and N_2 gas mixture. Energies **10**, 1170 (2017). https://doi.org/10.3390/en10081170
49. X. Yu, H. Hou, B. Wang, Prediction on dielectric strength and boiling point of gaseous molecules for replacement of SF_6. J. Comput. Chem. **38**, 721–729 (2017). https://doi.org/10.1002/jcc.24741
50. J. Jiao, D. Xiao, X. Zhao, Y. Deng, Analysis of the molecules structure and vertical electron affinity of organic gas impact on electric strength. Plasma Sci. Technol. **18**, 554–559 (2016). https://doi.org/10.1088/1009-0630/18/5/19
51. R.E. Wootton, M.R. Kegelman, A.W. Bauer, P.J. Chantry, T.W. Dakin, S.J. Dale, D.K. Davies, L.S. Frost, A. Lee, R.W. Lieberman, A.M. Sletten, J.B. Thompson, N.J. Zimmerman, Gases superior to Sf_6 for insulation and interruption. Electr. Power Res. Ins. **45**, 2513 (1982). https://doi.org/10.2172/6746595
52. R. Qiu, W. Zhou, Y. Zheng, S. Hu, H. Li, J. Yu, (2020) A simulation research on diffusion processes of discharging decomposition products of C_4F_7N/CO_2 in gas insulated transmission lines, 7th IEEE International Conference on High Voltage Engineering and Application, ICHVE 2020 - Proceedings pp 20–23. https://doi.org/10.1109/ICHVE49031.2020.9279468.
53. N. Tang, L. Chen, B. Zhang, X. Li, (2020) Experimental and theoretical exploration of C_4F_7N gas decomposition under partial discharge, 7th IEEE International Conference on High Voltage Engineering and Application, ICHVE 2020 - Proceedings pp 4–7. https://doi.org/10.1109/ICHVE49031.2020.9279726.
54. C. Kittel, D.F. Holcomb, Introduction to solid state physics. Am. J. Phys. **35**(6), 547–548 (1967). https://doi.org/10.1119/1.1974177
55. P.W. Atkins, J. De Paula, *Atkins' physical chemistry* (Oxford University Press, Oxford, 2014)
56. D.R. Lide, *CRC Handbook of Chemistry and Physics* (CRC Press, USA, 1992). https://doi.org/10.1016/0022-2860(92)85083-s
57. J.N. Bull, P.W. Harland, C. Vallance, Absolute total electron impact ionization cross-sections for many-atom organic and halocarbon species. J. Phys. Chem. A **116**, 767–777 (2012). https://doi.org/10.1021/jp210294p

IOP Publishing Journal of Physics B: Atomic, Molecular and Optical Physics
J. Phys. B: At. Mol. Opt. Phys. **53** (2020) 235201 (9pp) https://doi.org/10.1088/1361-6455/abbe2b

Double differential distributions of e-emission in ionization of N_2 by 3, 4 and 5 keV electron impact

Madhusree Roy Chowdhury[1,2], Dhaval Chauhan[2], Chetan G Limbachiya[2], Karoly Tőkési[3], Christophe Champion[4], Philippe F Weck[5] and Lokesh C Tribedi[1,*]

[1] Tata Institute of Fundamental Research, Colaba, Mumbai 400005, India
[2] M S University of Baroda, Vadodara 390001, India
[3] Institute for Nuclear Research, ATOMKI, Debrecen, Hungary
[4] Centre Lasers Intenses et Applications (CELIA), Bordeaux University, Talence, France
[5] Sandia National Laboratories, Albuquerque, NM 87185, United States of America

E-mail: lokesh@tifr.res.in and ltribedi@gmail.com

Received 3 July 2020, revised 31 August 2020
Accepted for publication 5 October 2020
Published 6 November 2020

Abstract

We report the measurement of the absolute double differential cross sections (DDCS) of secondary electrons emitted due to the ionization of N_2 molecule in collisions with fast electrons having energies between 3 and 5 keV. The emitted electrons with energies from 1–500 eV have been measured for different forward and backward emission angles. The measured DDCS have been compared with the state-of-the-art first Born approximation with correct boundary condition (CB1) model calculations as well as with the classical trajectory Monte Carlo (CTMC) method. From the measured DDCS, the single differential cross sections (SDCS) as a function of the emission energies have been computed and eventually the total ionization cross sections (TCS) have been derived. The TCS values are also compared with a semi-empirical calculation, namely, the CSP-ic (complex scattering potential-ionization contribution) model.

Keywords: ionization, electron impact, di-atomic molecule, DDCS, CB1, CTMC

Supplementary material for this article is available online

(Some figures may appear in colour only in the online journal)

1. Introduction

The interaction of a charged particle with an atom or molecule provides information about the fundamentals of dynamics involved in the few-body system being investigated. Depending on the energy and charge state of the projectile, different processes can occur between the two collision partners. The impact of electron on an atom or molecule, leading to single ionization of the target has been a subject of study over decades. Different mechanisms like ionization, excitation, elastic scattering, e–2e process etc [1] have been investigated over several years and many aspects of these processes are yet to be fully understood. The electron impact ionization of target atoms or molecules is not only important for understanding the collision dynamics but is also useful for other fields of research such as, mass spectrometry, plasma physics, astrophysics, stellar atmospheres and radiation chemistry etc [2–4]. Energetic electrons varying from few keV to hundreds of keV are present in the interplanetary medium. In the solar corona, different impulsive solar electron events are observed at energies between 2 and 15 keV. In the solar wind, the electrons have energy in the range from 20–200 keV [5]. In

* Author to whom any correspondence should be addressed.

addition, the nitrogen molecule deserves a special care since it is one of the residual gas in the fusion reactors. In such devices although the aim is to produce clean plasma to achieve high fusion performance, the impurities, such as, nitrogen or other noble gases are required to protect the plasma facing components from extreme heat loads coming from the hot plasma. The typical energy of electrons in the fusion chamber vary around a few hundreds eV but the complete energy distribution of electrons is very broad ranging up to a few tens of keV. Thus an accurate knowledge of the ionization cross sections by a few keV electron impact is not only important for basic understanding of the collision mechanisms, but also for the wide scale applications in astrophysics and fusion research. In recent times, fast ion and electron impact ionization studies on biomolecules have gained immense importance due to it is applicability in cancer treatment using hadron therapy technique [6]. These studies demand a better understanding of the interaction mechanisms involving relatively smaller but multi-electron molecules, such as N_2 or O_2 etc.

Among the different aspects of electron impact ionization study, the determination of total ionization cross sections of atoms and small molecules have been investigated extensively both in the experimental and theoretical framework. The double differential cross section (DDCS) measurements of the electrons emitted from a target atom/molecule provide a detailed understanding of the collision dynamics. Such experimental investigations serve as a powerful tool for testing the accuracy of different theoretical models. Most of the work on electron impact ionization focuses on impact energies varying from threshold to several hundreds of eV, with limited data existing in the higher energy regime [7]. Particularly, the high energy (a few keV) electrons are ideally suited to explore the applicability of the fundamental atomic collision models which are based on the perturbative approach. Some of the earlier work deal with the resonances in e-scattering from the N_2 at much lower energy, i.e., a few eV [8–14]. There are several theoretical and experimental studies on the e-impact ionization cross section [15–29]. However, the studies on the DDCS measurements for electron impact ionization [30–32] are very scarce. Besides providing information about the contribution of the valence shell electrons in the ionization process, the DDCS measurements also provide insight about the ionization from the inner shells of the target molecule. Such diatomic molecules are also well known candidates for studying the quantum mechanical aspects like Young type electron interference effect [33–35].

In this work, we have measured the e-DDCS for ionization of the N_2 molecule in collisions with fast electrons having energies between 3 and 5 keV. The experimentally obtained electron-DDCS have been compared with the two different theoretical models, namely, the CB1 (first Born approximation with correct boundary conditions) and the CTMC calculations. The interpretation of the cross sections for a multielectronic target system is a challenging task for theoretical models. The CB1 approximation has been successfully employed to calculate the ionization cross sections for varieties of large molecules, such as, biomolecules and PAH molecules under the collisions of fast electrons or fast heavy-ions [36–42]. Furthermore, in order to assess the possible impact of different descriptions of the molecular wave functions on the ionization cross sections, here we have also carried out the *ab initio* calculations by using two different descriptions of the N_2 molecule: the RHF/6-311G and CCSD/cc-pVTZ levels of theory. The main difficulty is caused by the many-body feature of the collision, involving the projectile, target nucleus and target electron(s). The CTMC method has been quite successful in dealing with the ionization process in ion-atom or ion-molecule collisions [43]. One of the advantages of the CTMC method is that the many-body interactions are exactly taken into account during the collisions on a classical level.

The structure of this paper is as following: in section 2 we have provided a brief outline of the experimental arrangement followed by a short note on the theoretical models in section 3. In section 4 we have dealt extensively with the experimental results and their comparison with the model calculations. Finally, the conclusion is added in section 5.

2. Experimental details

An electron gun capable of producing fast electrons with energies from 1–10 keV was mounted in a high vacuum chamber which was a 4-way-cross and maintained at a base vacuum of $\sim 1 \times 10^{-8}$ mbar. A differential pumping assembly was installed after the electron gun chamber. This was followed by the main scattering chamber which was maintained at a base pressure of $\sim 5 \times 10^{-8}$ mbar. The projectile electrons of energies 3, 4 and 5 keV were used in the present experiment. Two different sets of electrostatic lenses, deflectors and apertures were used to focus and collimate the electron beam. The projectile electrons collided with N_2 gas in the scattering chamber. The scattering chamber was flooded with the target gas at an absolute pressure of 0.1 mTorr which was measured using a capacitance manometer. The differential pumping arrangement was used to maintain the pressure difference between the interaction chamber and the e-gun chamber. The secondary electrons emitted from the target gas were energy analyzed using a hemispherical electrostatic energy analyzer with an extended collimator at the entrance of the analyzer. The energy selected electrons were detected by a channel electron multiplier (CEM) mounted at the exit end of the spectrometer. Extreme cleanliness was maintained inside the scattering chamber in order to avoid any stray electric and magnetic field near the interaction region which would otherwise deflect the low energy electrons. The collection of the lowest energy electrons accurately is difficult since any fringe field could reduce the transmission of these electrons and hence the experimental uncertainties are large in this region. The Earth's magnetic field was reduced to about 10 mG near the interaction region by using suitable μ metal shielding inside the scattering chamber. Two layers of thin μ metal sheets were used for this purpose. In addition, a pre-acceleration voltage of 6 V was applied at the entrance and exit slits of the analyzer to enhance the collection efficiency of the low energy electrons. The resolution of the spectrometer was about 6%. The front of the CEM was raised to +100 V, since the detection efficiency of CEM remains

constant ($0.87 \pm 10\%$) for electrons with energies between 100 and 600 eV (as known from the user manual of the CEM used [44]). The number of projectiles colliding with the target gas was obtained by measuring the beam current on a long Faraday cup which was electrically isolated from the main scattering chamber. The long Faraday cup was used to stop the flying away of the backscattered electrons from re-entering into the scattering chamber. A LabVIEW based data acquisition system was used for the entire data collection. The secondary electrons having energies from 1–500 eV were detected at 10 different angles between 30° and 145°. For every spectrum, the corresponding background spectrum was also collected in the absence of the gas which was subtracted from the electron spectrum obtained with the target gas. The statistical fluctuations varied from ∼2% for the lowest energy electrons in the forward angles to about 11% for the highest energy electrons in the backward angles. In addition, the errors are contributed from gas pressure fluctuations (∼5%), solid angle path length integral (∼10%), resolution of the spectrometer (∼10%) and detector efficiency (∼10%). The total uncertainties in each DDCS data was estimated to be about 18%–22%. Details about the analysis of the measured spectra is given in [45]. The experimental DDCS values are provided in a supplementary file (https://stacks.iop.org/JPB/53/235201/mmedia).

3. Theoretical models

3.1. CB1 model

The present ionization cross sections are calculated within the 1st Born approximation framework by using the partial-wave expansion formalism recently employed for describing the electron-induced ionization of isolated biomolecules [36–39]. In this approach, the incident/scattered electron is described by a plane wave whereas the ejected electron is modelled by a Coulomb wave associated to an effective target charge $Z_{\mathrm{T}}^{*} = \sqrt{-2n^2\epsilon}$ where n refers to the principal quantum number of each atomic orbital component used in the molecular target description (see hereafter) and the active electron orbital energy ϵ is related to the ionization energies B of each occupied molecular orbital by $\epsilon = -B$. Besides, it will be assumed that the passive (not ionized) electrons remain as frozen in their molecular orbitals during the collision, which permits us to reduce the electron target interaction potential to a one-active electron potential (see hereafter).

Under these conditions, the triply differential cross sections—hereafter denoted $\sigma^{(3)}(\Omega_{\mathrm{S}}, \Omega_{\mathrm{e}}, E_{\mathrm{e}})$—differential in the direction of the scattered electron Ω_{S}, differential in the direction of the ejected electron Ω_{e} and differential in the ejected energy E_{e} may be written as

$$\sigma^{(3)}(\Omega_{\mathrm{S}}, \Omega_{\mathrm{e}}, E_{\mathrm{e}}) = \sum_{j=1}^{N} \sigma_j^{(3)}(\Omega_{\mathrm{S}}, \Omega_{\mathrm{e}}, E_{\mathrm{e}}) \qquad (1)$$

where N is the number of molecular orbitals used in the description of the target and with $\sigma_j^{(3)}$ expressed as a weighted sum of the atomic triply differential cross sections $\sigma_{\mathrm{at},i}^{(3)}(\Omega_{\mathrm{S}}, \Omega_{\mathrm{e}}, E_{\mathrm{e}})$ corresponding to the different components involved in the description of the N_2 target (N_{1s}, N_{2s}, and N_{2p} orbitals), namely,

$$\sigma_j^{(3)}(\Omega_{\mathrm{S}}, \Omega_{\mathrm{e}}, E_{\mathrm{e}}) = \sum_i \xi_{j,i}.\sigma_{\mathrm{at},i}^{(3)}(\Omega_{\mathrm{S}}, \Omega_{\mathrm{e}}, E_{\mathrm{e}}) \qquad (2)$$

where the effective number of electrons $\xi_{j,i}$ as well as the corresponding binding energy are calculated in the gas phase with the Gaussian 09 software (see Frisch *et al* [46]). In order to assess the possible impact of different descriptions of N_2 molecular wave functions on the DDCS, *ab initio* calculations were carried out at both the RHF/6-311G and CCSD/cc-pVTZ levels of theory. The RHF/6-311G is a rather simple restricted Hartree–Fock description of the target with the medium accuracy Pople basis set 6-311G, while the CCSD/cc-pVTZ description is a more accurate coupled cluster calculation using both single and double substitutions from the Hartree–Fock determinant along with a much larger Dunning's correlation-consistent polarized basis set with triple-zeta. The first ionization energy corrected for zero-point vibrational energy (ZPE) was 16.900 eV with RHF/6-311G and 16.527 eV with CCSD/cc-pVTZ using Koopman's theorem. The ionization energy was further constrained to match the experimental value of 15.581 ± 0.008 for N_2 in the gas phase [47].

Thus, in the laboratory framework, the atomic triply differential cross sections $\sigma_{\mathrm{at,i}}^{(3)}$ were calculated from the atomic transition matrix element between the ground state to the 1st ionized level of the target. Then, by using the well-known frozen-core approximation which reduces the present multi-electron problem to a one active electron problem and considering the well-known partial-wave expansion of the plane wave as well as that of the Coulomb wave, the DDCS could be analytically expressed for each molecular orbital, the target ionization cross sections being simply obtained by summing up all the subshell contributions. Finally, singly differential and total cross sections were obtained after the numerical integrations over the scattering direction and the ejected energy spectrum, respectively.

3.2. CTMC model

The CTMC method is a non-perturbative method, where classical equations of motions are solved numerically [48–51]. In the present work the CTMC simulations were made in the three-body approximation, i.e. the many-electron target atom was replaced by a one-electron atom and the projectile ion was taken into account as one particle [52, 53]. For the target atom a central model potential has been used which is based on the Hartree–Fock method as developed by Green [54]. The potential can be written as:

$$V(r) = q\frac{Z - (N-1)\left(1 - \Omega^{-1}(r)\right)}{r} = q\frac{Z(r)}{r}, \qquad (3)$$

where Z is the nuclear charge, N is the total number of electrons in the atom or ion, r is the distance between the nucleus and the test charge q, and

$$\Omega(r) = \frac{\eta}{\xi}\left(\mathrm{e}^{r\xi} - 1\right) + 1. \qquad (4)$$

The potential parameters ξ and η can be obtained in such a way that they minimize the energy for a given atom or ion [55]. We treat the N_2 molecule as two N atoms in our simulation and accordingly we use $\xi = 1.179$ a.u. and $\eta = 2.27$ a.u for the N-atom. Further, this type of potential has certain advantages, because it has a correct asymptotic form for both the small and large values of r.

In the present CTMC approach, Newton's classical non-relativistic equations of motions for a three-body system are solved numerically for a statistically large number of trajectories for given initial conditions. We have used an ensemble of 5×10^7 trajectories. The equations of motion were solved using a standard Runge–Kutta method. A three-body, three-dimensional CTMC calculation is performed as described by Tőkési and Kövér [53]. The initial conditions of the individual collisions are chosen at sufficiently large internuclear separations from the collision center, where the interactions among the particles are negligible. These are selected in a similar fashion as described by Reinhold and Falcon [56] for non-Coulombic systems. A microcanonical ensemble characterizes the initial state of the target. The initial conditions were taken from this ensemble in such a way that initial binding energies of the N(2p) level ($E_b = -0.5343$ a.u.) and N(2s) level ($E_b = -1.371$ a.u.) were constrained. For ionization channel the energy and the scattering angles of the particles were recorded. These parameters were calculated at large separation of the projectile and the target nucleus.

The total and double differential cross-sections were computed using the following formulas:

$$\sigma = \frac{2\pi b_{\max}}{T_N} \sum_j b_j^{(i)}, \tag{5}$$

$$\frac{d^2\sigma}{dEd\Omega} = \frac{2\pi b_{\max}}{T_N \Delta E \Delta\Omega} \sum_j b_j^{(i)}. \tag{6}$$

In equations (5)–(6) T_N is the total number of trajectories calculated for impact parameters less than $b_{\max}$, and $b_j^{(i)}$ is the actual impact parameter for the trajectory corresponding to the ionization process under consideration in the energy interval ΔE and the emission angle interval $\Delta\Omega$ of the electron.

3.3. CSP-ic model for TCS

In addition to comparing the data with the CB1 and CTMC models, the total ionization cross section (TCS) data have also been compared with a semi-empirical model, namely the CSP-ic model [22, 57] which is used for calculating the ionization and excitation of varieties of molecules under electron impact. Since it has already been discussed in earlier papers we are providing a brief outline. Initially the total inelastic cross sections are calculated based on a complex scattering potential V_{CSC}, constructed using the target molecular charge density which is obtained by a linear combination of the atomic charge densities. This potential can be expressed as:

$$V_{CSC}(E_i, r) = V_{ST}(r) + V_{EX}(E_i, r) + V_{POL}(E_i, r) + iV_{ABS}(E_i, r) \tag{7}$$

While the real part of this interaction potential takes into account the static effect (V_{ST}), the exchange (V_{EX}) between the projectile and a target electron and the polarization (V_{POL}) of the charge density cloud, the imaginary part is an absorption term (V_{ABS}) [59], responsible for the loss of scattered flux into the allowed channels of electronic excitation and ionization [58]. The partial wave approach under the spherical approximation is used to calculate the complex phase shifts $\delta_l(k)$ which carry the signature of the interaction between the incident electrons and the molecule [60]. To compute the TCS we define a ratio between total ionization cross section and total inelastic cross sections, $R(E_i)$ [57], such that,

$$R(E_i) = 1 - c_1 \left(\frac{c_2}{U + a} + \frac{\ln U}{U} \right) \tag{8}$$

where $U = \frac{E_i}{I}$, E_i is impact energy and I is the ionization potential of the target. We evaluate the three constants c_1, c_2 and a to obtain $R(E_i)$ and hence the total ionization cross sections.

4. Results and discussions

4.1. Energy distribution at fixed emission angles

Figure 1 displays the absolute DDCS of the secondary electrons emitted from N_2 in collisions with 3 keV electrons. The DDCS spectra are shown for six different emission angles. The spectra fall by about four orders of magnitude in the measured emission energy range between 1 and 500 eV. The cross section is maximum in the lowest energy range corresponding to the soft collision mechanism and then falls rapidly with the increase in the emission energies. The soft collision mechanism involves very little momentum transfer from the projectile to the bound electrons of the target and hence these electrons are emitted for large impact parameter collisions. The intermediate part of the spectrum is normally dominated by the two-centre effect where the ejected electron is under the influence of both the projectile and the positively charged recoil target-ion. However, in case of electrons as projectiles, two centre effect does not play a major role unlike the case for a typical ion-molecule collision. The sharp peak observed at ~350 eV corresponds to the K-LL Auger electron emission. The measured DDCS have been compared with the CB1 model calculations. The calculations have been performed using two different descriptions of the target wave functions at the RHF/6-311G and CCSD/cc-pVTZ levels of the theory. Both the calculations have been shown in figure 1 (solid and dash-dot-dot lines) and it is seen that in the log–log scale, the two models almost merge with each other. This suggests that the description of the target wave functions has very limited impact on the DCCS in the energy range considered here. In case of the forward angles, the CB1 model calculations underestimate the data upto about 60 eV, beyond which it shows overall good agreement with the data. For the intermediate angles, around 90°, the theory matches qualitatively and quantitatively with the measured DDCS above 50 eV. However, in case of backward angles, the model underestimates

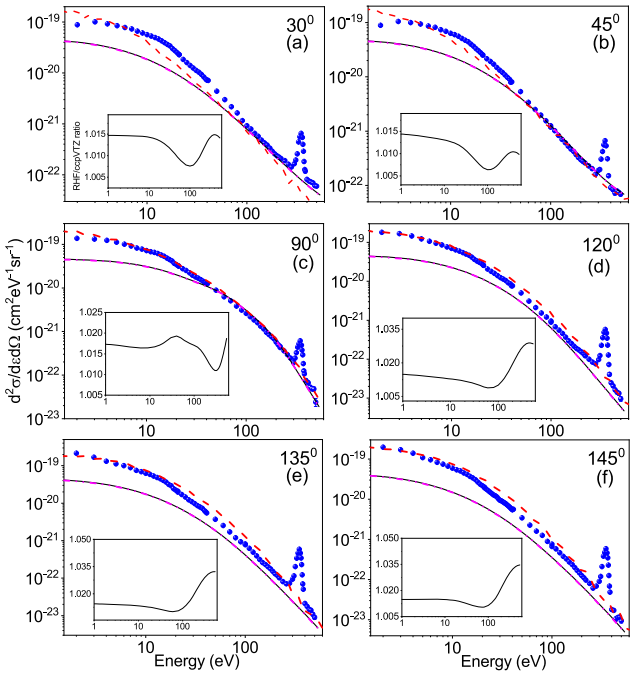

Figure 1. Absolute e-DDCS of N_2 in collisions with 3 keV electrons: The lines corresponding to the CB1 calculations with the RHF/6-311G (black solid line) and the CCSD/cc-pVTZ (magenta dash-dot-dot line) descriptions of the target wave function. The difference between these two calculations are too small and therefore the ratio between them are shown in the insets. The CTMC model calculations for 2N are shown by the red dashed lines.

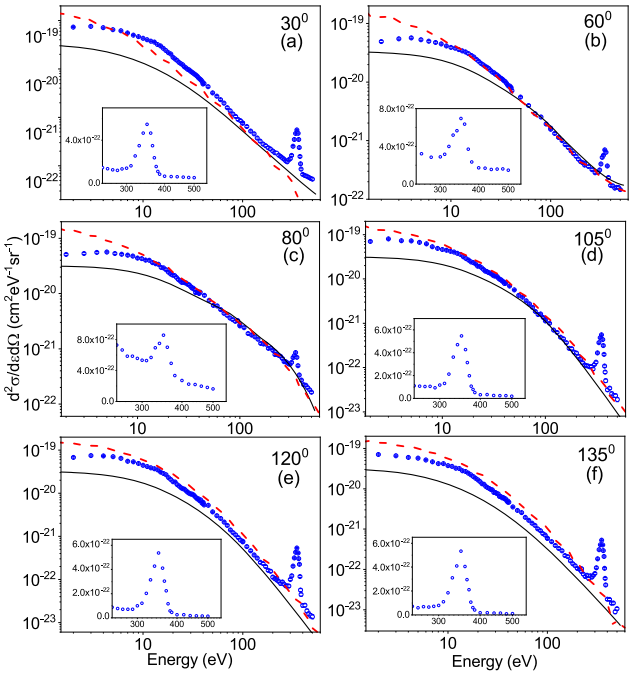

Figure 2. DDCS of secondary electrons in case of 4 keV projectile electrons. The CB1 calculations (with RHF/6-311G wavefunction) are shown by black solid lines. The CTMC calculations are shown by red dashed lines. Inset: K-LL Auger peak of nitrogen for each emission angle.

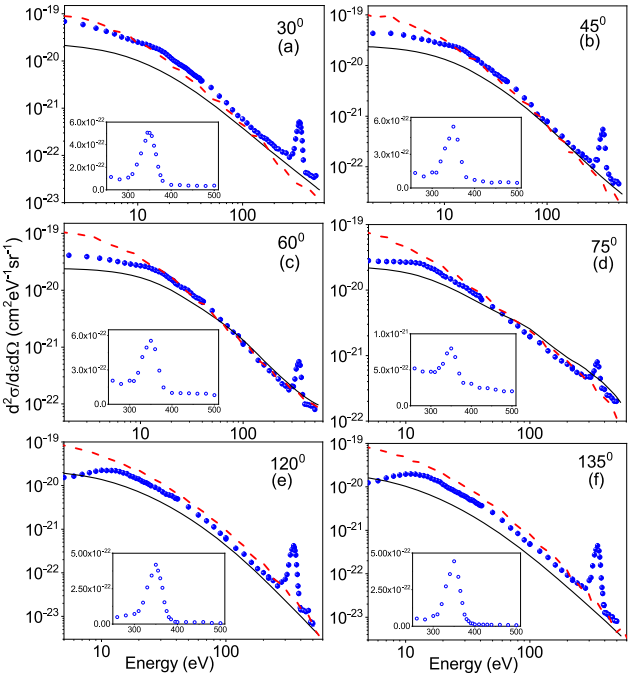

Figure 3. Similar to figure 2, except for 5 keV electrons.

the data over the entire spectra, with maximum discrepancy occurring in the low emission energies. The ratio between the CB1 predictions using two different wave functions is found to vary very little i.e. from 1.01 in the forward angles to 1.04 for the higher backward angles (see insets in figure 1). The experimental data have also been compared with CTMC model calculations for twice the atomic nitrogen or 2N (red dashed line). Overall an excellent agreement is observed with this model over the entire energy regime. In figures 2 and 3, we have shown the energy dependence of the e-DDCS for the projectile energies 4 and 5 keV, respectively. In both the cases the CTMC model is seen again to match well with the data points except for the lowest energy electrons, where it predicts slightly higher cross sections. On the other hand, the CB1 model show a good qualitative agreement reproducing the shape of the energy distribution accurately. However, this model quantitatively underestimates the data below 70 eV for all the angles. For higher beam energy i.e. at 5 keV (figure 3) the CB1 model although predicts somewhat different cross sections from the experiment, but the difference is quite less compared to that for the 3 keV and 4 keV electron beam. The insets in each panel in figures 2 and 3 show the magnified view of the K-LL Auger peak.

Figure 4 displays the theoretical (CB1) DDCS values as a function of the ejected electron energy for various emission angles. The calculated values are shown for incident electron energy of 3 keV. It may be noticed that in the low energy region, all the curves corresponding to the different emission angles bunch together. This region is dominated by the soft collision mechanism for which the DDCS remains almost independent of the emission angles. With the increase in the emission energies, the spectra corresponding to the intermediate angles, (i.e., 75°, 80° and 90°) start going up whereas the spectra for the forward and backward angles show a steady

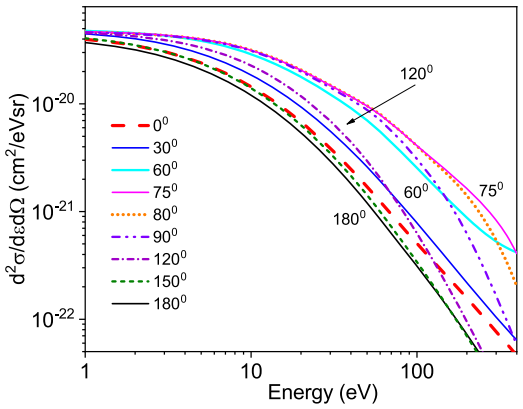

Figure 4. Theoretical (CB1) DDCS for different emission angles for 3 keV electron beam.

fall. The separation among different lines represent the angular distributions.

4.2. Angular distribution at fixed emission energies

To have a better understanding of the features seen in figure 4, the absolute DDCS of the ejected electrons as a function of different emission angles have been displayed in figure 5 corresponding to the projectile beam energy of 3 keV. The six plots shown in figure 5 expand over the entire emission energy range revealing the signature of different features at different parts of the spectrum. In figure 5(a) an almost flat distribution is observed corresponding to the soft collision mechanism which is dominated by large impact parameter events. For higher electron emission energies, a peak like structure starts appearing around 80° which sharpens further with the increase in the emission energies. This peak is due to the binary nature of collision i.e. the direct two-body free-electron scattering between the incident electron and the target electron while the recoil-ion remains passive. The CB1 model (black solid and magenta dash-dot-dot lines) show a qualitative agreement only but quantitatively underestimates the data, except in the peak region, where it matches well with the measured quantities. With the increase in the emission energies, it is seen that the DDCS values for the forward angles are slightly higher compared to those for the backward angles. For ejected electron energy 160 eV (figure 5(d)), the measured DDCS for forward angle is 1.6 times higher compared to the backward angle, whereas for 260 eV, the difference goes up to 2.6 times (figure 5(f)). These numbers, i.e. forward–backward angular asymmetry parameters, are close to that predicted by the CB1 model.

It is seen that the CTMC model show very good agreement with the data at 7 eV (figure 5(a)). However, with increase in emission energies, it is observed that the CTMC model predicts a higher cross section for the backward angles compared to that for the forward angles. Thereby the forward-backward angular asymmetry is not reproduced properly by the CTMC model unlike the cases for the experimental measurements and the CB1 model. Similar features are also observed for the impact energies of 4 keV (figure 6) and 5 keV (figure 7). In order to understand and correct this behavior we made some

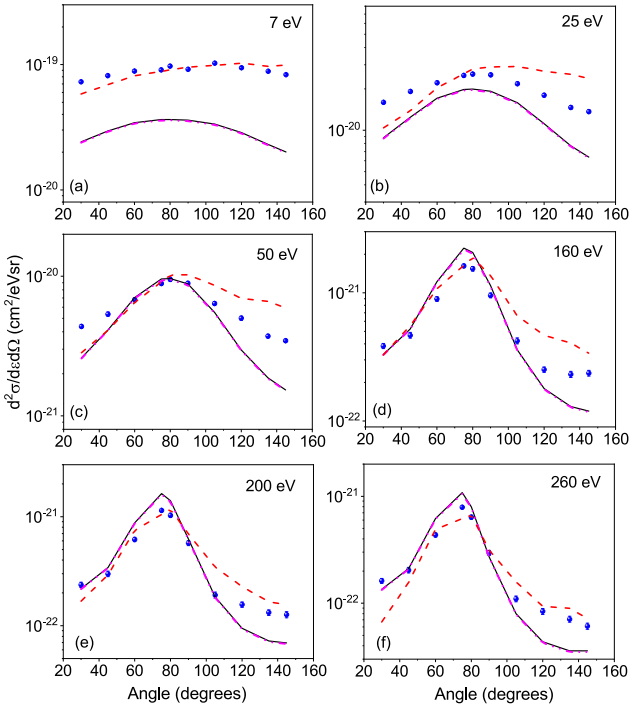

Figure 5. Angular distributions of e-DDCS for fixed secondary electron energies in case of incident energy 3 keV. Black solid and magenta dash-dot-dot lines represent the CB1(RHF/6-311G) and CB1(CCSD/cc-pVTZ), respectively. The CTMC calculations are shown by red dashed lines.

initial tests on the strength of the projectile electron and target electron interactions as modelled in the CTMC approach. As a result of the standard calculations (shown in the figures), the interaction between the two electrons is kept 'ON' during the entire motion of the particles till the asymptotic limit. However, as a initial test we also performed the simulations by switching off the e–e interaction in the exit channel. This indicated certain improvement in the distribution. However, further systematic calculations are required to be performed to improve the angular distribution. We conclude that the present CTMC model overestimate the strength of the electron–electron interactions particularly in the exit channel. The projectile electron sweep out the ejected target electron from the forward angles to the backward ones. The detailed analysis of this effect is in progress and will be published elsewhere.

4.3. Single differential cross section

Integrating the e-DDCS spectrum over the emission energy or emission angle gives us the SDCS. Integrating over the emission energies, we obtain the SDCS i.e. $\mathrm{d}\sigma/\mathrm{d}\Omega_\mathrm{e}$, as a function of angles which is given by:

$$\frac{\mathrm{d}\sigma}{\mathrm{d}\Omega_\mathrm{e}} = \int \frac{\mathrm{d}^2\sigma}{\mathrm{d}\Omega_\mathrm{e}\mathrm{d}\epsilon_\mathrm{e}}\mathrm{d}\epsilon_\mathrm{e}. \tag{9}$$

Similarly, integrating over the emission angles, we get the SDCS as a function of the emission energy:

$$\frac{\mathrm{d}\sigma}{\mathrm{d}\epsilon_\mathrm{e}} = \int \frac{\mathrm{d}^2\sigma}{\mathrm{d}\epsilon_\mathrm{e}\mathrm{d}\Omega_\mathrm{e}}\mathrm{d}\Omega_\mathrm{e}. \tag{10}$$

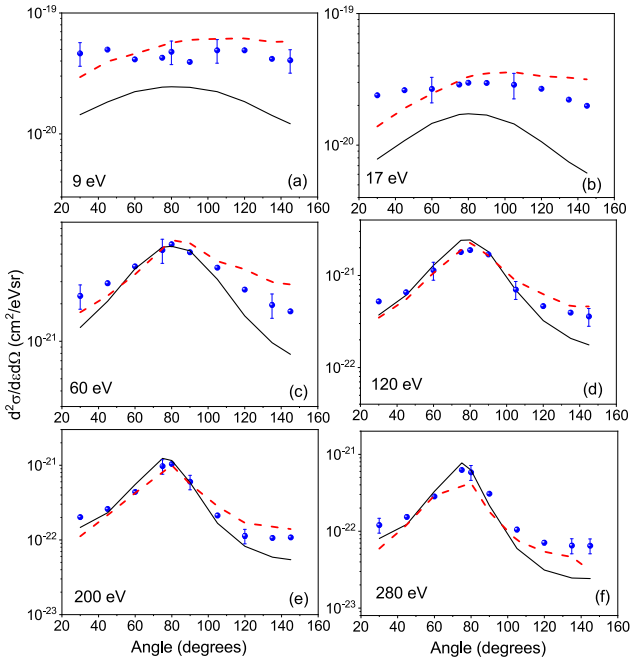

Figure 6. Similar to figure 5, shown for 4 keV electrons. The absolute errors are shown for some data points.

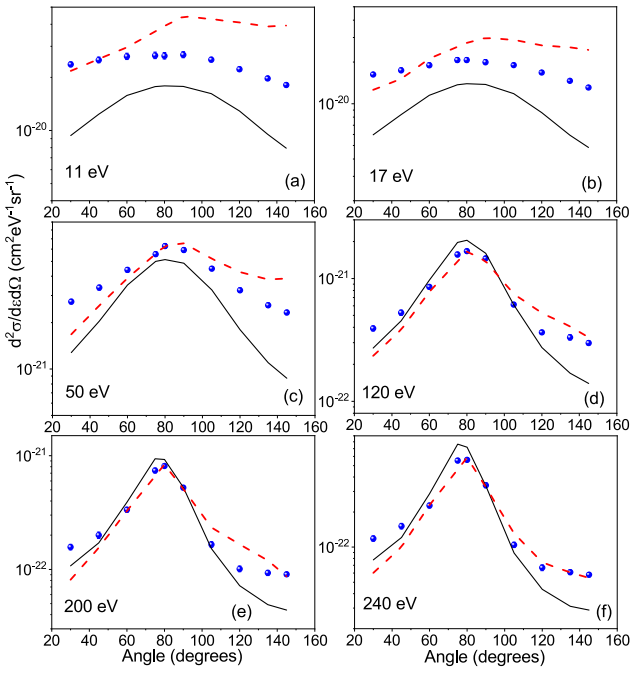

Figure 7. Similar to figure 5 for incident energy 5 keV.

Figure 8 displays the SDCS i.e., $d\sigma/d\epsilon_e$ as a function of the emission energies corresponding to 3, 4 and 5 keV incident energies. For all the three beam energies, the CB1 model predicts lower cross sections compared to the data upto ∼50–60 eV, beyond which one can observe a very good agreement. The discrepancy is largest for incident energy 3 keV and least for the 5 keV electrons. The measured DDCS have also been compared with the CTMC model (red dashed line). Overall an excellent agreement is observed with the CTMC

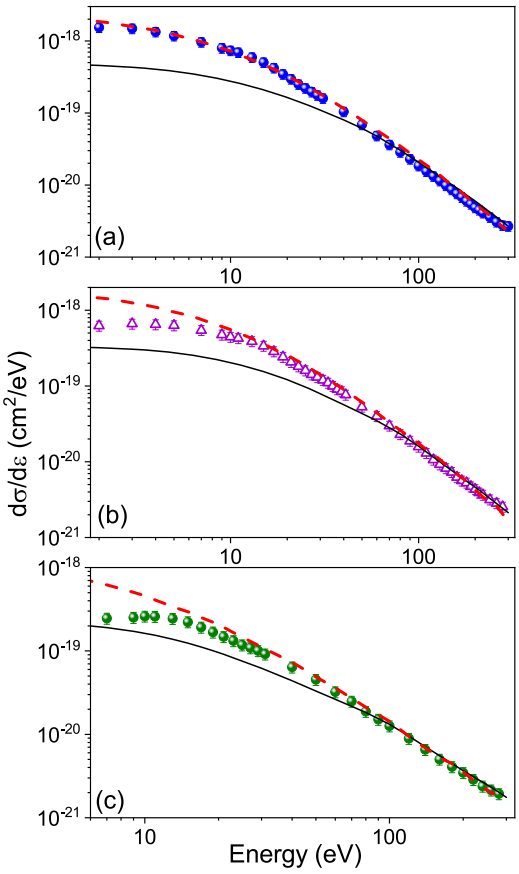

Figure 8. $d\sigma/d\epsilon$ as a function of emission energies for (a) 3, (b) 4 and (c) 5 keV incident energies; data compared with CTMC (red dashed line) and CB1 (black solid line) models.

model over the entire energy regime for all the three beam energies under investigation. However, in case of 4 and 5 keV (see figures 8(b) and (c)), the model overestimates the data for the lowest energy electrons only by a little amount.

4.4. Total ionization cross section

Integrating the SDCS over the emission energies or emission angles gives the total ionization cross section. The TCS were obtained by integrating over the electron energies between 1 and 500 eV and over the emission angles from $\theta = 0°$ to $\theta = 180°$. The data points below 30° and above 145° were estimated by extrapolation to obtain the total cross section and the difference was found to be about 11%–13%. It was observed that the TCS values derived by integrating the SDCS over the emission angles and energies varied very little i.e. only by ∼0.3%–0.4%. In figure 9, the experimental and theoretical TCS values have been displayed which includes the data obtained for the incident energies of 7 keV [61] as well as for the 6 and 8 keV [62]. The total contribution of the K-shell ionization (σ_{K-LL}) for 3, 4 and 5 keV beam energies are 0.23 Mb, 0.21 Mb and 0.19 Mb, respectively, whereas, the TCS at these three energies were found to be 26.3 Mb, 16.8 Mb and 14.2 Mb.

From figure 9 it is seen that the CB1 model falls well below the present experimental data but provides an excellent

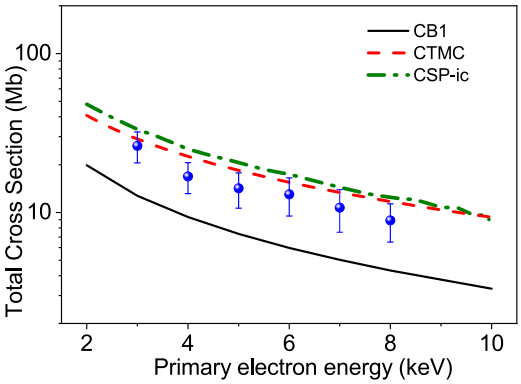

Figure 9. Total ionization cross section as a function of incident electron energy along with the predictions of three different models, i.e. the CB1, CTMC and CSP-ic.

qualitative agreement with the observed energy-dependence. The CTMC model, on the other hand, falls a bit higher compared to most of the data points but mostly within the experimental uncertainties which are about 22%–27%. The present TCS values are found to be lower than the existing data [7] by about 20% to 40% (not shown). The CTMC calculations also fall below these existing data and the difference increases for higher energy. The CB1 model is closer to the present measurements and has a large deviation from the existing data. The TCS values predicted by the CSP-ic model overestimates the measured data for all the energies, but provides a good qualitative behavior regarding the energy dependence. This discrepancy could be due to the consideration of the spherical charge density of the N_2 molecule and other approximations [63] used in the semi-empirical model. It is to be noted that the TCS calculations obtained using the two *ab initio* models, (CB1 and CTMC), lie below and just above the experimental values, respectively. The CTMC model provides closest agreement to the present data.

5. Conclusions

We have measured the absolute DDCS, SDCS and TCS of the secondary electron emission in ionization of N_2 under the impact of 3, 4 and 5 keV fast electrons for emission angles between 30° and 145°. The experimental DDCSs spectra have been compared with the CB1 model calculations with two different target wave functions as well as with the CTMC model for twice of atomic nitrogen. No significant difference has been observed between the two sets of the CB1 model calculations corresponding to the two wave functions at the RHF/6-311G and CCSD/cc-pVTZ levels of theory. This suggests that the description of the target wave functions have very limited impact on the DDCS in the energy range considered here. The CTMC model provided a very good agreement with the measured data for the entire emission spectra except for certain energy-angle window region. The CB1 model predicted lower cross section values compared to the experimental data for all emission energies, with maximum discrepancy lying in the low emission energy region. Although the CTMC gives the closest representation to the experimental values, the forward–backward angular asymmetry of the DDCS is not reproduced properly by the CTMC model unlike the CB1 model and hence further investigations are required. The derived TCS values have been compared both with the *ab initio* CB1 and CTMC calculations as well as with the semi-empirical CSP-ic model. While qualitatively both the CB1 and the CSP-ic models show similar energy dependence, the CTMC gives the closest representation to the measured TCS values within experimental uncertainties.

Acknowledgment

One of the authors (M R C) would like to acknowledge the financial assistance from CSIR for the execution of this project. We acknowledge the technical support provided by Mr Nilesh Mhatre and Mr. W Fernandes. Sandia National Laboratories is a multi-mission laboratory managed and operated by National Technology and Engineering Solutions of Sandia, LLC., a wholly owned subsidiary of Honeywell International, Inc., for the US Department of Energy's National Nuclear Security Administration under Contract DE-NA0003525. The views expressed in the article do not necessarily represent the views of the US DOE or the United States Government.

ORCID iDs

Chetan G Limbachiya https://orcid.org/0000-0003-2845-1244
Karoly Tőkési https://orcid.org/0000-0001-8772-8472
Lokesh C Tribedi https://orcid.org/0000-0002-9282-9734

References

[1] Mark T D and Dunn G H (ed) 1985 *Electron Impact Ionization* (Wien: Springer)
[2] Bartschat K and Kushner M J 2016 *Proc. Natl Acad. Sci.* **113** 7026
[3] Becker K H and Tarnovsky V 1995 *Plasma Sources Sci. Technol.* **4** 307
[4] Janev R K (ed) 1995 *Atomic and Molecular Processes in Fusion Edge Plasmas* (New York: Plenum)
[5] Jeffrey N L S, Kontar E P and Fletcher L 2019 *Astrophys.* J **880** 136
[6] Sanche L 2005 *Eur. Phys. J.* D **35** 367
[7] Schram B L, De Heer F J, van der Wiel M J and Kistemaker J 1965 *Physica* **31** 94
[8] Golden D E 1966 *Phys. Rev. Lett.* **17** 847
[9] Mathur D and Hasted J B 1977 *J. Phys. B: At. Mol. Phys.* **10** L265
[10] Weatherford C A and Temkin A 1994 *Phys. Rev.* A **49** 2580
[11] Morgan L A 1986 *J. Phys. B: At. Mol. Phys.* **19** L439
[12] Kennerly R E 1980 *Phys. Rev.* A **21** 1876
[13] Sun W, Morrison M A, Isaacs W A, Trail W K, Alle D T, Gulley R J, Brennan M J and Buckman S J 1995 *Phys. Rev.* A **52** 1229
[14] Garcia G, Perez A and Campos J 1988 *Phys. Rev.* A **38** 654
[15] Schram B L, Moustafa H R, Schutten J and De Heer F J 1966 *Physica* **32** 734
[16] Rapp D and Englander-Golden P 1965 *J. Chem. Phys.* **43** 1464
[17] Straub H C, Renault P, Lindsay B G, Smith K A and Stebbings R F 1996 *Phys. Rev.* A **54** 2146

[18] Hwang W, Kim Y K and Rudd M E 1996 *J. Chem. Phys.* **104** 2956
[19] Madison D H and Al-Hagan O 2010 *J. Phys. B: At. Mol. Opt. Phys.* **2010** 1
[20] Margreiter D, Deutsch H, Schmidt M and Mark T D 1990 *Int. J. Mass Spectrom. Ion Process.* **100** 157
[21] Mark T D 1975 *J. Chem. Phys.* **63** 3731
[22] Joshipura K N, Gangopadhyay S S, Kothari H N and Shelat F A 2009 *Phys. Lett.* A **373** 2876
[23] Deutsch H, Becker K, Matt S and Mark T D 2000 *Int. J. Mass Spectrom.* **197** 37
[24] Hudson J E, Hamilton M L, Vallance C and Harland P W 2003 *Phys. Chem. Chem. Phys.* **5** 3162
[25] Toth I, Campeanu R I, Chis V and Nagy L 2008 *Eur. Phys. J.* D **48** 351
[26] Freund R S, Wetzel R C and Shul R J 1990 *Phys. Rev.* A **41** 5861
[27] Keiffer I J and Dunn G H 1966 *Rev. Mod. Phys.* **38** 1–35
[28] Kim Y K and Desclaux J-P 2002 *Phys. Rev.* A **66** 012708
[29] Itikawa Y 2006 *J Phys. Chem. Ref. Data* **35** 31
[30] Opal C B, Peterson W K and Beaty E C 1971 *J. Chem. Phys.* **55** 4100
[31] Opal C B, Beaty E C and Peterson W K 1972 *At. Data Nucl. Data Tables* **4** 209
[32] Goruganthu R R, Wilson W G and Bonham R A 1987 *Phys. Rev.* A **35** 540
[33] Chatterjee S, Kasthurirangan S, Kelkar A H, Stia C R, Fojón O A, Rivarola R D and Tribedi L C 2009 *J. Phys. B: At. Mol. Opt. Phys.* **42** 065201
[34] Roy Chowdhury M, Stia C R, Tachino C A, Fojon O A, Rivarola R D and Tribedi L C 2016 *Phys. Rev.* A **94** 052703
[35] Gao J, Madison D and Peacher J L 2005 *Phys. Rev.* A **72** 032721
[36] Champion C, Hanssen J and Hervieux P-A 2004 *J. Chem. Phys.* **121** 9423
[37] Milne-Brownlie D S, Cavanagh S J, Lohmann B, Champion C, Hervieux P-A and Hanssen J 2004 *Phys. Rev.* A **69** 032701
[38] Champion C, Dal Cappello C, Houamer S and Mansouri A 2006 *Phys. Rev.* A **73** 012717
[39] Champion C 2013 *J. Chem. Phys.* **138** 184306
[40] Agnihotri A N *et al* 2012 *Phys. Rev.* A **85** 032711
[41] Agnihotri A N, Nandi S, Kasthurirangan S, Kumar A, Galassi M E, Rivarola R D, Champion C and Tribedi L C 2013 *Phys. Rev.* A **87** 032716
[42] Biswas S, Champion C, Weck P F and Tribedi L C 2017 *Sci. Rep.* **7** 5560
[43] Jorge A, Horbatsch M, Illescas C and Kirchner T 2019 *Phys. Rev.* A **99** 062701
[44] *Channel Electron Multiplier* (Germany: Dr. Sjuts Optotechnik GmbH)
[45] Chowdhury M R and Tribedi L C 2017 *J. Phys. B: At. Mol. Opt. Phys.* **50** 155201
[46] Frisch M J *et al* 2009 *Gaussian 09, Revision A.02* Gaussian, Inc Wallingford
[47] Trickl T, Cromwell E F, Lee Y T and Kung A H 1989 *J. Chem. Phys.* **91** 6006
[48] Abrines R and Percival I C 1966 *Proc. Phys. Soc.* **88** 861
[49] Olson R E and Salop A 1977 *Phys. Rev.* A **16** 531
[50] Tőkési K and Hock G 1994 *Nucl. Instrum. Methods Phys. Res.* B **86** 201–4
[51] Tőkési K and Hock G 1996 *J. Phys. B: At. Mol. Opt. Phys.* **29** L119–25
[52] Tőkési K and Kövér Á 1999 *Nucl. Instrum. Methods Phys. Res.* B **154** 259–62
[53] Tőkési K and Kövér Á 2000 *J. Phys. B: At. Mol. Opt. Phys.* **33** 3067–77
[54] Green A E S 1973 *Adv. Quantum Chem.* **7** 221
[55] Garvey R H, Jackman C H and Green A E S 1975 *Phys. Rev.* A **12** 1144
[56] Reinhold C O and Falcon C A 1986 *Phys. Rev.* A **33** 3859
[57] Joshipura K N, Vinodkumar M, Limbachiya C G and Antony B K 2004 *Phys. Rev.* A **69** 022705
[58] Swadia M, Thakar Y, Vinodkumar M and Limbachiya C 2017 *Eur. Phys. J.* D **71** 85
[59] Staszewska G, Schwenke D W, Thirumalai D and Truhlar D G 1983 *Phys. Rev.* A **28** 2740
[60] Vinodkumar M, Limbachiya C, Barot A and Mason N 2013 *Phys. Rev.* A **87** 012702
[61] Roy Chowdhury M, Stia C R, Tachino C A, Fojon O A, Rivarola R D and Tribedi L C 2017 *Eur. Phys. J.* D **71** 218
[62] Tribedi L C *et al* unpublished
[63] Limbachiya C, Vinodkumar M, Swadia M and Barot A 2014 *Mol. Phys.* **112** 101